The Design and Development of a Novel Beta Ti Alloys with Low Elastic Modulus for Biomedical Application

Submitted by

MOSHOKOA NTHABISENG ABIGAIL

A Master's Research dissertation submitted in fulfilment of the requirements for the degree of

MASTER OF TECHNOLOGY

In

ENGINEERING METALLURGY

In the

Faculty of Engineering and the Built Environment

At the

UNIVERSITY OF JOHANNESBURG

SUPERVISOR: Dr Babatunde Abiodun Obadele

CO-SUPERVISOR: Ms Lerato Raganya

: Prof Ronald Machaka

: Prof Elizabeth Makhatha

Date of submission

07/2020

DECLARATION

I NTHABISENG ABIGAIL MOSHOKOA hereby declare that this master's research dissertation is wholly my own work and has not been submitted anywhere else for academic credit either by myself or another person. I understand what plagiarism implies and declare that this proposal is my own ideas, words, phrase, arguments, graphics, Figures, results and organisation except where reference is explicitly made to another's work. I understand further that any unethical academic behaviour, which includes plagiarism, is seen in a serious light by the University of Johannesburg and is punishable by disciplinary action.

Signed Date 17/07/2020

DEDICATION

This dissertation is dedicated to Almighty GOD, to my loving parents: Mrs MOKGADI MARGRET MOSHOKOA and the late Mr MOREPIWA JOHANNES MOSHOKOA. To my sister MAGDELINE MOSHOKOA.

ACKNOWLEDGEMENT

My gratitude goes to my supervisor, thank you Dr Babatunde Obadele from Botswana International University of science and technology, thank you for your supervision and the immense support you have shown me, you were academically incredible with your advices and supervision. My appreciation goes to Prof Ronald Machaka and Dr Robert Tshikudo the CAM from CSIR for the warm welcome to be one of the team at the CSIR (AME), thank you for the support and all the advices. My profound thankfulness to my co-supervisor Ms Lerato Raganya, thank you so for the mentorship. I have learned a lot from you about this research world. Thank you for accepting me to be your master's student and to be under your Thuthuka Funding. My gratitude goes to Prof Elizabeth Makhata for University of Johannesburg, Department of Metallurgy, thank you for all the advices and support you have shown me.

I would like to thank the University of Johannesburg for giving me this opportunity to study my master's degree within the institution, the CSIR, AME department for granting the opportunity to conduct my experiments and get laboratory training in their department. The National Research Fund (NRF) and DSI for funding the project under Lerato Raganya Thuthuka funding. My gratitude goes to everyone at the CSIR (Lusanda Fikeni, Stephen Masete, Suzan Nchabeleng, Marry Mojalefa, Ndumiso Nguni, Solly Motoung, Khoro Malabi, Pierre Rossouw, Martin Williams, Lerato Raganya and Mandy Madiogoe) for assisting me with every experimental preparation and obtaining experimental results. To Mintek (Edson Mahuma and Melannie Smith) for assisting me with arc melting process. To the University of Pretoria, the Department of Mineral science (Carel Coetzee, Lwazi, Thulani Mukharati) for assisting with SEM analysis and Electropolishing and Wiebke Grote for XRD analysis.

To the Moshokoa family (Mom, sisters, brothers, niece and nephews) thank you so much for the support, the road was not easy at all, but you held my hand to the end. To my sister Magdeline Moshokoa, thank you for the support and advices you gave me, you truly stuck by me with this research work, you experience all those stress with me and for that thank you so much. Lastly, my gratefulness goes to the following people for supporting me through this research journey: Dineo Moshokoa, and Moshokoa Joyce. Finally, thank God for giving me the protection and strength to go on until the finish line.

ABSTRACT

The aim of this work was to design and develop a β Ti-type based alloy with a low elastic modulus close to that of the human bone. It's imperative for the elastic modulus of the implant to match that of human bone in order to avoid the stress shielding effect which is explained as the difference in the transfer of mechanical stress from the implant to the bone. Currently commercially available Ti6Al4V alloy that is being used for biomedical application is reported to have some drawbacks such a higher elastic modulus as compared to the bone and the release of toxic elements of V and Al are reported to cause health issues. Therefore, the development of β-Ti alloy with low elastic modulus and non-toxic element has gained great research interest. This research work focus on the composition design of a binary Ti-Mo alloys (10.02, 10.83, 12.89 and 15.05 wt% Mo) using the cluster plus glue atom model and using the β stabilizing predictions methods such as Moeq, Kβ stability index, e/a ratio and the d-orbital map to predict the stability of the β phase in binary Ti-Mo alloys. The alloys were fabricated using the commercial Arc re-melting furnace with a water-cooled copper mould. Solution treatment of the as-cast ingots in a ceramic furnace took place at a temperature of 1100℃ for 1 h and then the ingots were quenched in ice water. The solution treated alloys were compressed in-order to examine the deformation behaviour. All the processed samples (as-cast, solution treated and compressed) were characterized for phase and microstructural properties using the X-ray diffraction (XRD), Optical microscope (OM), Scanning electron microscope (SEM), and Electron backscatter diffraction techniques (EBSD). The mechanical properties of all the sample in all conditions (as-cast and solution treated) were investigated using the tensile test, 3-point bend test, compression test and Miro-Vickers hardness. The as-cast XRD peaks, OM and SEM micrographs results illustrated the equiaxed β structure and secondary orthorhombic martensitic α″ phase, whereas the EBSD map showed the existence of the omega phase in addition to the α″ phase and bcc β phase. The micro-Vickers hardness and the elastic modulus of the as-cast alloys decreased when the Mo content increased, whereas the bending strength and other tensile properties oscillated as the Mo content increased. The microstructure and phase evolution of the solution treated alloys analysed using XRD, OM and SEM showed a decrease in the quantity of the orthorhombic martensitic α″ phase and an increase in the bcc β phase with an increase in the Mo content. While the EBSD maps illustrated the presence of the omega phase

which decreased with an increase with Mo content. The micro-Vickers hardness of the solution treated alloys increased as the Mo content increased whereas the elastic modulus decreased with a Mo content of Ti-15.05 wt% Mo. The bending properties and tensile properties of the solution treated alloys were fluctuating. Compressive strength of solution treated alloys increased but significantly decreased when the Mo content was found to be Ti-15.05 wt% Mo. The deformation behaviour of the designed alloys analysed using the OM, EBSD, tensile properties and micro-Vickers hardness showed that when the Mo content increased the volume fraction of the parallel deformation plates of stress induced transformation was decreasing and the amount of wider deformation bands and thinner bands were becoming dominant. The experimental results of all the binary Ti-Mo alloys in as-cast and solution treated conditions were found to be inconsistent with the theoretical results predicted by the β stabilizing prediction methods because of the precipitation of the secondary phases of martensitic and omega phase. The predicting method such as Mo equivalence, the e/a ratio and the K_{β} showed theoretically all the studied alloys will only retain the β phase upon quenching from the β phase region without the precipitation of the secondary phases. The d-electron method predicted that only Ti-10.02wt% Mo and Ti-10.83wt% Mo will form secondary phases upon quenching.

LIST OF ABBREVIATIONS

OM -	Optical Microscope
SEM -	Scanning Electron Microscope
EBSD –	Electron Backscatter Diffraction
XRD -	X-ray Diffractometer
Hv-	Micro-Vickers Hardness
E-	Elastic Modulus
GPa-	Giga Pascals
β -	Beta
α -	Alpha
ω –	Omega
S.T –	Solution Treatment
AC –	As-cast
CT –	Compression Test
BS –	Bending Strength
IPF –	Inverse Pole Figures
UTS -	Ultimate tensile strength
Y.S -	Yield Strength
Ti -	Titanium
Mo -	Molybdenum
Nb -	Niobium
Sn -	Tin
Ta -	Tantalum
Cr -	Chromium
TEM -	Transmission Electron Microscope
Mo_{Eq} -	Molybdenum Equivalence
e/a ratio-	electron valence per atom
K_{β} -	The Co-efficient of beta stability
Ms -	Martensitic start temperature
M_f -	Martensitic finish temperature
SIM-	Stress Induced Martensitic
Bcc-	Body centred cubic

TABLE OF CONTENTS

LISTS OF FIGURES

LIST OF TABLES

PUBLISHED PAPERS

1. Nthabiseng Moshokoa, Lerato Raganya, Ronald Machaka, Babatunde Abiodun Obadele and Elizabeth Makhatha. (2020). Microstructural and mechanical properties of Ti-Mo alloys designed by the cluster plus glue atom model for biomedical applications. International Journal Advanced of Manufacturing Technology. https://doi.org/10.1007/s00170-020-06208-7.
2. Nthabiseng Abigail Moshokoa, Lerato Raganya, Babatunde Abiodun Obadele, Peter Olubambi and Ronald Machaka. (2020). The effect of solution treatment on the microstructure and mechanical properties of as-cast Ti-Mo alloys. 10.1016/j.matpr.05.784.
3. Lerato Raganya, Nthabiseng Abigail Moshokoa, Babatunde Abdiodun Obadele, Peter Olubambi and Ronald Machaka. (2020). Study of the microstructure and crystal orientation of as-cast Ti-10.2Mo-19.5Nb alloy. 10.1016/j.matpr.05.785.
4. Lerato Raganya, Nthabiseng Abigail Moshokoa, Babatunde Abdiodun Obadele, Peter Olubambi and Ronald Machaka. (2020). Investigation of the tensile properties of heat treated Ti-Mo alloys. 10.1016/j.matpr.05.782.
5. Moshokoa NA, Raganya LR, Obadele BA, Olubambi PA and Machaka R (2019). Effect of Mo content on the microstructural and mechanical properties of as-cast Ti-Mo alloys.IOP conf. Ser: Mater.Sci.Eng.655.012025.
6. Raganya LR, Moshokoa NA, Obadele BA, Olubambi PA and Machaka R (2019). The Microstructural and Mechanical Characterization of the β-type Ti-11.1 Mo-10.8 Nb alloy for biomedical application. IOP conf. Ser: Mater.Sci.Eng.655.012025.
7. Moshokoa NA, Mukhudwana TV, Raganya M L, Lekgoathi JL, Obadele BA and Olubambi PA. (2018). Spark plasma sintered Ti6Al4V-ZrO2 bio composites: Optimization of ball milling and turbula mixing of powders and their subsequent sintering parameters. IOPconf.Ser: Mater.Sci.Eng.430.012035.

CHAPTER 1: INTRODUCTION

1.0 BACKGROUND

Biomedical materials which are natural or artificial are used as structures and implants in human beings with the intention of replacing lost or diseased biological structures and refining the quality of life Long and Rack (1998) , Geetha *et al.*(2009) and Gepreel and Niinomi (2013). Navarro, Michiardi and Castan (2008) reported that the demand of artificial instruments made of biomedical materials to substitute dysfunctional hard tissues within the population of aged groups who suffers from diseases such as arthritis and joint pains has significantly increased. In biomedical application, an orthopaedic implant of different organs in the human body such as intravascular stents, heart valves, cardiac simulator and replacement implants in knees and knees hips are in need of replacement, Navarro, Michiardi and Castan (2008) and Zhang *et al*.(2011).

According to a report by Long and Rack (1998), orthopaedic implants utilized for hip and knee joints replacements have high pre-requisites because of challenges such as osteoarthritis (inflammation in the bone joints), osteoporosis (weakening of the bones) and trauma that can lead to pain or loss in function of the tissue. These challenges result in a gradual degradation in the mechanical properties of the bones because of loss of the function for the self-healing process. Orthopaedic implant failure can be caused by the following reasons: fragments generation, metal ions release and foreign body response in the human body, a difference of modulus between the bones and the implants or too low strength to maintain the load Gepreel and Niinomi (2013).

The design and development of orthopaedic materials must possess certain requirements in-order to avoid revision surgery. Amongst the requirements outstanding biocompatibility, low elastic modulus and high strength are one of them. Biocompatibility is the development of a dependable attachment connecting the implants and the adjacent bone without and over-riding fibrous tissue and infection Viceconti *et al.* (2000). The low elastic modulus close to the bone is required to avoid the stress shielding effect. The stress shielding effect explained by CA (1988) as the insufficient load transfer from the artificial implant to the close remodelling bone which lead to bone resorption and eventually loosening of the prosthetic devices.

Based by the above considerations, metals and alloys have been used as load bearing implants. To date chromium-based alloys, stainless steel, Ti and its alloys are mostly used for orthopaedic implants Navarro, Michiardi and Castan, (2008), Liu *et al.* (2015). Stainless steel and Co-Cr alloys suffers from two drawbacks such as Ni, Co and Cr elements that have been reported to be associated with diseases when discharged from the implant into the human body Long and Rack (1998). Okazaki and Gotoh (2005) reported that the release of Ni may results in a number of skin related diseases such as dermatitis; the presence of Co, carcinogenicity and neurological symptoms after years of implantation; and the release of Cr, negative effects on the kidneys, liver and blood cells via oxidation reactions Evans (1986). The last challenge associate together with stainless steel and Co-Cr based alloys is that they both illustrates a higher elastic modulus than that of the bone (210 GPa and 240 GPa respectively) that result in stress shielding effect and eventually implant failure Chen and Thouas (2015).

Titanium and its alloys have appeared as assuring metallic implant materials since the 20th era due to their distinctive properties such as low young‘s modulus, large ductility, high strength, good corrosion and wear resistance Niinomi and Nakai (2011), Marker *et al, (*2018) and Zhang *et al (*2018). Commercially pure titanium (CP-Ti) was initially used as a biomaterial for orthopaedic implant application because of their ability to promote rapid osteointegration Chen *et al* (2017). However CP-Ti suffers from low mechanical strength and low fatigue strength that excludes its use in load bearing applications Mitragotri, (2015). It was replaced by Ti6Al4V alloy because of its properties such as biocompatibility, improved strength and good corrosion resistance.

Ti6Al4V alloy is commonly used in the manufacturing of orthopaedic prosthesis such as knee joint and hip replacement because of its outstanding properties such as high specific strength, excellent corrosion resistance, low elastic modulus and superior biocompatibility as measured to those of stainless steel and Co-Cr metallic materials Sidambe (2014). However, the advantages of this alloy are not enough to avoid implant failure because Ti6Al4V suffers from two major drawbacks: Firstly, the release of Al and V ions from the parent material to the implant is reported to cause adverse health issues. Aluminium ions is reported to increase the capability for the development of Alzheimer’s disease during long term implantation Keda *et al.* (2002), whereas Vanadium ions are able to alter the kinetics of the enzymes activity associated with the

inflammatory response cells Yu *et al* (1993) , Okazaki (1996). The second drawback is that Ti6Al4V alloy exhibit a modulus (110GPa) higher than that of the human bone (10-40GPa). The mismatch in the elastic modulus results in a stress shielding effect. The transfer of mechanical stress through an interface from the implant to the adjacent bone to avoid implant failure is achieved by the stress shielding Sumner *et al* (1998).

Therefore, the development and design of beta type (β-type) Ti alloys having non-toxic and allergy free elements such as Mo, Nb, Ta, Zr and Sn have attracted and still attracting considerable attention especially for orthopaedic implants application due to the properties such as low elastic modulus and excellent biocompatibility. The work aims to design and develop a binary beta Ti alloy with a low elastic modulus close to the bone for biomedical application. This will be a preliminary study on the 1st step towards achieving a pathway to studying potential Ti-Mo alloys for orthopaedic implants. In this study, Ti will be micro-alloyed with Mo because it's a strong beta stabilizer Polmear (2006) , Lu *et al.*, (2013) and relatively cheaper than other β stabilizing elements. According to various studies available in literature, a comparatively lower content of 10 wt% Molybdenum is required to stabilize the β phase in binary alloys. Ho *et al* (1999) reported that at a composition of 10wt% Mo can be stabilized β phase, at least 35wt% Nb and 70 wt% are required to stabilize the β phase in binary Ti-Nb and Ti-Ta binary alloys, respectively Zhou and Niinomi, (2009) ,Yong *et al*, (2003) and Lee CM, Ju CP, (2002).

1.1 RESEARCH PROBLEM

Ti6Al4V alloy is a material of choice for manufacturing orthopaedic implants for biomedical applications because of its exceptional properties such as high density, low strength to ratio and lower elastic modulus as measured to stainless steel and Co-Cr alloys. However, its drawback such as the release of toxic ions such as Al and V from the implant into the body and its high modulus than that of the human bone motivate for the design and development of β –type Ti alloy that consist of non-toxic elements such as Nb, Mo, Ta, and Sn to replace the toxic elements and lower the elastic modulus in Ti6Al4V is of research interest. Up to date the lowest elastic modulus reported is about 78GPa in metastable Ti-15Mo binary alloys after annealing Niinomi, (1998).

Many aspects need to be taken into consideration while studying the design and development of low elastic modulus of β type Ti alloys for biomedical application. The reasons are motivated by the various parameters that affects the elastic modulus of β-Ti alloys such as the phase and microstructural features which are governed by the amount and type of alloying elements, lastly is the stability of the β phase and the processing route used. Therefore, the challenges that the research study might come across are: Firstly, to select an approach in designing the binary β-type Ti alloys with high stability and low elastic modulus that will provide physical background of the optimum choices of the compositions as there were principally formulated by the trial and error method. Secondly to control the enough composition of alloying element to be added to Ti that will be enough towards retaining the β phase and supressing the precipitation of the martensitic phases and omega phase. Thirdly is to control the phases evolution during casting and heat treatment.

1.2 AIM AND OBJECTIVES

This study is aimed at developing a β Ti-Mo type based alloy as a preliminary study towards achieving a pathway to studying potential Ti-Mo alloys with properties as close to those of the bone as possible to reduce the difference in elastic modulus (reduces stress shielding effect) between the human bone and implanted materials. The aim will be covered with the following objectives:

1. Design the composition using the cluster plus glue atom model
2. Establish the stability of the β phase in Ti-Mo alloys using β stabilizing prediction methods, such as the molybdenum equivalence, the electron valence per atom (e/a) ratio, the coefficient of β stability (K_β) method and the Bo and Md stability map.
3. Fabricate the designed alloys using Vacuum Arc re-melting process technique, solution treatment using a ceramic furnace and deform them using compression test.
4. Examine the effect of Mo on the microstructural evolution of as-cast and solution treated Ti-Mo alloys by using XRD, SEM, OM and EBSD.
5. Analyse the influence of microstructure towards the mechanical properties of as-cast and solution treated Ti-Mo alloys using a tensile test and bending Test.
6. Evaluate the microstructural evolution of Ti-Mo alloys after deformation using OM and EBSD.

1.3 JUSTIFICATION OF THE RESEARCH

Engh CA, (1988) and Sumner et al., (1998) defined the stress shielding phenomenon as the inadequate loading of bone due to large difference in the young's modulus between the bone and the implant devices in hip and knee joint prosthesis has raised serious concerns over the years because this phenomenon leads to bone resorption and eventually implant failure The rapid growth in the population of aged people and young people involved in accidents (traffic accidents or sports accidents) around the developing countries have led to an ever increasing need for materials required for biomedical applications. Nabeel *et al.*, (2012) reported that over 7 million Brane mark systems implants have been placed in human bodies and over a million spinal rod implantations have been completed in the year 1980-2000. It is not only replacement surgeries that have increased but also the revision surgeries in hip and knee implants. These revision surgeries cause pain for the patients and they require a lot of money. It's been reported by Implants, (2008) that the total number of surgeries is expected to increase by 137% and 607% by 2005 and 2030. The development of a low-cost implant material with low young's modulus is of urgency because its success will benefit the old aged population, all the young sports people and the biomedical manufacturing companies.

1.4 SCOPE OF THE STUDY

The primary focus of this research study will be based on the design and development of β type Ti alloy with an elastic modulus close to that of human bone (cortical bone) by studying the influence of solution treatment process on microstructural and mechanical properties of as-cast binary Ti-Mo alloy and to investigate the deformation mechanism on the solution treated Ti-Mo alloy after compression test. The compositions will be designed using the cluster plus glue atom model and this research study will only be focused on the four designed compositions: Ti-10.02wt% Mo, Ti-10.83wt% Mo, Ti-12.89wt% Mo and Ti-15.05wt% Mo. The reason we started at Ti-10.02wt% Mo alloy was motivated by the findings of Bania PJ 1990 where it was reported that a Moeq of 10wt% or more can stabilize the beta phase, the other (Ti-10.83wt%Mo and Ti-12.89wt%Mo composition were chosen because of the less work reported in literature regarding them and the Ti-15.05wt% Mo alloy was chosen in order

to compare with available literatures. The β predictions methods such as Mo equivalence, the e/a ratios found in literature were used to predict the stability of the β phase. Elemental powders of Mo and CP-Ti were the as-received powders. The powders will be manufactured using the commercially available arc-re-melting furnace into ingots. The ingots will be solution treated and quenched in icy water and their microstructural and mechanical properties will be studied. To investigate the deformation mechanism, compression test was conducted for all the solution treated alloys and their microstructural evolution were studied.

1.5 ETHICAL STATEMENT

There were no ethical issues associated with this research.

1.6 OUTLINE OF THE DISSERTATION

This dissertation is organised as follows:

Chapter 1 presents Background and introduction of the research study, the Aims and Objectives, Research problem and justification of research study. Chapter 2 gives brief literature review, which describe current knowledge of β-Ti alloys, Ti-Mo binary system and fabrication process. This is followed by literature on solution treatment and as-cast Ti-Mo alloys. In Chapter 3, detailed experimental methods, characterization techniques and the corresponding equipment used in this research study were stated. Chapter 4 introduce experimental results and discussion of the effect of microstructural and mechanical properties of Ti-Mo alloys in as-cast, solution treatment conditions and their deformation behaviour. Lastly, chapter 5 provided summary of the research study and provide recommendations relating to future work.

CHAPTER 2: LITERATURE REVIEW

2.0 Introduction

This chapter present literature review on the β Ti alloys as the 3rd class of Ti alloys. This chapter will focus on the binary β-Ti alloys that are being developed for biomedical application. The cluster plus glue atom model and the β stabilizing prediction methods will be discussed. The microstructural characteristics and phase formation after quenching from the β transus temperature will be considered and their effect on the mechanical properties especially the young's modulus will be discussed. The deformation behaviour of binary β Ti alloys will be discussed and the techniques used to determine the deformation behaviours will also be discussed in the form of experimental work reported by other authors.

2.1 Ti and its alloys

2.1.1 Effects of alloying Elements

Titanium is allotropic, under ambient pressure, pure titanium exists as either an α phase or the β phase depending on temperature. At temperatures above 882℃ known as the β transus temperature, α phase transforms into the β phase, below the β transus temperature the hexagonal close packed phase (hcp),α is stable Polmear (2006). The β transus temperature can be altered by alloying elements. Alloying elements in titanium alloys are classified as neutral, α stabilizers or β stabilizers. Alloying elements such as Al, Ga, B, La, C, O and N are classified as α stabilizers because they raise the β transus temperature as their concentrations increases. Alloying elements such as Zr and Sn behave neutral and they slightly decrease the β transus temperature. Key alloying elements that can affect the β phase are transition metals such as V, Mo, Nb, Ta, Cu, Ni, Fe, Co, Au and Pt and are classified as β stabilizers because of their ability to lower the β transus temperature (Gerd, 2003). Welsch, (1993), C, (2003) and Gerd, (2003). Figure 2. 1 below shows different alloying elements and how they affect the stability of the alpha (α) and β phase.

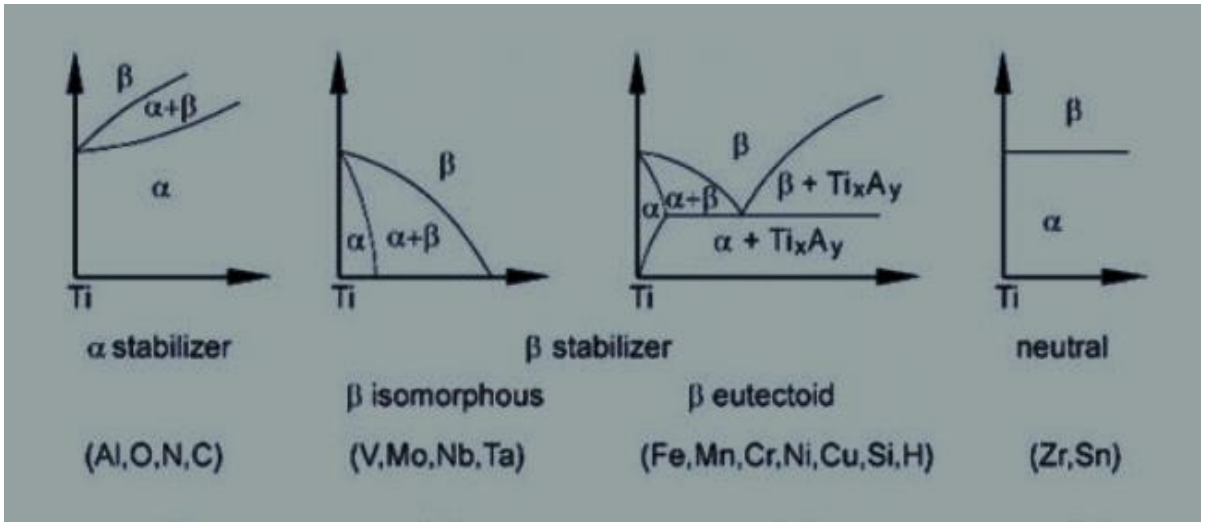

Figure 2. 1: Schematic drawings of the effect of alloying additions on equilibrium phase diagrams of Ti-alloys. (Gerd, 2003)

2.1.2 Classification of Ti and its alloys

Titanium is commonly characterize into four groups based on their phase content as α type alloys, near α type alloys, α+β type alloys and β type alloys Geetha *et al.*, (2009).The α type alloys consist of α phase only and an example of this type is CP-Ti alloys. The near α type alloys consist of α phase and small amount of β phase Sidambe, (2014). The α-type Ti alloys and the near α type Ti alloys have similar properties such as excellent corrosion resistance, good weldability and high creep resistance. However this type of alloys suffers from low strength at room temperature and they cannot be heat treated due to the hcp structure being stable Zheng (2013).

The α+β type alloys have a higher content of β stabilizers than near Ti alloys. They retain higher fraction of β phase about 5-30vol% Geetha *et al* (2009). They possess properties such as excellent fabricability, high strength at room temperature and moderate strength at high temperature. As compared to α type alloys, β type Ti alloys are heat-treatable and their properties can be optimized by heat treatment. Amongst the α+β type Ti alloys, Ti6Al4V is the most widely used for manufacturing of orthopaedic implants applications because of its biocompatibility and low strength however the elastic modulus and vanadium and aluminium ions released from the implant motivated for the development of β- type Ti alloys.

2.1.3 Metastable β-Ti alloys

Metastable beta type Ti alloys are defined as titanium alloys with enough concentration of β-stabilizer (such as Mo, Nb, and Ta), to retain 100% beta upon quenching above the β-transus temperature (882° C) to room temperature. This implies that there is enough beta stabilizing content to prevent passing through the martensite start (M_s) upon quenching, thus supressing the formation of martensitic phases Bania and Parris, (1990). β- type Ti alloys have attracted considerable attention especially in orthopaedic implant application because of their outstanding properties such as improved mechanical properties, low elastic modulus, good fatigue resistance, superior bio-corrosion resistance, no allergic challenges and excellent biocompatibility regardless of their high cost relative to other alloys Ankem and Greene, (1999), Abdel-hady, Hinoshita and Morinaga,(2006).

A schematic pseudo binary isomorphous diagram explained by Bennett (2018) is displayed in Figure 2. 2 below. The diagram shows the alpha α phase fields, the α+β phase field and the β phase field. The phase boundary drawn in bold are equilibrium boundaries and only drawn above the 200 °C temperature where diffusion is fast enough to reach equilibrium. The dotted line indicates the non-equilibrium martensite start temperature (M_s), the martensitic finish temperature (M_f), the variation in content between the athermal omega phase and isothermal omega phase. The hcp α′ martensite phase forms at lower concentrations of beta stabilizing elements, whereas the orthorhombic α" martensite phase forms at higher concentrations of these beta stabilizing elements upon quenching from above the β transus temperature. For example Davis, Flower and West, (1979) reported that in binary Ti-Mo alloys the HCP α′-martensite phase forms at Mo concentration between 1 and 4wt% and the orthorhombic martensite α"- phase occurs between the Mo concentration of 4 and 10wt%.

The metastable phase located between the β_c and β_s occurs when adding higher content of β stabilizer. The β_c is the minimum critical level of β stabilizer for metastable β alloy to retain β completely upon quenching above the β transus region and β_s is the minimum amount of β stabilizer to form a stable β alloy. The Metastable β alloys consist of the bcc β phase but can also contain small volume fraction of martensitic phases or the athermal omega phase depending on the composition and process technique Banerjee

and Williams,(2013). According to Davis *et al*, (1979), Bania and Parris, (1990), a Mo concentration of more than 10 wt%, the martensitic transformations are completely supressed upon quenching from above the T_β, forming only the metastable β phase. Enough beta stabilizing elements (above the β_s) leads to the formation of stable β phase.

The metastable athermal omega precipitates during rapid quenching from above the beta transus temperature in the absence of diffusion. He, (1973), Moffat and Larbalestier, (1988). The isothermal omega precipitates out by atomic diffusion during aging at temperatures below 500 ℃ Sukedai *et al* .(2011). The isothermal omega phase forms during aging in a temperature of 100-500 ℃ and higher alloying content. Isothermal omega phase is a continuation of the athermal omega phase because it depends on the holding time and the quenching rate, more especially, the volume fraction of isothermal omega increases with increasing holding time and decreasing quenching rate until precipitation reaches saturation Devaraj *et al.*(2012).

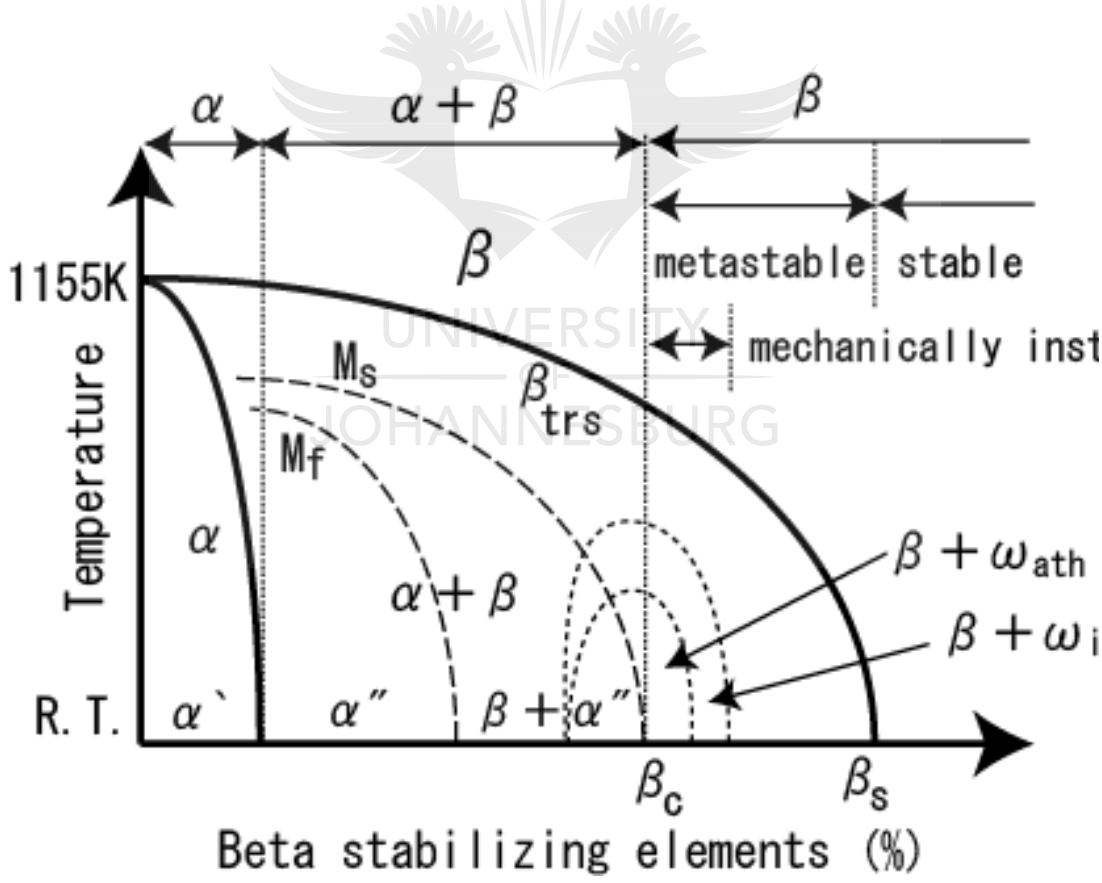

Figure 2. 2: A schematic diagram of binary isomorphous phase diagram. Bennett, (2018)

2.1.4 Types of beta type stabilizing element

According to Metallurgy and Technology, (2000), beta stabilizing elements in β titanium alloys are classified into two types: Isomorphous and eutectoid type as illustrated in table 2.1 below. Generally, isomorphous beta stabilizers have high β_c (β critical) values, they decompose to form α+β only without the formation of compound. The eutectoid beta stabilizers have lower β_c values and are more potent to suppressing the beta transus, they tend to form alpha + compound upon decomposition and they can be added elementally at relatively low cost.

Table 2. 1: list of frequently used beta stabilizers and their respective β_c value Metallurgy and Technology (2000).

β -Stabilizer	**Type**	**β_c (wt %)**
Molybdenum	Isomorphous	10.0
Niobium	Isomorphous	36.0
Tantalum	Isomorphous	50.0
Vanadium	Isomorphous	15.0
Tungsten	Isomorphous	25.0
Cobalt	Eutectoid	6.0
Copper	Eutectoid	13.0
Chromium	Eutectoid	8.0
Iron	Eutectoid	4.0
Manganese	Eutectoid	6.0
Nickel	Eutectoid	8.0

2.2 Phase Transformation in metastable β type Ti alloys.

In β Ti-alloys, the excellent mechanical properties possessed depends on the final microstructure evolution and formation of phases formed either during solution treatment or thermomechanical processing. Three different phase transformation found in in β Ti alloys phases can be classified into β, hexagonal α, martensitic hexagonal α' or orthorhombic α″ and ω (athermal or isothermal omega phase). The different phases and phase transformations will be discussed in this section.

2.2.1 The martensitic phase.

Martensitic transformation occurs by diffusion-less or shear (displacive) solid state motion. The transformation requires a cooperative movement of atoms, resulting in a microscopically homogeneous transformation of the bcc into the hcp crystal lattice. The driving force of this transformation is usually by mechanical deformation or by a change in temperature Av (2001), Gerd (2003). Two different crystal structures namely: the hexagonal martensite denoted as α' and the orthorhombic martensite denoted as α″ can occur when quenching of bcc β phase of pure Ti and dilute Ti alloys from above the transus temperature. The hexagonal martensite has the same crystal structure as the HCP α phase, but it differs in that it retains the β composition, Davis, *et al* (1979) .

Amongst the two-crystal structure, the alpha (α') is the most prevalent type because it can occur in two limiting morphologies such as massive or lath martensite (high purity Ti and very dilute alloys and acicular martensite in alloys with slightly solute content. The acicular martensite occurs as an intimate mixture of individual α plates each having a different variant of the Burgers relation. The orthorhombic martensite seems to occur mainly in Ti-alloys with β stabilizers of the transition metals such as Mo, Nb, Ta and W etc. The lattice parameters of α″ are strongly dependent on the solute content Gerd, (2003).

2.2.2 The omega phase

The omega phase (ω) is a metastable phase in Ti-based alloys with a hexagonal structure. The designed primitive metastable hexagonal crystal phase of omega (ω) accompany the matrix phase when the bcc lattice becomes unstable in some of the IV transition metals and alloys group Pd, (1954) and Sikka, (1982). Sikka, (1982) reported that it is generally accepted that the transformation mechanisms are the (111) collapse model which was developed by Fontaine *et al* (1970) to explain the dependency of temperature and composition on the diffuse ω reflection and reversible athermal formation. The model can be viewed as a collapse of (111) lattice planes of the bcc structure in a sequence shown in the Figure 2. 3.

The ω phase is an important feature in metastable β alloys. The formation of the ω phase can affect mechanical properties of β phase Ti alloys Banerjee, (2006). The size of ω phase is very small in metastable β Ti alloys, it is varied from less than 6 nm in the as-quenched condition to about 300 nm just before its transformation to α Sikka, (1982)

and American, Corporation and Oaks, (1969). Ho, *et al* (1999), Oliveira *et al.*, (2007) were not able to detect the omega phase using the XRD technique, however Sabeena *et al.*, (2013) reported the presence of the omega phase using the VLM XRD technique. It is generally, important to supress the deleterious and harmful precipitation of omega (ω) phase which increases strength and improves super-elastic property at the expense of the value of elastic modulus. The elastic modulus increased with increasing the volume fraction of the ω phase as the elastic modulus of the ω phase is higher than that of β and martensite phases Hao *et al*, (2006). Ho, (2008) studied the effect of omega phase on mechanical properties of Ti-Mo alloys for biomedical applications using the TEM technique. The presence of the omega phase was found in Ti-10Mo and Ti-20Mo alloys and it affected the mechanical properties negatively.

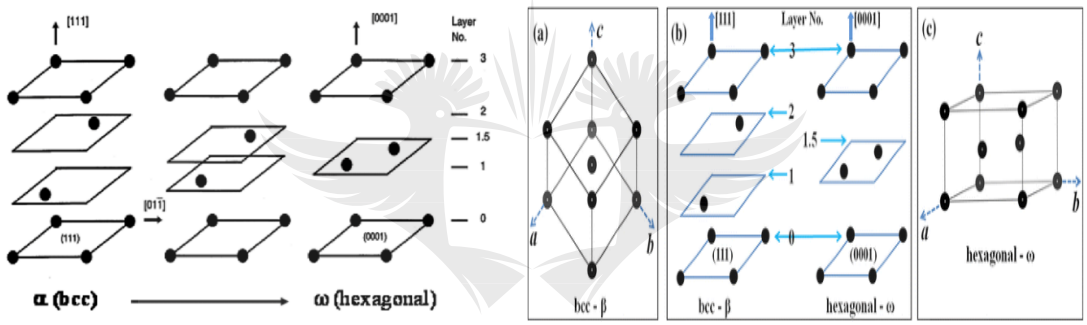

Figure 2. 3: Schematic illustration of ideal ω formation from bcc structure Sikka, (1982)

The effect of β stabilizing element (M) concentration on the microstructural evolution and elastic modulus of Ti-M binary alloys not designed by the cluster plus glue atom model and no prediction methods have been reported. For example, Ho et al 1999 investigated the structure and properties of a series of binary Ti-Mo alloys ranging from 6-20 wt% Mo in as-cast condition. The results show that 7.5 wt% Mo alloy consisted of orthorhombic martensitic α″ phase that show the lowest mechanical properties such as bending modulus, bending strength and micro-Vickers hardness because the α″ phase is an intermediate phase between bcc and hcp and its transition to orthorhombic requires small strain that are required to produce dislocated hexagonal structures Davis *et al* (1979).

When the Mo content increased to 10wt% the beta phase was stabilized. The mechanical properties of the alloys that displayed the β phase for example 10 and 20

wt% showed higher mechanical properties such as the bending modulus, bending strength and micro-Vickers hardness. The authors stated that the reasons for the increase in the mechanical properties may be due to the solid solution strengthening effect. Oliveira *et al.*, (2007) also studied the microstructural characterization of Ti-Mo alloys with various composition of Mo in as-cast condition (4, 6, 8, 10, 15 and 20 wt. %) using XRD technique. The XRD results showed that the mixture of hcp α′ and orthorhombic α" phase were remarked in Ti-4 wt% Mo, adding more Molybdenum content to 6 and 8wt% Mo, the only phase present was α" phase which was coherent with the results reported by Ho *et al* (1999).

According to the authors experimental s results the beta phase could not be retained at 10wt% Mo as reported by Bania and Parris, (1990), Ho *et al*, (1999) because of the presence of orthorhombic martensitic α″ peaks. The XRD results reported by the authors were not able to detect the omega phase due to its detection limit. Chen Yu-yong *et al* (2006) also investigated the microstructure and mechanical properties of a series of binary Ti-Mo alloys with Mo content from 5, 10, 15 and 20 wt% Mo in as-cast condition using optical microscopy, XRD, Vickers hardness and compression test. They found out that the XRD results were comparable to those reported by Oliveira and Guastaldi, (2008) with 10 wt% Mo and contradicting those reported by Bania and Parris, (1990), Ho *et al* (1999). The lowest elastic modulus and compressive strength they reported to be found in Ti-20 wt% Mo and the highest elastic modulus and compressive strength were found in Ti-5 wt% Mo alloy. They didn't report about the presence of omega phase.

The influence of heat treatment on binary Ti-Mo alloys on the microstructure and elastic modulus have been reported. For example, Cardoso *et al.*, (2014) also studied the impact of composition on the microstructure, Vickers hardness and elastic modulus in Ti-Mo alloys in solution treatment condition. The as-quenched results illustrated that when increasing the Mo content from 3 to 15w% Mo, the martensitic phase is supressed and the β phase is retained. The highest elastic modulus and hardness were reported in 9 wt% Mo alloy and the lowest were reported in 7.5 wt% Mo alloy. Aging of solution treated, and quenched samples showed the precipitation of the orthorhombic martensitic and HCP phase. The highest hardness after aging was attributed by the presence of the omega phase and all the composition showed that over-aging within

80h at various aging temperatures. Sabeena *et al.* (2013) studied different thermal transformation products of β phase in Ti-Mo system with 1,7,15 and 25 wt% Mo alloys using the XRD, SEM and hardness techniques. The alloys were homogenised and then quenched in water. The XRD results showed peaks of α′ phase at 1wt% Mo, at 7 wt% Mo there were only peaks of α″ phase, at 15 and 25 wt% Mo the alloy consisted of peaks of β phase only.

The micro-hardness increased when the Mo content increased until at 15 wt% Mo and then it increased at 25 wt% Mo. Davis *et al* (1979) studied the microstructure of martensite on a sequence of Ti-Mo alloys after solution treatment and water quenching of (2, 3, 4, 6, 8 and 10 wt% Mo) as a function of molybdenum content and crystal structure. The phases and microstructure they have analysed show that all the alloys in the range of 2-8 wt% Mo transformed to martensite upon quenching. According to the authors the Ti-2 wt% Mo alloy exhibited a coarse plate-type martensite consisting of large parallel sided key plates with partitioned regions filled with progressively smaller inferior plates and the other region were characterized of massive type martensite with lamellar colonies of parallel plates. The structure changed with increase in the molybdenum content, at Ti-10 wt% Mo the alloy consisted of untransformed equi-axed grains of β-phase.

Wang *et al.* (2016) also examined microstructural characteristics and mechanical properties of Ti-10, 15 and 20 wt% Mo alloys in solution treated condition. They used the XRD and OM techniques for microstructural characterization and tensile properties were studied for mechanical properties. Their XRD results showed that Ti-10 wt% Mo alloys exhibited peaks of α″ phase and β phase which were contradicting findings reported by Bania (1990), whereas Ti-15 and 20 wt% Mo alloys show only peaks of β phase. The optical micrographs result of Ti-10 wt% Mo exhibited fine acicular martensitic structure dispersed homogeneously over the big grain of the β matrix. The α″ plates were seen to be nucleating on the β grain boundaries and ending in the interior of β grains during quenching. Ti-15 and 20 wt% Mo alloys were characterised by equi-axed β grains with average grain size of about 500 μm indicating that no martensite plates were detected by optical microscope in this alloy. The elastic modulus of Ti-15 wt% Mo was higher than that of Ti-10 and 20 wt% Mo.

Tensile properties results showed a decrease in the yield strength and ultimate tensile strength from Ti-10 wt% Mo - Ti-15 wt% Mo, the two alloys exhibited large plastic strain because their elongation were higher (24% and 28% respectively). Ti-20 wt% Mo show higher yield stress and UTS but lower elongation. The fracture surfaces after tensile test were studied using the SEM technique and the results show that Ti-10, 15 and 20 wt% Mo contained dimples with various sizes indicating ductile fracture characteristics. Ti-10 and 15wt% Mo fracture were micro-void coalescence but Ti-15 wt% Mo exhibited bigger dimples in the fracture surface than in Ti-10 wt% Mo alloy and this illustrated that Ti-15wt% Mo was more ductile. Ti-20 wt% Mo exhibited equally ductile failure and brittle fracture due to large dimples and cleavage facets.

2.3 Alloy Design

In the past decade extensive research towards the development of binary Ti-Mo alloys witch have low elastic modulus were designed using trial and error method with no physical background and in addition to the trial and error method, there are several methods that were proposed in predicting the stability of the beta phase such as d-electron by Morinaga (2016), the Mo equivalent value method Gordin *et al.* (2004) ,the average electron concentration (e/a) predicted by Ikehata *et al*(2004) and the Beta stabilizing index calculated by Moiseev and Antipov, (1995). Recently Wang *et al.*, (2015) designed the cluster plus glue atom to attain the compositional method with the aim of achieving a low elastic beta-Ti solid solution alloys with higher structural stabilities.The design approaches are discussed in details as follows:

2.3.1 The Cluster plus Glue Atom Model

Cluster plus glue atom model according to Wang *et al.* (2013), was 1st proposed to explain the following: the composition of stated low elastic β-Ti alloys, to design and to analyse alloys of base centred cubic (bcc) structural stability.. Singh, (1994) reported that the maximum displacement that is between solute and the solvent atoms in the base centred cubic (BCC) solid solution alloys are anticipated to the strong chemical interaction that occurs in the first and second nearest neighbouring shell around the solute atoms. The solute centred CN14 rhombic dodecahedron polyhedron represented in Figure 2. 4 consist of 8 solvent atoms of the 1st neighbour shells (red atoms) and 6 solute atoms of the 2nd neighbour shell (blue atoms). This was chosen as the cluster in

the cluster plus glue atom model for BCC structure , Hao and Wu (2011). The composition formula is demonstrated in equation 2.1

$$[(\text{Centre})\text{-}(\text{Shell})_{14}]\ (\text{Glue})_{1\text{ or }3} \qquad \textit{equation 2.1}$$

The component elements in this model are arranged in a way that they correspond to the enthalpies of mixing (ΔH) with the base Ti. According to equation 2.1, the centre is the strongly bonded part and is centred by an element like Mo, Sn which have a negative enthalpy of mixing with the base Ti, the shell atom is the base element like Ti then the glue atom site is relatively bonded to the cluster- shell atom which are preferentially comprised of elements such as Nb which have a positive enthalpy of mixing with the base element Ti. Zhou, (2000) stated that in a binary Ti-Mo system, Ti-11Mo alloy with lower limit for β stabilization is expressed with a cluster formula of $[(\text{Mo-Ti}_{14})]$ Ti. The monotectoid point of $Ti_{88}Mo_{12}$, where β-Ti solid solution was the most stable as interpreted by 1:1 cluster model type $[MoTi_{14}]\ Mo_1$, by substituting the glue atom side by a more weakly bonded Ti atom, results in $[MoTi_{14}]Ti_1$ which is less stable but with lower E value, Zhou, (2000).

Wang *et al.* (2015) investigated the microstructure and the stability origins of the low elastic modulus in the $[(\text{Mo, Sn})\text{-}(\text{Ti-Zr})_{14}]$-Nb alloy series to reveal the relationship between the low E property and the β structural stability. Their experimental results revealed that the lowest elastic modulus of 48 GPa was found when the cluster formula was $[(Mo_{0.5}, Sn_{0.5})\text{-}\ (Ti_{13}Zr_1)]\ Nb_1$, with a microstructure composed of the omega, orthorhombic martensitic and beta phase. The studies reported by Wang *et al.*, (2013) and (2015) on the cluster plus glue atom model of two Ti-Mo binary alloys, most ternaries and quaternaries Ti-Mo based alloys have motivated the design of a range of compositions of Ti-Mo binary alloys using the cluster plus glue atom model to assess their relationship between low E and microstructure for biomedical application since there are less reported work on Ti-Mo binaries designed by the cluster plus glue atom model.

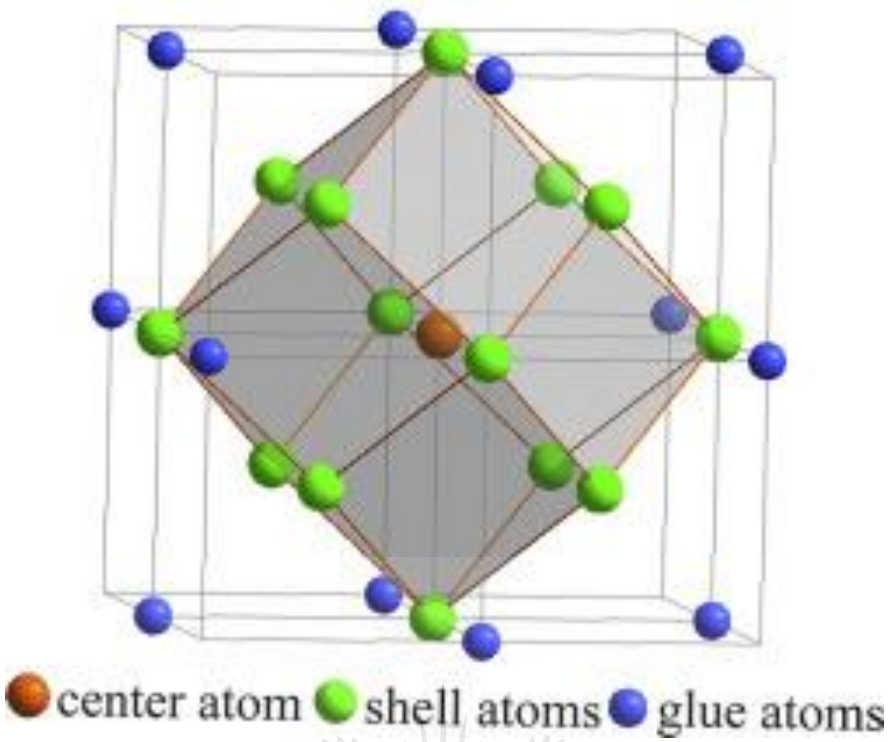

Figure 2. 4: The CN14 rhombic dodecahedron polyhedron as the cluster in BCC structure.

2.3.2 The Molybdenum Equivalence

Generally β titanium alloys is categorized as titanium alloys that contain a β parent phase stabilised to room temperature and that exhibits excellent strength, however additional sub-classifications can be made depending on the formation of non-equilibrium phase which compete with the equilibrium phases following the addition of β stabilizers. The stability of the β phase in titanium alloys depend on the addition of different content of transition metals. The most popular parameter to determine the stability of beta is the Molybdenum equivalence in wt% (Mo_{eq}). The Mo_{eq} is defined by G, (1993) as the number of beta phase stabilizing elements, alpha phase stabilizing elements and neutral elements required to retain 100% of the β phase after quenching from above the β transus temperature to room temperature. The Mo_{eq} utilize Mo as an arbitrarily chosen baseline and normalizes other elements to an equivalent Mo value. The equation is given by Bania (1990) as:

$$(Mo_{eq})_B = 1.0\,Mo + 0.67\,V + 0.44\,W + 0.28\,Nb + 0.22\,Ta + 2.9\,Fe + 1.6\,Cr + 0.77\,Cu + 1.11\,Ni + 1.43\,Co + 1.54\,Mn - 1.0\,Al. \quad \textit{equation 2.2}$$

According to equation 2.2, the constant before each alloying element concentration occur as the ratio of the critical concentration of Mo to retain 100% of the metastable bcc β phase after quenching from above the transus temperature to room temperature and prevent the formation of the martensitic phases. Bania, (1994) reported that a Mo_{eq} value of 10.0 wt% in Ti-Mo alloys will be sufficient to stabilize the β phase during quenching and the T_β tends to decrease with increasing the Mo_{eq}**.** A higher value of Mo_{eq} indicates a heavily stabilized alloy. Aluminium remain subtracted because it is an alpha (α) phase stabilizing element. In their studied Wang *et al.*,(2015) calculated a Mo_{eq} of 11.8 for a binary $Ti_{88.21}Mo_{11.79}$ and the elastic modulus after casing was reported to be 116 GPa.

2.3.3 The d-electron Design Method

The d-electron alloy design method proposed by Kuroda *et al.*, (1998) was experimentally confirmed to give guidelines on the selection of alloying elements, to forecast the phase stability of alloys, their properties and predicting the plastic deformation mechanism of β Ti alloys Brozek *et al.* (2016). In these method electronic structures for BCC alloys are calculated and two parameters are identified theoretically: Bo which is the bond energy that measures the covalent bond strengths between Ti and an alloying element, the 2nd one is the d-orbital energy level (Md) which relates with the electronegativity and the metallic radius of elements. The prediction method is clarified in detail in section 2.4.1 under deformation mechanism. The average electronic parameters given as Bo and Md are defined by equation 2.3

$$Md=\Sigma x_i\,(Md)_i \text{ and } Bo=\Sigma x_i\,(Bo)_i \qquad \textit{equation 2.3}$$

2.3.4 The Beta Stabilizing Index

The beta stabilizing index (K_β) remains yet another approach used to determine the stability β in Ti alloys. The beta stabilizing index is given in equation 2.4, Where C_i – is the composition of β stabilizing element and β_{Ci} – is the critical beta concentration or the concentration at which β phase is expected to be stable Moiseev and Antipov, (1995). If the K_β is in the range of 1-1.5 ($1 < K_\beta < 1.5$) then the β phase in the alloy was found to be metastable, beyond this value the β phase found to be stable.

$$K_\beta=C_i/\beta_{Ci} \qquad \textit{equation 2.4}$$

2.3.5 The e/a ratio.

The e/a ratio is used to predict the formation of athermal omega phase in Ti alloys Ikehata *et al.* (2004) and the ratio is the average number of valence electron in each atom of Ti-Mo binary alloys According Ikehata *et al.* (2004) the formation of athermal omega phase is at its maximum e/a ratio of 4.13 and minimum at 4.30, above this minimum point (4.30) the β phase becomes the dominant phase. Laheurte *et al.* (2010) reported on the as-quenched microstructures as a function of e/a values of multi-component alloys. Their e/a ratio was ranging from 4.0 – 5.0 as shown in the diagram in Figure 2. 5. According to the diagram the stability of a fully β phase in titanium alloys have been calculated to be between the e/a ratio of 4.20 and 5.0. The equation is given as:

e/a ratio = $(v_1m_1 + v_1m_2 + v_3m_3 + v_nm_n)$ /100 *equation 2.5*

where V_n is the total number of valence electron in the valence shell of the n^{th} element and m_n is the atomic percentage of the n^{th} element.

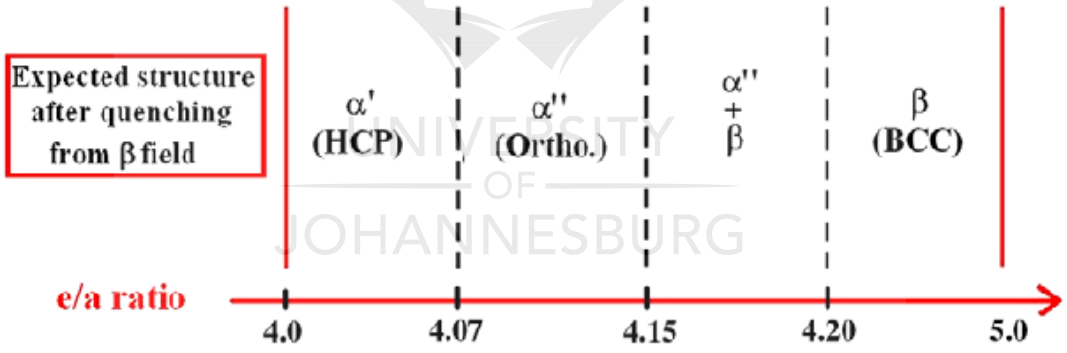

Figure 2. 5 : Expected Ti-Mo alloys structure after quenching with regard to the electron to atom ratio scale (e/a ratio) (Laheurte *et al.*(2010).

2.4 Deformation mechanisms in metastable β-Ti alloys

Deformation mechanism that includes the following: hexagonal close packed (hcp) α' martensite phase, the orthorhombic α″ martensite phase, the hcp ω phase and twinning, transpires by conventional viscous slip and stress-induced transformations. Metastability of beta (β) phase throughout tensile, compressive or creep loading process allows stress-induced transformations to occur which can significantly influences the

mechanical response Kolli (2018). The occurrence of stress induced mechanism which depends on the β phase stability can influence the mechanical response of a material. The deformation mechanism of metastable β Ti alloys generally include dislocation slip, mechanical twinning and stress-induced phase transformation Banerjee and Williams, (2013). The movement of various deformation mechanisms are quantified by Mo_{eq} as a function of β-phase stability and microstructure for example the metastable phase present after heat treatment, Hanada (1987), Ankem (1999), Grosdidier *et al* (2000) and Bhattacharjee (2005).

According to Kim, (2006), deformation that occur via stress-induced α″ martensite has grown much attention in the biomedical and micromechanics application because of its properties that result in shape memory effect and pseudo-elastic or super-elastic behaviour. However, the formation of martensite during deformation may include deleterious effect for structural application by promoting significant stress inhomogeneity in the microstructure and lower ductility when compared with other alloys deforming only by slip Karase *et al.*(2003). Instead, it may nucleate at pre-existing α″-phase in the microstructure that formed during heat treatment. The phase nucleates at relatively small strains in order to accommodate deformation and the formation of the α″-phase that is responsible for a lower yield stress but higher work hardening rates at some β phase Ti alloys Grosdidier *et al.*(2000), for example when the β phase stability increase the yield stress increase and the bulk of the α″- phase decrease in Ti-Nb-Sn alloys Ankem (2010).

Deformation by stress-induced HCP ω phase and twinning has grown significance in application where reliability is vital because of its ability to affect the mechanical properties such as the yield stress, ductility and strain hardening of β phase Ti alloys. During tensile deformation, metastable β phase Ti alloys with high Mo_{eq} values have shown the ability to supress the development of the martensite phases and exhibit a range of stress induced transformation and mechanical properties. In general, Ti alloys containing sufficient β-phase stability to prevent martensite formation often deforms by a combination of stress induced {332} <113> twinning and hcp ω phase formation with the ω phase predominantly nucleating inside the deformation twins Hanada and Izumi (1986), Zhang *et al.*(2005). A significant increase in the β-phase stability supresses the formation of the ω phase leaving {332} <113> twinning as the dominant stress induced

transformation during deformation. Whereas slip dominates in alloys with even higher Mo_{eq} values.

A β-Ti alloy after heat treatment with a microstructure that consist of phases such as metastable martensite phases or the hcp ω phase will serve as nucleation sites for stress-induced transformation during deformation. Depending on the alloying composition and the β-phase stability, a mixture of more than one stress-induced deformation mechanism and slip may also occur. In general, as the value of Mo_{eq} increases, the stress-induced deformation mechanism follow the sequence α' → α″ → ω + twinning → twinning → twinning + slip → slip, overlap in the mechanism activity attributed by microstructural features such as grain size or the presence of metastable phases may promote or suppress a particular mechanism (Kolli (2018). The existence of different stress-induced transformation during deformation can be described by the phase-stability diagram based on the d-orbital energy level Md and the mean bond order Bo (Kuroda *et al.*(1998).

2.4.1 The d-electron alloy design method

Morinaga and Yukawa (1997) proposed a semi-empirical integrative method in the 1990s called the d-electron method. Extensive experiments confirmed that this method can be utilised as guidance in selection of adapted contents of specific alloying elements, it can predict the stability of phases and alloy properties as well Morinaga M (1985). Electronic structures for various elements can be calculated for BCC Ti alloys and two alloying parameters can be determined theoretically by employing the molecular orbital method. One of the parameters is the bond order (Bo) which is a measure of covalent bond strength between Ti and an alloying element. The second one is the mean d-orbital energy level (Md), which correlates with the electronegativity and the metallic radius elements. For Titanium alloys, the average values of Bo and Md are defined by taking the compositional averages of the parameters and denotes them as $\bar{B}o$ and $\bar{M}d$. Electronic parameters Bo and $\bar{M}d$ are calculated from the following expression:

$$\bar{M}d = \Sigma X_i (Md)_i \text{ and } \bar{B}o = \Sigma X_i (Bo)_I \qquad \textit{equation 2.6}$$

where X_i is the molar fraction of the i elements and $(Md)_i$ and $(Bo)_i$ is the numerical values of Md and Bo for each alloying element.

The d-electron design method results in a semi-empiric stability map called the Bo and Md map. This method is used to develop high temperature α-type alloys Morinaga M, Yukawa N, Maya T (1988), high strength β-type alloy, high corrosion resistant alloys, and β type Ti alloys for bio-implant application Kuroda *et al.*, (1998).

The general Bo and Md map is shown/ illustrated in Figure 2. 6. Morinaga (2016) proposed that the lower part of Bo and Md map is where the Bo value is less than 2.84 and the part where the Bo value is between 2.84 and 2.96 (eV) was extended by Abdel-Hady, Hinoshita and Morinaga, (2006). The alloy position varies as the alloy composition changes with the average composition of Bo and Md parameters. The stability of the β phase increase with increasing content of the β-stabilizing elements in different Ti-M binary alloys (M=V, Cr, Mo, Nb and Ta) , Abdel-Hady, Hinoshita and Morinaga, (2006). Different zones of deformation modes can be drawn on the map when the β phase's chemical stability decrease and the main deformation evolves from dislocation slips to mechanical twining then to stress induced martensitic transformation .The boundaries such as slip/twin, Ms=RT (room temperature) and Mf=RT are plotted on the map and can be regarded as important reference in designing new β Ti-alloys due to their indication to predict mechanical stability in metastable β phase. The map can also be used to predict as-quenched properties of Ti-alloys and it can be used to select compositional ranges where the 3 deformation mechanisms (dislocation slip, mechanical twinning and stress-induced martensitic transformation) are competitive in β phase alloys.

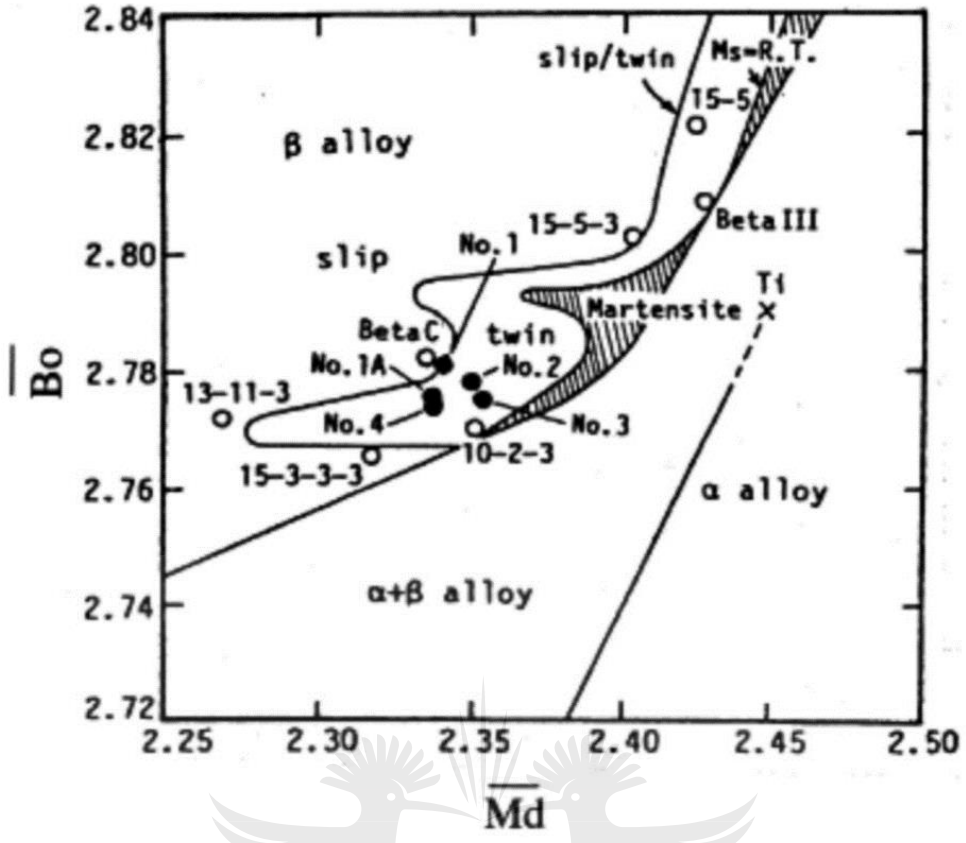

Figure 2. 6: A typical Bo and M̄d stability phase maps Kuroda *et al.*(1998).

2.4.2 Literature study on deformation mechanism of Ti-Based alloys.

This section is based on papers published by other authors who used the Bo and Md map found in literature to predict the deformation mechanism in beta Ti alloys. The aim of this study is to show that there is currently less published work on the deformation mechanism of binary Ti-Mo alloys after compression using the Bo and Md map. The gap have motivated for the study on the deformation mechanism of binary Ti-Mo alloys designed by the cluster plus glue atom model and other prediction tools.

Kuroda *et al.* (1998) investigated new β type titanium alloys composed of non-toxic elements designed using a new alloy design method based on the molecular orbital of electronic structures proposed by Morinaga and Yukawa (1997). The designed alloys were homogenised at 1273K for 21.6 Ks and they were cold rolled to 75% reduction after homogenization the alloys were then solution at 1117K for 1.8 Ks and then aged at different temperatures 673, 723 and 773 K for 10.8 Ks. Their microstructural results showed that the average β grain size of Ti-29Nb-13Ta-4.6Zr was approximately 23μm,

Ti-16Nb-13Ta-4Mo alloy was approximately 30μm and the average grain size of Ti-29Nb-13Ta-2Sn was approximately 28 μm. The mechanical properties illustrated that the solutionized designed alloy has lower strength and equivalent or greater elongation when compared with these of conventional titanium alloys such as Ti6Al4V. The tensile strength of Ti-29Nb-13Ta-4Mo after aging at 673 K was found to be more brittle. The moduli of elasticity of as-solutionized and aged designed alloys were lower compared with those conventional titanium alloys for medical implants.

Buzatu *et al.*, (2019) investigated the influence of the bond order, energy level of metal d-orbital, ratio of valence electrons/atom and influence of the addition of W. The alloying element was made with intent of obtaining a high strength and corrosion resistance. They started with the additions of Ti-15Mo up to 11 wt. % W. They discovered that a non-uniform dendrite structure of the as-cast alloy was observable, and the EDS showed a uniformly distribution of elements in the alloy. The Vickers micro-hardness measured ranged between 300-350 HV and the elastic modulus of the deformed material was low (29.5GPa) with no visibility of cracks after compression. The addition of W into Ti-15Mo alloy decreased the Md insignificantly but increased the Bo. They discovered that based on the $\bar{B}o$ and $\bar{M}d$ map (in Figure 1) the Ti-15Mo alloy is allocated in the β phase region and the addition of W lead to better positioned the alloy in β phase region. The stability of Ti-15Mo can be increased by increasing the Bo value and decreasing the Md value. The addition of W in Ti-15Mo leads to an increase in the e/a ratio and the Mo_{eq}.

Sadeghpour *et al.*(2018) evaluated the consistency of the d-electron method in predicting the deformation mechanisms of the complex multi-element β Ti alloys. They introduced a new composition to the existing Ti-5553 alloy that has the same composition but different predicted β phase stabilities to investigate and compare the deformation mechanisms and mechanical properties. The initial composition was Ti5Al-5Mo-5v-3Cr and the d-electron method was used to design three new compositions; Ti-4Al-7Mo-7V-3Cr (Ti-4733), Ti-3Al-5Mo-7V-3Cr (Ti-3573) and Ti-3Al-8Mo-7V-3Cr (Ti-3873) alloys.

The ingots of the mentioned alloys were melted using vacuum arc melting, homogenized and hot forged for 4h at 1000℃, they were then rolled at 750℃ and they were solution treated at 1000℃ for 30min and quenched in water. The deformation

behaviour was characterized using uniaxial compression at room temperature. For microstructural characterizations the specimen was evaluated using different techniques such as XRD, OM, TEM and EBSD. According to the Bo and Md map the 3 designed alloys: Ti-4733, Ti-3573 and Ti-3873 were situated in martensite borders, martensite plus twin border and twin plus slip border respectively, this implied that the alloys deformation mechanism were stress induced martensite (SIM) transformation, SIM plus twinning mechanism and twinning plus slip deformation respectively. The compressive results showed that the yield strength of the designed alloys were found to be higher than the reference alloys and those reported by Nyakana *et al.*(2005) and Ren *et al.*(2013).

The XRD pattern of the initial microstructure of the Ti-5553 and Ti-3573 alloys after solution treatment displayed athermal omega phase peaks in addition to the β matrix. The EBSD maps microstructure of the solution treated alloys displayed equi-axed phase β grains with an average diameter that was between 150-250 μm without any evidence of martensitic α″ phase in the matrix. They concluded that these results agreed with the predictions made by the d-electron method for two alloys: Ti3573 and Ti3873 but were in contradiction with Ti4733 and Ti-5553.

The SAED (selected area electron diffraction) pattern was taken to confirm the presence of the omega phase as seen in the XRD. The SAED pattern of Ti-3573 alloy indexed as [110] zone axis shows additional spots at 1/3[112] and 2/3[112] positions of the β reflections which represented the athermal omega phase and this was found in Ti-5553 alloy. The deformation mechanism of the compressed alloys was studied by various techniques. Interrupted compression test at a strain up to 10% was performed on the studied alloys. The microstructures analysed using optical microscope showed 3 types of deformation: a group of thin parallel plates, wide bands and polyline or wavy thin lines.

Alloy Ti-5553 and Ti-4733 possessed the thin parallel plates and wavy lines deformation whereas the Ti-3873 alloys illustrated the wavy lines type deformation only. The thin lines were related to stress induced martensitic transformation whereas the wavy lines were related to deformation by slip. The XRD patterns of the compressed alloys displayed that Ti-5553 and Ti-4733 alloys displayed both α″ peaks and β peaks

and Ti-3573 displayed week α″ phase peaks and β phase, these alloys underwent SIM transformation and slip during deformation.

The EBSD inverse pole Figures maps of the deformed samples didn't show the presence of any twins, but few α″ martensite bands were visible inside the grains in alloy Ti-5553 and Ti-4733. The image quality maps of Ti-5553 and Ti-4733 alloys identified a deformation mechanism by slip and SIM transformation only. The Ti-3873 alloy showed wide deformation bands and they were indexed as mechanical twin that was visible in one of the grains in the IPF maps.

Laheurte *et al.* (2010) investigated and compared mechanical properties such as elastic modulus, yield strength and stress induced martensitic transformation ability. The results were discussed in relation to their respective position in the Bo and Md electronic diagram. The new formulated alloys from the reference Ti-29Nb-13Ta-4.6Zr as follows: Ti-29Nb-11Ta-5Zr (TN11TZ) and Ti-29Nb-6Ta-5Zr (TN6TZ) were fabricated by a cold crucible levitation melting technique, they were then homogenised at 1223 K for 12 h under inert argon atmosphere and they were cold rolled with controlled reduction in thickness of 1.90. The alloys were solution treated at a temperature of 1173 K for 2h and quenched in ice water. The alloys were characterised using different techniques such as XRD, OM, TEM and a tensile test was performed. The three alloys show a decrease with the d-electron parameters (average Bo and Md) when the Ta content was decreasing.

The e/a ratio was used to predict the stability of the β phase, and the stability limit was calculated to be around 4.20. The stability limit was reasonably connected with the results of the three alloys as they possessed an e/a ratio values between 4.21 and 4.25, form those values the authors made predictions that the TN6TZ system will present a martensitic start temperature very close to room temperature with low mechanical stability of β phase upon deformation. The optical micrographs results displayed equi-axed grains with an average diameter of approximately 50 μm. Only β grains were visible on these micrographs with no evidence of α″ precipitation in the beta matrix. Also, the absence of the α″ phase was detected by the X-ray diffraction profile in TN6TZ and TN11TZ alloys, this implied that the Ms Temperature was below room temperature. They reported that the possible precipitation of nano-sized omega phase

could not be detected using the optical microscope technique due to its small particle size.

Their experimental results were in agreement with those reported by Niinomi (2008) on the TN13TZ system. The solution treated TN6TZ alloy was cold rolled with a very high rolling rate of 160% were analysed for microstructural characteristics using TEM, the results show that the alloy was perturbed with very high density of dislocation and high-volume fraction of stress induced α″.

Marteleur *et al.*(2012) reported on the development of alloy design procedure for super-elastic properties of Ti alloys that can be extended to their plastic properties. The study confirms the activation of several deformation mechanisms and a large work hardening rate. The binary Ti-12wt% Mo alloy was proposed for this study, it was designed using the d-orbital map and according to the map, the alloy was predicted to have the twinning +SIM and twinning deformation mechanism. It was processed by cold crucible levitation melting, they were cold rolled, recrystallized and water quenched. The alloy was characterised using the EBSD, TEM, XRD techniques etc.

The EBS maps results show that at a tensile strain of0.05 the alloy was accommodated by a combination of several deformation mechanisms. Mechanical twinning was activated at a strain of 0.05, the twining system were indexed as {332} <113> twins in bcc β phase. There were observations of bands which were identified as mechanically induced α″ that occurred at nano scale showing that the strain was accommodated at different microstructural scales. Besides the mechanical twining, features of the deformed microstructure were indexed as hexagonal close packed α' phase which was confirmed by the XRD but not anticipated to be found within this alloy.

This study thus highlights the fact that the enhanced mechanical behaviour of the Ti-12wt% Mo alloy relies on a complex combination of several deformations such as: stress induced martensitic transformation and intense mechanical twinning associated with the formation of ω phase.

Min *et al.*(2014) investigated the evolution of {332} <113> twining structures at various tensile strains in a Ti-15Mo alloy by optical microscope combined with EBSD analysis to examine the correlation between twinning structure and straining behaviour. The alloy was prepared by cold crucible levitation melting, hot forged, hot rolled and

then homogenized followed by air cooling. The EBSD inverse pole Figure maps of deformation microstructures displayed plate-like features apparent within the grains identified as {332}{113} twins. The twins became denser and thicker with increasing strain, with the colour contrast from the matrix becoming more pronounced within grains at a greater strain of 0.17. The average area fraction of twins as measured by OM rapidly increased to 40% at a strain of 0.05 and it gradually increased to 52% at a strain of 0.12.

Min *et al.*(2012) investigated the effect of elemental distribution on the deformation modes further, namely the dislocation slip and the {332} <113> twinning and on the tensile properties in a Ti-15Mo-5Zr alloy and to discuss the possibility of improvement in the tensile properties by controlling the deformation microstructure. The alloys were fabricated using a cold crucible furnace, the as-cast alloys were heat treated at 1273K for 3.6Ks, they then hot forged at the same temperature into block of various sizes and it was hot rolled into a plate at 1173 K followed by air cooling. The plate was cut into different sizes and they were solution treated at 1173 K for 3.6Ks and then water quenched. The alloys were characterized for microstructural analysis using different techniques such as XRD, OM and EBSD. The mechanical properties were tested using a tensile test.

The OM results show the cold rolled and solution treated alloys were composed of a series of bands with higher density that were parallel to the rolling direction, while the Hot rolled and solution treated alloy had no band. The alloys composed of a β phase in all the sample with no significant difference in the grain size. The XRD profile indicated diffraction peaks for the athermal ω phase. The cold rolled and solution treated samples show a high yield strength and significant uniform elongation whereas the hot rolled and solution treated samples were composed of the highest yield strength with an elongation of 12%. The optical micrographs of the deformed alloys that were solution treated showed plate-like features with {332} <113> twins. The fracture cold rolled, and solution treated alloys were composed of the same features, but the twins were heavily deformed and some of them were lenticular in shape, this means the sample deformed by dislocation slip and twinning.

CHAPTER 3: EXPERIMENTAL METHODS

3. Introduction

In this chapter, the author introduces the experimental procedure and software used for designing, casting, heat treatment and characterization of the designed alloys. The research experiment consists of two materials or system, commercially pure titanium (CP-Ti) and Molybdenum (Mo). Alloy compositions were designed using cluster plus glue atom model. An Arc melting furnace was used for fabricating the alloys, solution treatment was carried out on the as-cast alloys and the solution treated alloys were compressed to further study the deformation mechanism. Different characterization techniques were utilized to investigate the microstructural properties and the mechanical properties. The whole process is summarised in the flow diagram in Figure 3.1.

The cluster formula, the nominal composition, calculated values of Moeq, e/a ratio, Kβ stabilizing index, the Bo and Md values of the designed alloys are listed in Table 3.1, their formulas and equations are explained in the literature review in Chapter 2, section 2.2. As illustrated in Table 3.1, the beta stabilizing prediction methods such as Moeq of the designed alloys range between 10.02wt% (a minimum composition reported by Bania PJ) and 15.05wt%, the K_β stability index of the designed alloys were in the range of 1.0-1.51 and the e/a ratio was in the range between 4.20-4.30. These methods predicted that all the designed alloys will retain the β phase and supress the formation of secondary phases of martensitic and omega upon quenching from the β field.

The average Bo and Md stability map in Figure 3.2 were used to predict the stability of the phases and the deformation behaviour. According to the stability map, the Ti-10.02wt% Mo is situated at the omega region and on the martensitic start boundary, this designed alloy is predicted to form +β α″+ω phase, the Ti-10.83wt% Mo was situated between the omega and β boundary and it was predicted to form β+ω upon quenching, the Ti-12.89wt% Mo and Ti-15.05wt% Mo alloys were located within the β site which indicated that they will form the β phase only upon quenching.

The stability map was also used to predict the deformation mechanism of alloys. The Ti-10.02wt% Mo alloy located between the martensitic boundary line and the twin

region. This alloy was predicted to deform by stress induced martensitic and by twinning. The Ti-10.83wt% Mo alloy is situated between the slip and twin region, implying that the alloy was predicted to deform by slip and twinning. The Ti-12.89wt% Mo and Ti-15.05wt% Mo are situated at the slip region predicting that these alloys will only deform by slip only.

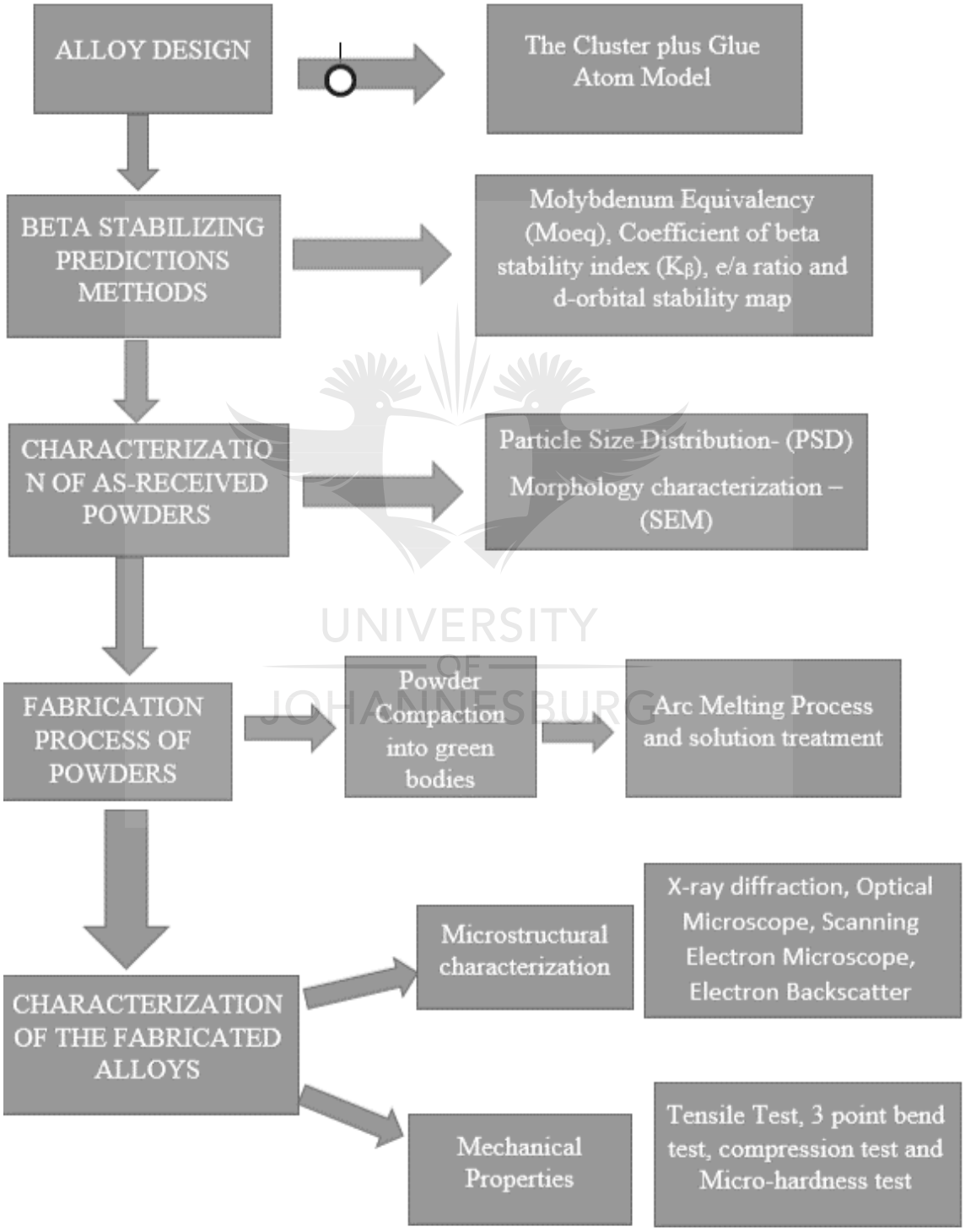

Figure 3.1: Flow Diagram of the experimental procedure.

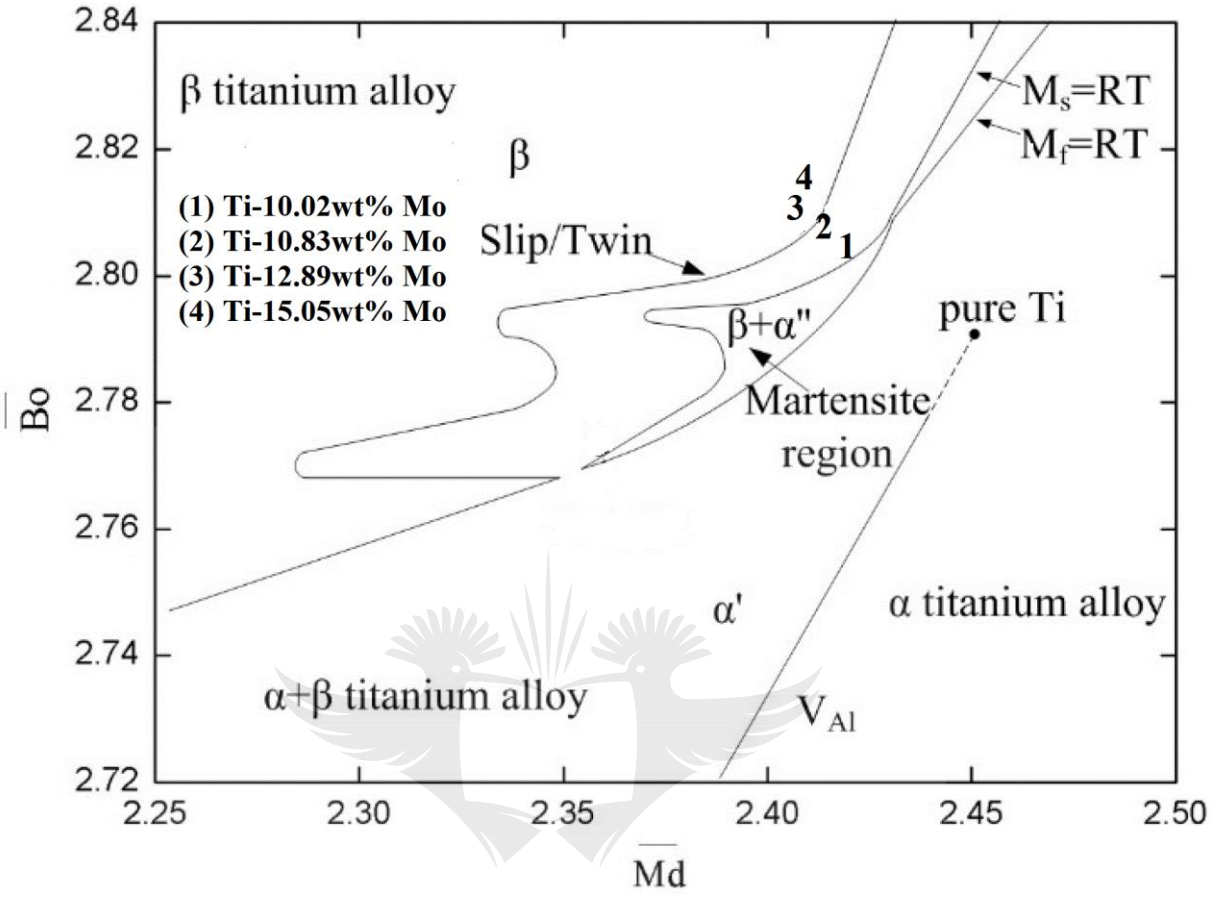

Figure 3. 2: The Bo and Md stability phase map showing the positions of the designed alloys. (Kuroda *et al.*(1998).

Table 3. 1: Cluster Formula**,** Nominal Compositions and calculated values of Mo_{eq}, e/a ratio, Kβ and the average Bo and Md.

Cluster Formula	Composition [wt.%]	Mo_{eq} (wt. %)	e/a ratio	K_β stabilizing index	Bo	Md
$[(Mo)\text{-}(Ti)_{14}]\ Ti_4$	Ti-10.02 Mo	10.02	4.20	1.00	2.804	2.4215
$[(Mo)\text{-}(Ti)_{14}]\ Ti_{2.5}$	Ti-10.83 Mo	10.83	4.24	1.08	2.806	2.4188
$[(Mo)\text{-}(Ti)_{14}]\ Mo_{0.1}\ Ti_{0.9}$	Ti-12.89 Mo	12.89	4.26	1.29	2.809	2.4133
$[(Mo)\text{-}(Ti)_{14}]\ Mo_{0.3}\ Ti_{0.7}$	Ti-15.05 Mo	15.05	4.30	1.51	2.812	2.4077

3.2 Materials and fabrication process

3.2.1 Characterization of as-received powders

CP-Ti and molybdenum powders were sourced from the CSIR and Alfa Aesar respectively. The two powders were characterized for morphology and particle size using the Joel scanning electron microscope (SEM) and Microtract particle analyser equipment as shown in Figure 3.3 respectively. The morphology of the as-received powders (CP-Ti and Mo) were irregular in shape with the average particle size of 28.07 µm and 16.83 µm respectively as shown in Figure 3.4.

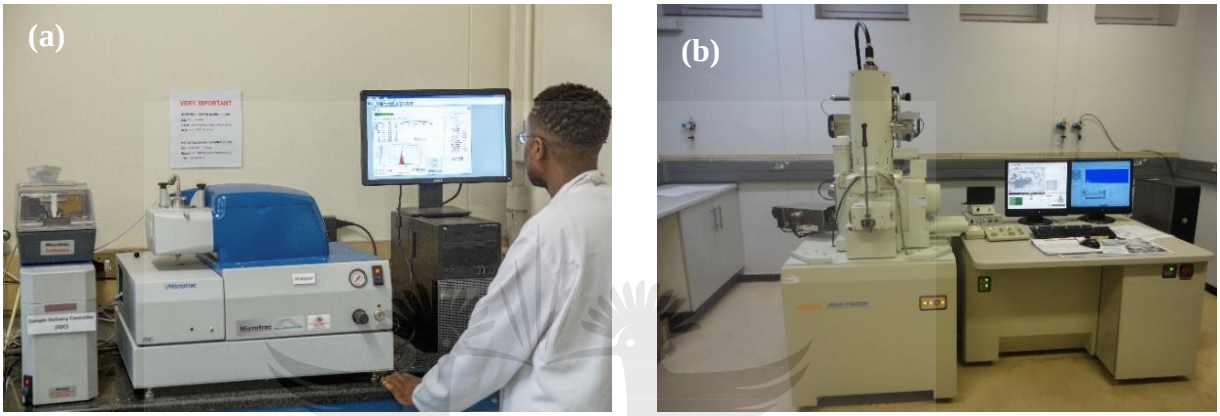

Figure 3. 3: (a) Particle size analyzer and (b) Scanning electron microscope.

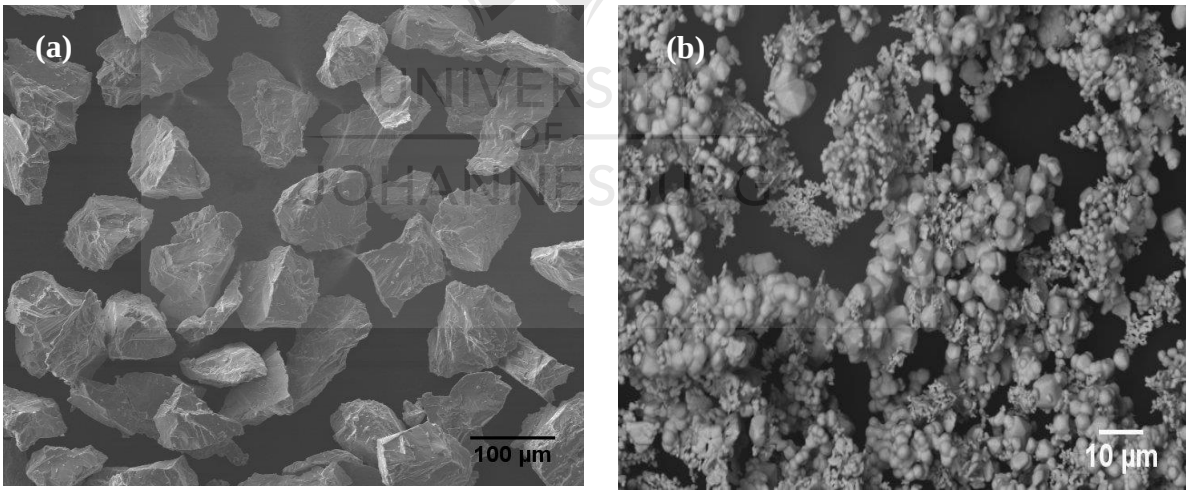

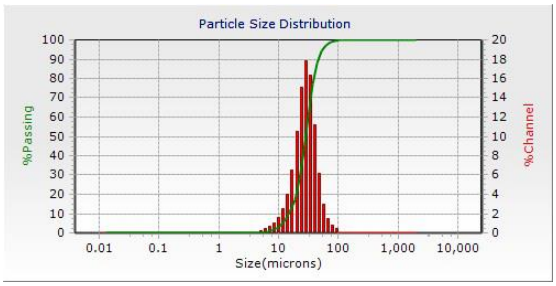

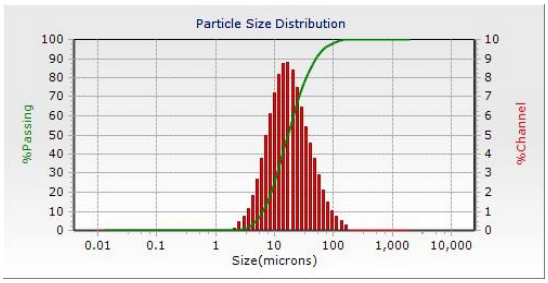

Figure 3. 4: SEM morphology and particle size distribution of as received (a) CP-Ti and (b) Mo powders

3.2.2 Powder Compaction / Powder Pressing

The two elemental powders were weighed into plastic containers according to the compositions given in Table 3.1. The weighed powders were cold compacted into green bodies using the VLP series Cold compaction machine or pressing machine. The powders were pressed to shape in a rigid steel die with some cylindrical specimens with a diameter of 100 mm to produce 100 g green bodies. The steel die was cleaned with ethanol to avoid contamination and ACRAWAX®C dispersion was applied to the die to avoid stickiness during removal. Figure 3.5 (a &b) shows the VLP series machine and the compressed 100g green body sample respectively.

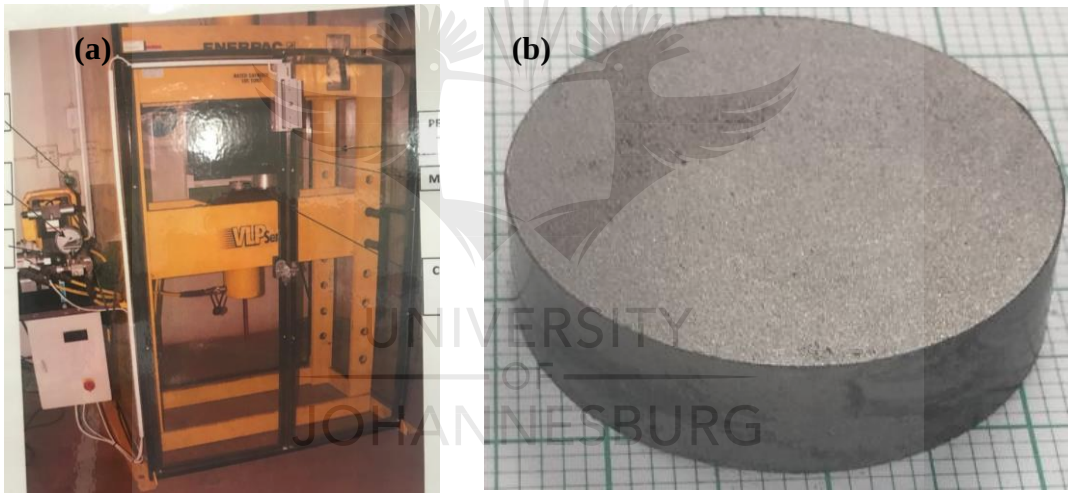

Figure 3. 5:(a) Pressing machine and (b) 100 g green body (Ø 100 mm).

3.2.3 Vacuum Arc re-melting process and Solution Treatment

The compacted green bodies were melted using a commercially Arc re-melting furnace at Mintek, South Africa. The furnace consists of the following water-cooled copper crucible, a tungsten electrode and oxygen getter. The furnace was purged with argon prior melting. Each ingot weighed 100 g. In the melting process the ingots were re-melted 3 times, flipped between each melting in-order to ensure chemical homogeneity. Figure 3.6 shows the commercially arc re-melting furnace. The ingots after casting were solution treated using a Ceramic Kiln Furnace (see Figure 3.7) at the CSIR with a temperature of 1100 ℃ for 1 h. The ingots were quenched in a bucket of icy water (see

Figure 3.7). The solution treated alloys were sectioned into 3 x 3 x 7 mm sizes for compression test using An Instron™1342 machine.

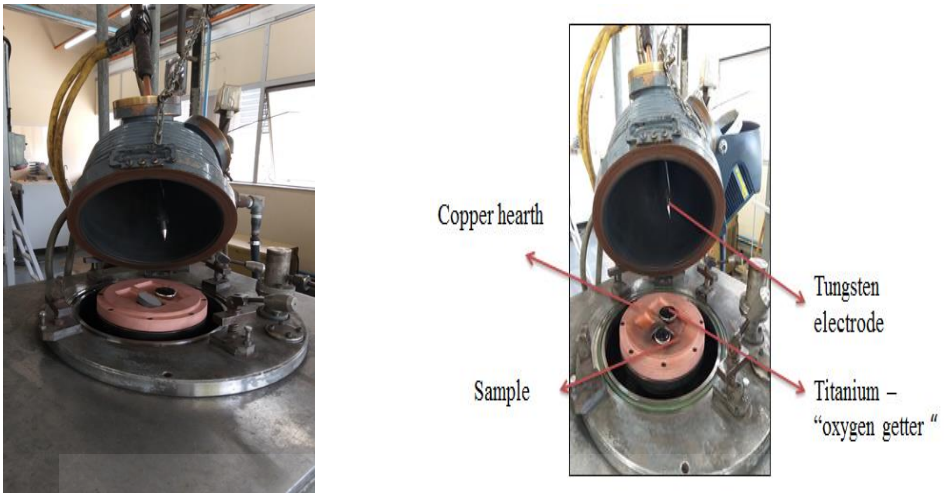

Figure 3. 6: Vacuum Arc re-melting furnace

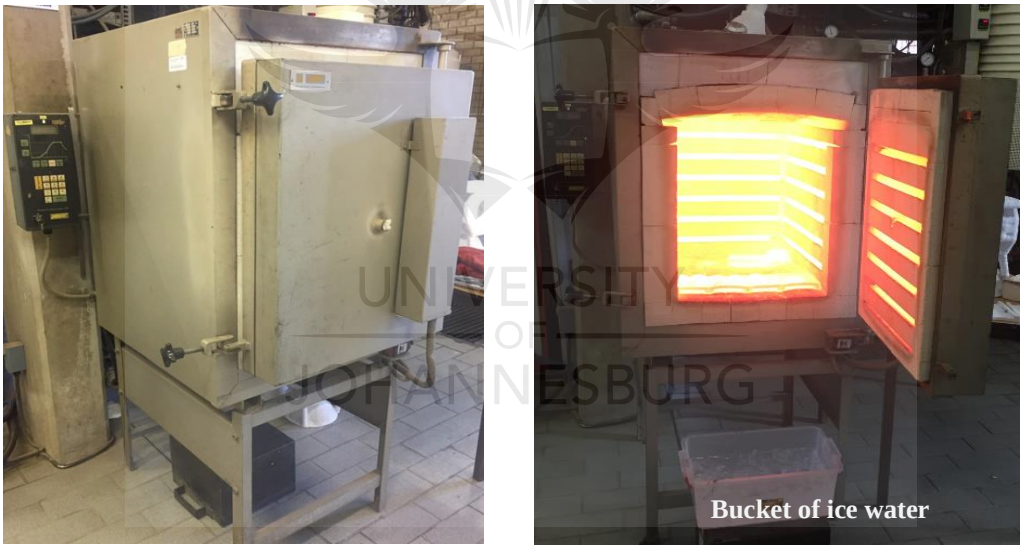

Figure 3. 7:Heat treatment furnace (Ceramic Kiln Furnace)

3.3 Sample preparations

The samples for optical and SEM analysis were sectioned into different sizes using the precision cut-off cutting machine (Brilliant 250X and 221X). For density measurement the ingots were sectioned into half and for mechanical properties, the samples were prepared according to each test specification measurement. The machined samples for OM and SEM were mounted by using a Beuhler simpliment 1000 mounting machine with conductive phenolic hot mounting resin. The specimens for OM and SEM were

ground and polished by conventional technique as presented in Table 3.2. The prepared specimens were etched using Kroll etchant ((92 ml distilled water, 8 ml HNO_3 and 2 ml HF) at different times (1-60 s) for microstructural analysis. Etching of samples refers to the selective removal of material from the surface in order to develop surface features which are related to the microstructure of the bulk material

Table 3. 2: Grinding and polishing steps for specimen preparation

Step	Grit/Pad	Speed (rpm)	Force (N)	Time(min)	Lubricant
1	800 SiC	150	15	2	Water
2	1000 SiC	150	15	2	Water
3	1200 SiC	150	15	2	Water
4	3 μm	300	20	4	3μm diamond suspension + water
5	Colloidal silica	300	20	8	Colloidal silica + water

3.4 Archimedes density measurement (Water Displacement Methods)

The densities were determined using Archimedes principles. The OHAUS machine/equipment that was used to determine the densities is shown in Figure 3.8. The rig consists of the following: a mass balance, a bridge and a specimen support structure. The function of bridge is used to support the beaker above the balance pan and the specimen support is connected to the balance pan. A wire basket connected to the specimen support hangs into the water and contains the specimen. The whole technique involves two measurements:

- Weight of the sample in air, labelled as A
- Weight of the sample in distilled water, labelled as B

The measurements were repeated 5 times for each sample and the average density was recorded. The relative or apparent densities (g/cm^3) were calculated using equation 3.1.

Relative Density (ρ) *=Experimental density / Theoretical density *100 equation 3.1*

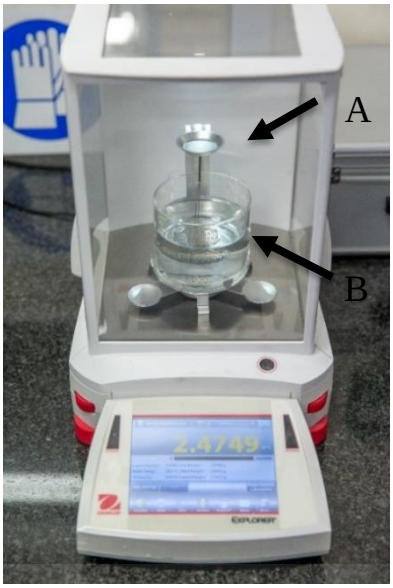

Figure 3. 8: The Density Kit

3.5 Microstructural characterization

3.5.1 Optical microscopy and Scanning Electron Microscope

Optical microscopy is the primary tool for morphological characterization of microstructure in science and engineering fields. The optical microscope is an assembly of 3 separate systems: the illuminating system which provides the source of light illuminating the sample, the sample stage that holds the sample in position and the imaging system. Leica CTR 4000 fitted with Leica DMI500M camera Optical microscope was used to take Images at various magnification from the lowest to the highest (5X- 20X) and Image J was used to analyse or distinguish different phases and the presence of porosity on each sample / specimen.

SEM (scanning electron microscopy) is a tool for observing specimen's surfaces. Samples that consist of fine electron beam, secondary electrons are emitted from the specimen surface. The characteristic information one can obtain from the SEM include: Topography which is the surface features of an object, morphology which is the size and shape of the particles and elemental composition. The microstructure, fracture surface and elemental composition of the specimens (both as-cast and solution treated) were obtained using SEM equipped with EDS (Joel: JSM-6510). The samples were analysed at different magnifications using both secondary electrons and backscatter electrons.

3.5.2 X-ray diffraction Analysis

X-ray diffraction (XRD) is one of the techniques for identification and characterization of crystalline solids, each crystalline solid has its unique characteristic X-ray powder pattern which is used as a fingerprint for its identification. The technique is based on the diffraction of X-rays by the sample in different directions. Waves of wavelength comparable to the crystal lattice spacing are strongly scattered or diffracted (Shetty, Kusminski and Scherer (2009). In this study X-ray diffraction determination of the alloys were executed on a Philips Xpert pro PANalytical powder diffractometer in θ – θ configuration with an X'Celerator detector for phase identification. The patterns were run with Co-Kα radiation with a secondary monochromatic (λ = 1.789Å). Analysis of the diffraction pattern was done using the Origin software and to identify different phases, literature was used as comparison. Figure 3.9 shows the XRD machine.

Figure 3. 9: X-ray diffraction machine

3.5.3 Electron backscatter diffraction (EBSD)

EBSD was used to further identify the microstructure, phase and deformation structures of the Ti-Mo samples. Prior to the EBSD observations, the samples were prepared by electro-polishing technique to remove any debris material from metallic work piece, to polish and deburr the metal parts. Landolt (2018) Electropolishing process was conducted using a Struers polishing machine at 30 V for 80 s. The perichloric acid from Struers with no precise composition was used as an electrolyte. Samples (one sample per alloy) were sectioned from A-3point test specimens and compression specimens from each alloy and were polished then cleaned with water and ethanol. The samples

were put in a sealed container to avoid oxidation and thereafter taken for EBSD analysis. Figure 3.10 shows the Struers electro-polishing machine.

Electron backscatter diffraction (EBSD) is a common laboratory technique used to measure crystal orientations and diffraction patterns from crystalline samples in the scanning electron microscope Humphreys (2004) and Britton *et al.* (2016). Such pattern analysis continues to be carried out using modern software algorithms to produce excellent data sets that can be questioned or interpreted for crystallographic texture, grain orientation, grain shape and local deformation structure. The EBSD scans for the Ti-Mo alloys in this study were performed using Zeiss Cross Beam 540 equipment, operating at 25 kV and 10 nA to image the samples. The EBSD analysis were performed using an Oxford NordLys Max^3 detector and Oxford Aztec analysis software. The samples were analysed at different places with no specification of a place of analysis. Figure3.11 shows the EBSD machine.

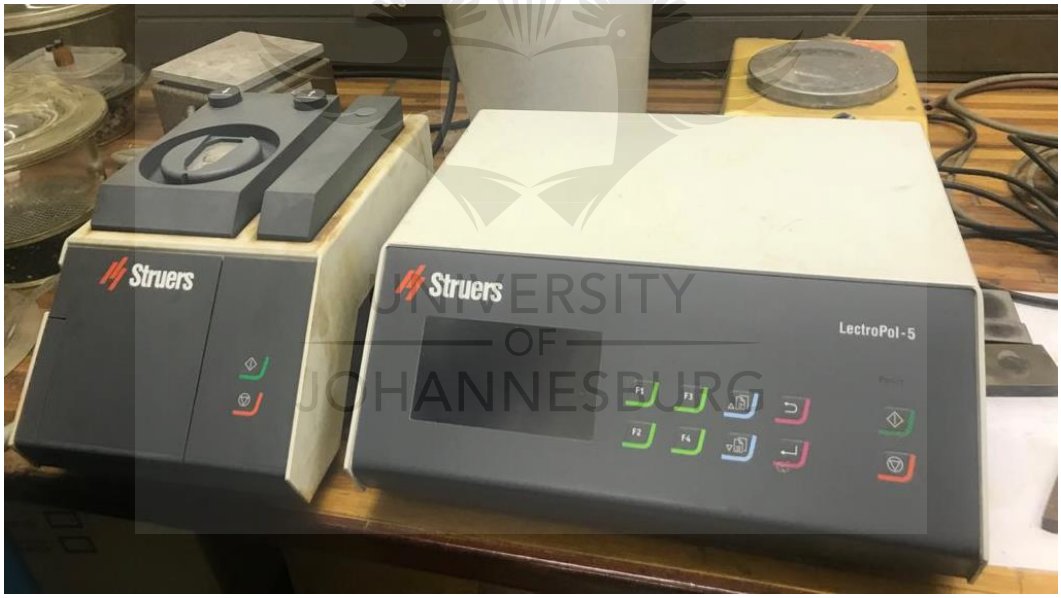

Figure 3. 10 : Struers Electropolishing machine

Figure 3. 11: EBSD machine

3.6 Mechanical testing of as-cast and solution treated ingots

Mechanical testing or engineering tests are performed to determine various mechanical properties of materials such as strength, hardness, elastic modulus and ductility.

3.6.1 Vickers Microhardness test

Hardness test is important as it relates to other properties such as strength, brittleness and ductility of that material. ZWICK ROELL (see Figure 3.12), Vickers Microhardness indenter was used to measure the hardness of the Ti-Mo alloys. A small diamond indents was made with a load of 500 gf for 10 s. The two diagonals made after 10 indentations per sample were measured microscopically and their average values calculated.

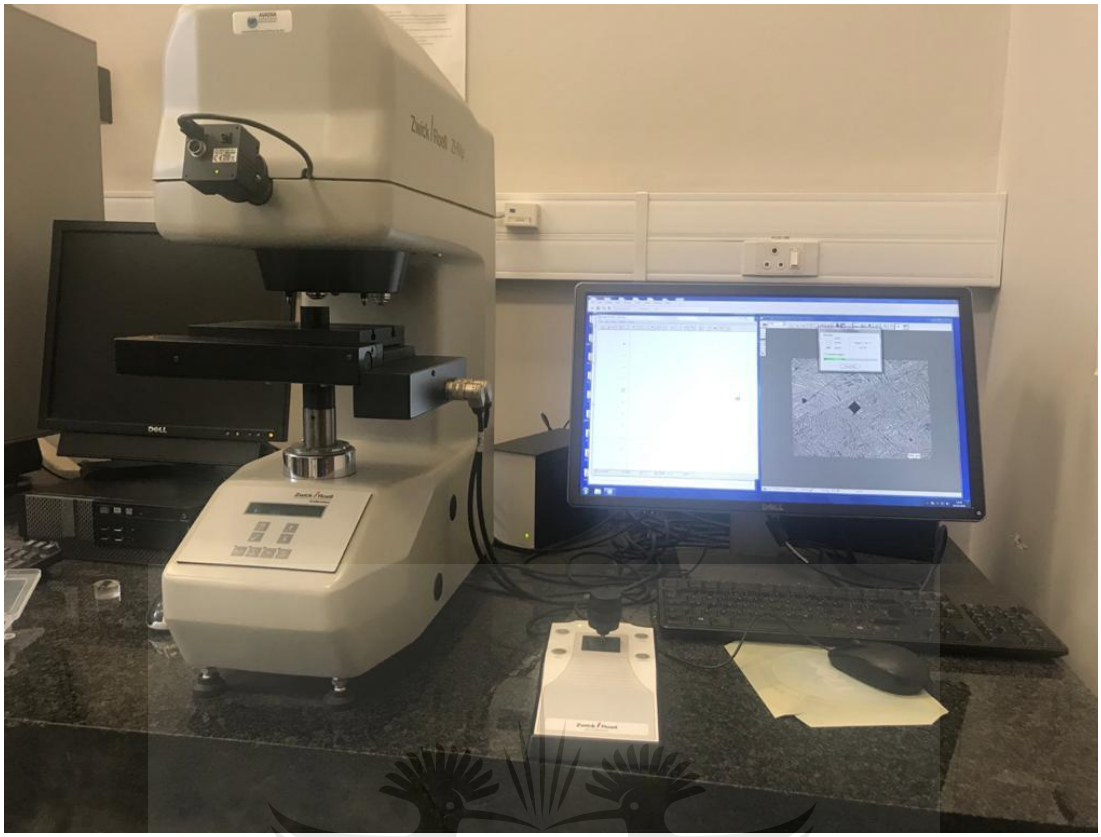

Figure 3. 12: Vickers micro-hardness machine

3.6.2 Tensile test

Tensile test is used to measure or study the stress-strain relationship of metals, Mp (2002). Tensile test uses an extensometer to apply measured force to a test specimen. The core product of a tensile test is a load vs elongation which can be converted into a stress strain curve. Values such as strain, stress, modulus of elasticity, tensile strength, yield point/strength, ductility and elastic limit can be determined or gauged. Tensile specimens with a gauge of 48 X 5 X 3 mm were cut from as-cast and as-quenched alloys by EDM. The dimensions of the samples are illustrated in Figure 18. An Instron^{TM}1342 tensile tester fitted with 50 kN load cells was used to conduct the tensile test at room temperature with a constant crosshead speed of 0.5 mm/min. The tensile strain was measured using an extensometer attached to the gauge section of the test specimen. The extensometer was removed to prevent damage before the specimen can fracture. The average tensile test data given (Yield strength, Ultimate tensile strength, elastic modulus and elongation) in this study were taken from three tensile experiments for each alloy.

3.6.3 A 3-point bend test

A 3-point bend test were carried out using an Ingstron^{TM}1342 testing machine and the dimensions are also illustrated in Figure 3.13. The bending strength of the studied alloys were determined according to ASTM: D790-03. The equation of the bending /flexural strength is given as.

$$\sigma_f = 3PL/2bw_2 \qquad \textit{equation 3.2}$$

Where σ_f is the bending strength (MPa), *P* is the load (N), *L* is the span length (mm), *b* is the specimen width (mm) and *w* is the thickness of the specimen (mm). The dimensions of the specimens were: *L*= 30 mm, *b*=4.0 mm and *w*=3.0mm. The average bending strength were taken from at least 3 specimens under the same conditions (testing temperature of 20ºC and testing rate of 2.0 mm/min).

3.6.4. Compression Test

The compressed samples were analysed using the Ingstron^{TM}1342 machine. 3 samples with a dimension of (5mm X 3mm X 3mm) from each alloy were subjected to compression test at room temperature, and the compressive strength was analysed.

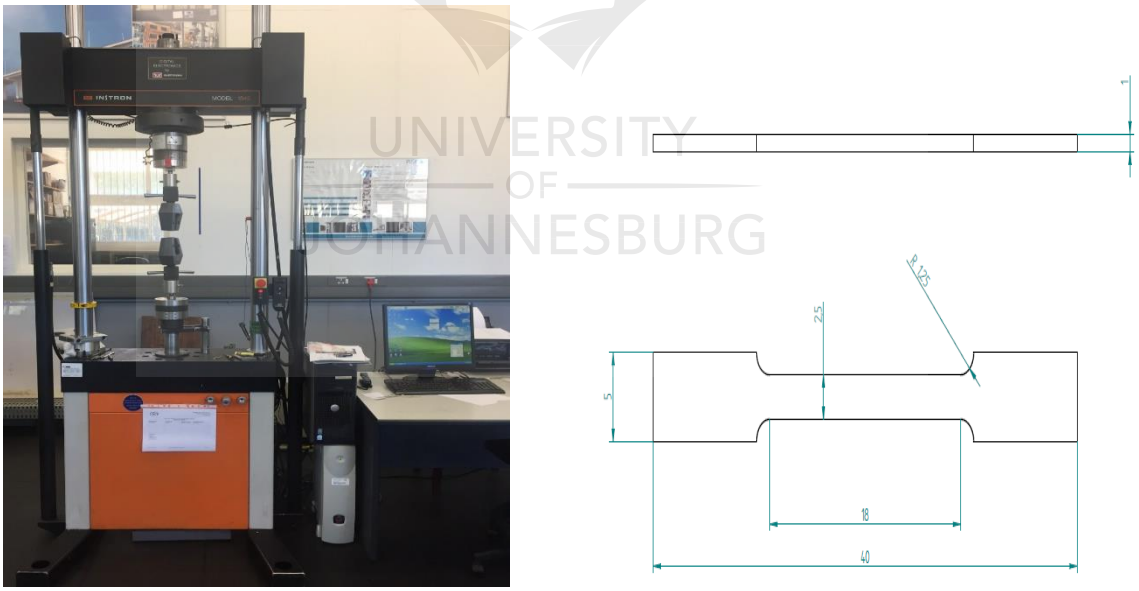

Figure 3. 13 : (a) Three point and tensile test machine and (b) schematic diagram of the tensile and 3 point bend test specimens.

CHAPTER 4: RESULTS AND DISCUSSION

4.0 INTRODUCTION

This chapter introduces the experimental results of Ti-Mo alloys in as-cast, solution treated conditions. The chapter is divided into different sections: section 4.1 discusses the densities of Ti-Mo alloys in AC (as-cast) and ST (solution treatment) conditions. Section 4.2 is based on the phase and microstructural evolution of AC and ST Ti-Mo alloys. Sub-section 4.2.1 examines the XRD patterns of AC, ST and CT (compression test), while subsection 4.2.2 and 4.2.3 show the microstructural evolution between AC and ST. The microstructural evolution of Ti-Mo alloys after compression test (CT) are explained in section 4.4. Subsection 4.3.1-4.33 explains the effect of microstructural evolution on the mechanical properties of Ti-Mo alloys in AC and ST conditions, whereas subsection 4.3.4 is based on the compression properties of the solution treated alloys. Section 4.4 is based on the deformation behaviour of Ti-Mo alloys of the solution treated after compression test.

4.1 Archimedes Densities of Ti-Mo alloys in as-cast and solution treated conditions

The densities of the designed alloys in as-cast and after solution treatment were found to be significantly increasing with an increase with the β stabilizing content. The increase in the density was attributed to Mo comprising of a higher melting point and density than titanium. The results are summarised in Table 4. 1.

Table 4. 1: Archimedes Densities of As-cast and Solution treated alloys.

Mo Content (wt %)	Density (As-Cast) (g/cm^3)	Density (Solution treated) (g/cm^3)
Ti-10.02wt% Mo	4.818	4.778
Ti-10.83wt% Mo	4.819	4.830
Ti-12.89wt% Mo	4.839	4.894
Ti-15.05wt% Mo	4.889	4.922

4.2 Phase analysis and microstructural evolution of Ti-Mo alloys in as-cast, solution treated conditions and after compression.

4.2.1 X-ray diffraction of As-Cast, solution treated and compressed Ti-Mo alloys

X-ray diffraction was conducted to identify the constituent phases in the as-cast Ti- Mo alloys. The XRD patterns of as-cast Ti-Mo alloys are presented in Figure

4. 1.It was evident that from the XRD patterns, all the as-cast Ti-Mo alloys comprised of both orthorhombic martensitic α″ phase and bcc β phase peaks. The omega phase peaks could not be detected using the XRD technique due to its low detection limit. The XRD peaks changed from double peaks of orthorhombic martensitic to those of single beta peaks as the Mo content increased. The highest peak intensity was that of β phase at 2θ=52º and it was evident in Ti-15.05Mo alloy. The highest orthorhombic martensitic peak intensity was at 2θ=45º, whereas the lowest β peak intensity was observed to be at around 2θ=68º. The XRD patterns of Ti-10.02 Mo alloy was consistent with the results found by Oliveira *et al*, (2007) in as-cast condition but different from the experimental results reported by Bania, (1994). It was reported that β phase was retained at Mo content of 10, whereas the XRD results for Ti-15.05 Mo was inconsistent with the results reported by Martins *et al.* (2011). All the Ti-Mo alloys were not in agreement with the experimental results found by Chen *et al (* 2006), Davis *et al* (1979), Ho,*et al* (1999) in as-cast conditions. Comparing the XRD results of binary Ti-Mo alloys with other binary β Ti alloys such as Ti-Nb, and Ti-Sn reported by Lee, (2002) and Hsu *et al*., (2009) respectively, it was shown that the XRD patterns of the compared alloys consist of two phase of α″ and β just like the Ti-Mo alloys even at higher composition of Nb and Sn in as-cast condition. The XRD patterns of the studied alloys in as-cast condition were significantly different from those reported in literature. This discrepancy may be attributed by the difference in the XRD diffractometer equipment, the XRD patterns for this study were determined using the Co-Kα radiation with a secondary monochromatic λ=1.789Å, whereas the XRD patterns reported in literature were characterized using the Cu-Kα radiation with a monochromatic of λ=1.544Å.

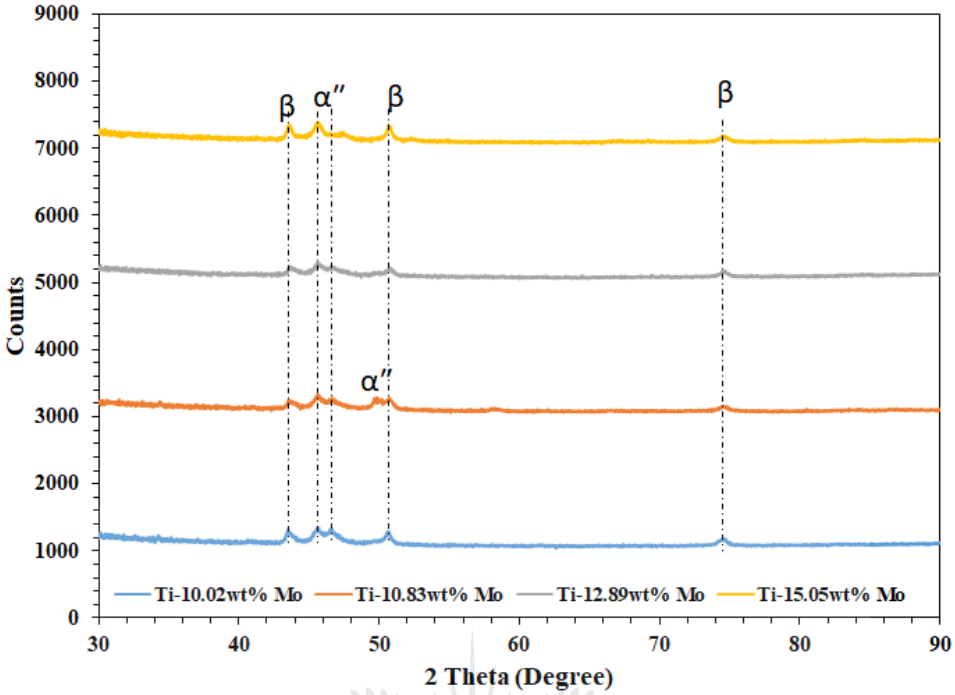

Figure 4. 1: X-ray diffraction of Ti-Mo alloys in as-cast condition.

X-ray diffraction was conducted to identify the constituent phases in the as-cast, solution treated and compressed Ti-Mo alloys. The XRD patterns are presented in Figure 4. 2-Figure 4. 5. The XRD pattern for Ti-10.02 Mo shown in Figure 4. 2 shows this alloy transformed into two phases upon quenching from the β transus temperature as it was comprised of high-volume fraction of orthorhombic martensitic α″ phase peaks and lower fraction of bcc β phase peaks after casting and solution treatment. It was evident that the change in temperature from casting to solution treatment resulted in the transformation of a new bcc β phase peak at about 2θ= 48º. This peak was observed to be broader, wider and higher than the one at 2θ=45º. The XRD pattern after compression test were comprised of high-volume fraction of bcc β phase peaks than the orthorhombic martensitic α″ phase peaks. The XRD patterns that occurred after compression test resulted in the suppression of the α″ peak and evolution of β phase at 2θ=75º. The highest peak positioned at 2θ=45º. Increasing the Mo content to Ti-10.83Mo as illustrated in Figure 4. 3, the XRD pattern shows that the alloy transformed in two phases after casting and quenching as it was comprised of both orthorhombic martensitic α″ phase peaks and bcc β phase peaks. It was evident that the double α″ peak in Ti-10.83Mo from a high intensity single peak of Ti-10.02Mo at 2θ=59º was attributed to the low martensitic start temperature during casting as compared to the one

in Ti-10.02Mo. There was no evidence of new peaks after solution treatment and the highest peak was found to be that bcc β at about 2θ=45º that was not evident in Ti-10.02Mo after solution treatment, the highest peak transformed due to the Ms temperature being lower than in Ti-10.02Mo during quenching. The XRD peaks that occurred after compression test showed peaks of bcc β phase only with the highest peak positioned at about 2θ=45º and 2θ=65º.

A further increase in the Mo content to 12.89 Mo as displayed by the XRD pattern in Figure 4. 4, showed that after casting (AC), the XRD pattern were composed of equal volume fraction of both the orthorhombic martensitic α″ phase peaks and bcc β peaks. The α″ peak at 2θ=57º became smaller as compared to the peak seen at Ti-10.02, Ti-10.83Mo alloy and this was because of the continuous decrease in the Ms temperature during casting. The transformation after solution treatment showed that amongst the bcc β peak, there was a single peak of α″ at 2θ=78º, which implied the martensitic start temperature was decreasing and reaching room temperature. The compressed XRD peaks of this alloy were comprised of bcc β peaks only with the highest peaks positioned around 2θ=45º. Increasing the Mo content to 15.05, the XRD pattern displayed in Figure 4. 5 illustrated that after casting the only peaks that were evident were that of orthorhombic martensitic α″ phase and bcc β phase. It was evident that the volume fraction of α″ phase decreased significantly as compared to the other alloys while the bcc β peaks increased significantly. The highest peak was positioned around 2θ=51º. The XRD pattern after solution treatment and compression test were comprised of bcc β peaks only with the highest peaks positioned around 2θ=45º. It was evident in the XRD patterns from Figure 4. 2-Figure 4. 5, that peaks of α″ decreased and bcc β with shaper peaks increasing with an increase in Mo content. The results implied that as the Mo content increased the MS (martensitic start) decreased to room temperature and retained the β phase. No peaks of the ω phase were detected by the XRD technique after casting, solution treatment and compression test because of its low detection limit.

The XRD results of the solution treated Ti-10.02Mo and Ti-15.05Mo alloys were in agreement with the results found by Cardoso *et al.*(2014), Wang *et al.* (2016) where they reported corresponding peaks of α″ and β phase in Ti-10.02Mo alloy after solution treatment and peaks of β phase in Ti-15Mo alloy. Zhao *et al.*(2012) also reported on the presence of peaks β phase in Ti-15Mo alloy. It was challenging to compare Ti-

10.83Mo and Ti-12.89Mo alloys after solution treatment to the results found in literature due to less published work found in literature. It was also challenging to compare the XRD pattern after compression test due to less published work found in literature. The XRD patterns of the studied alloys after solution treatment were significantly different from the ones reported in literature and this discrepancy may be attributed by the difference in the XRD diffractometer equipment, the XRD patterns for this study were determined using the Co-Kα radiation with a secondary monochromatic λ=1.789Å, whereas the XRD patterns reported in literature were characterized using the Cu-Kα radiation with a monochromatic of λ=0.1541Å.

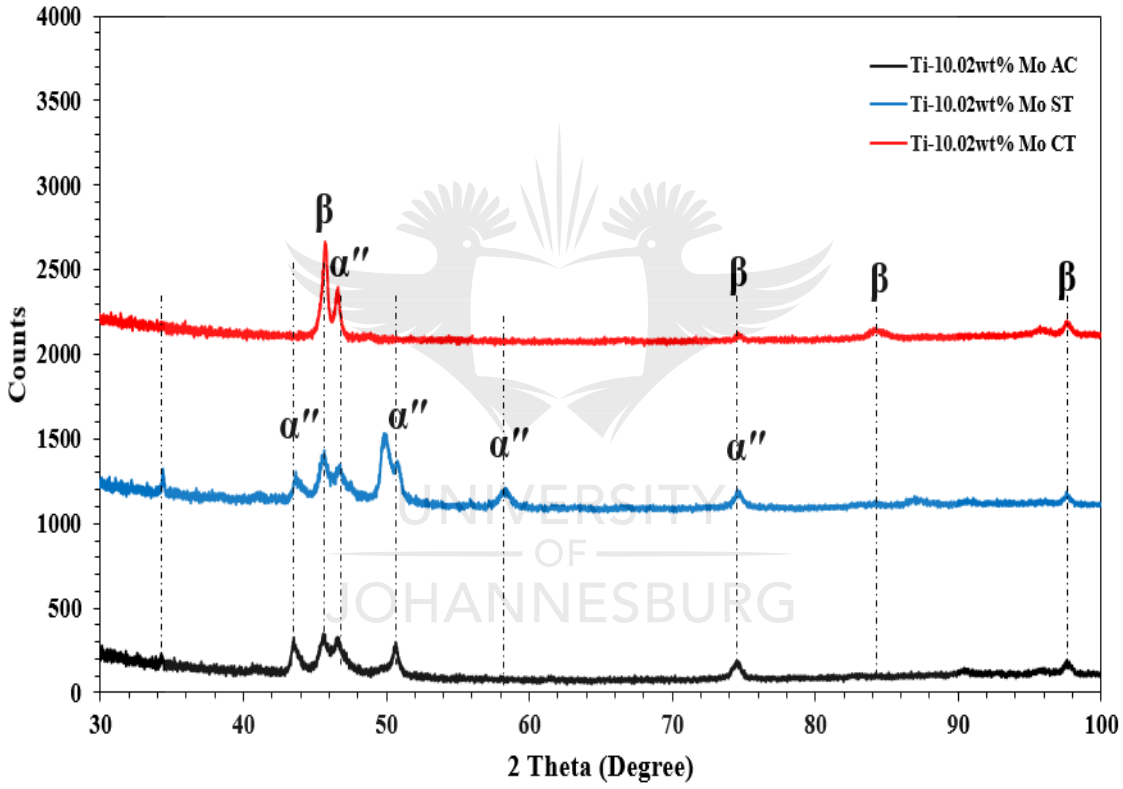

Figure 4. 2: XRD patterns of Ti-10.02wt% Mo alloys in AC, ST AND CT condition

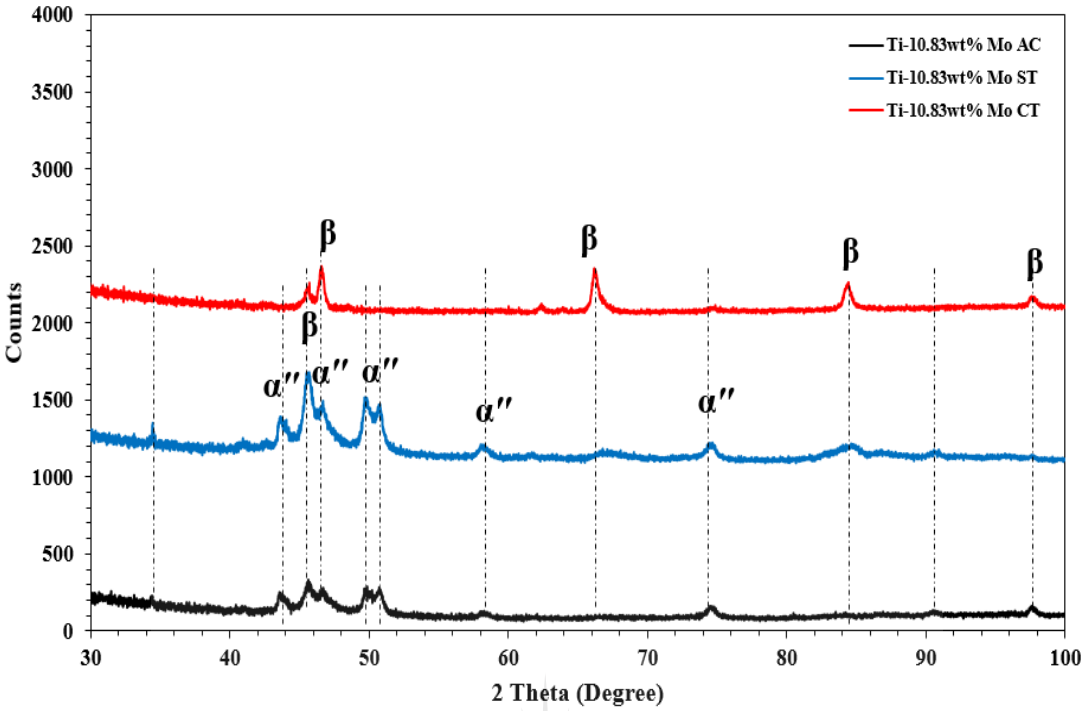

Figure 4. 3: XRD Profiles of Ti-10.83wt% Mo alloys in AC, ST and CT condition

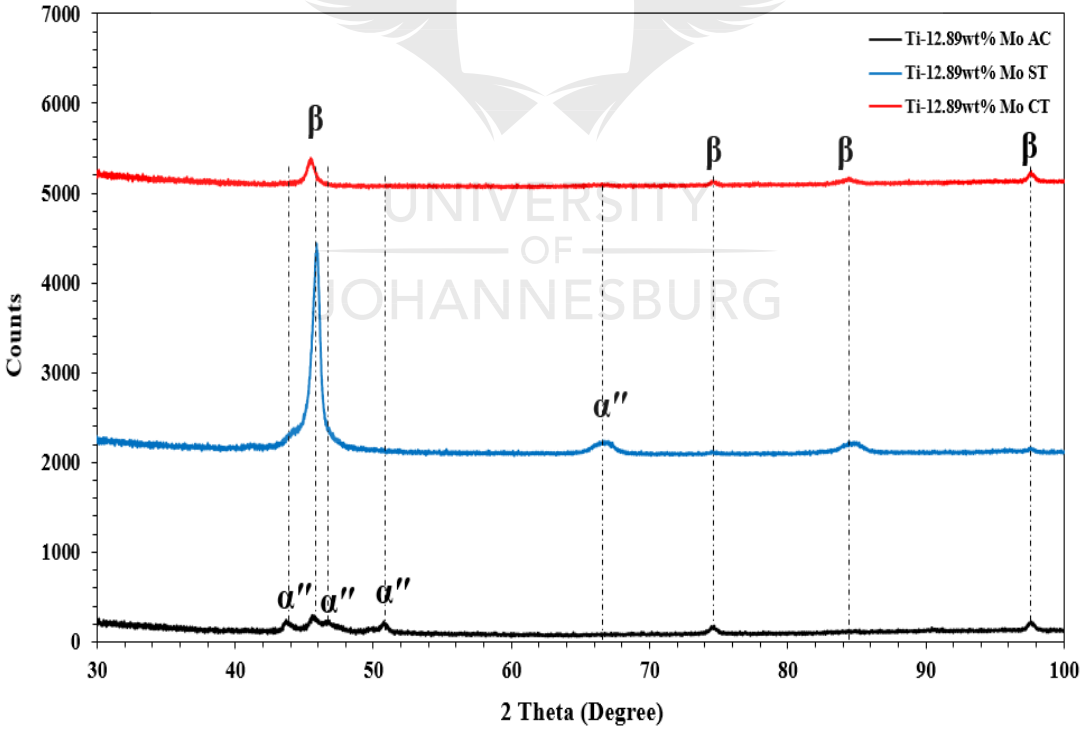

Figure 4. 4:XRD patterns of Ti-12.89wt% Mo alloy in AC, ST and CT condition

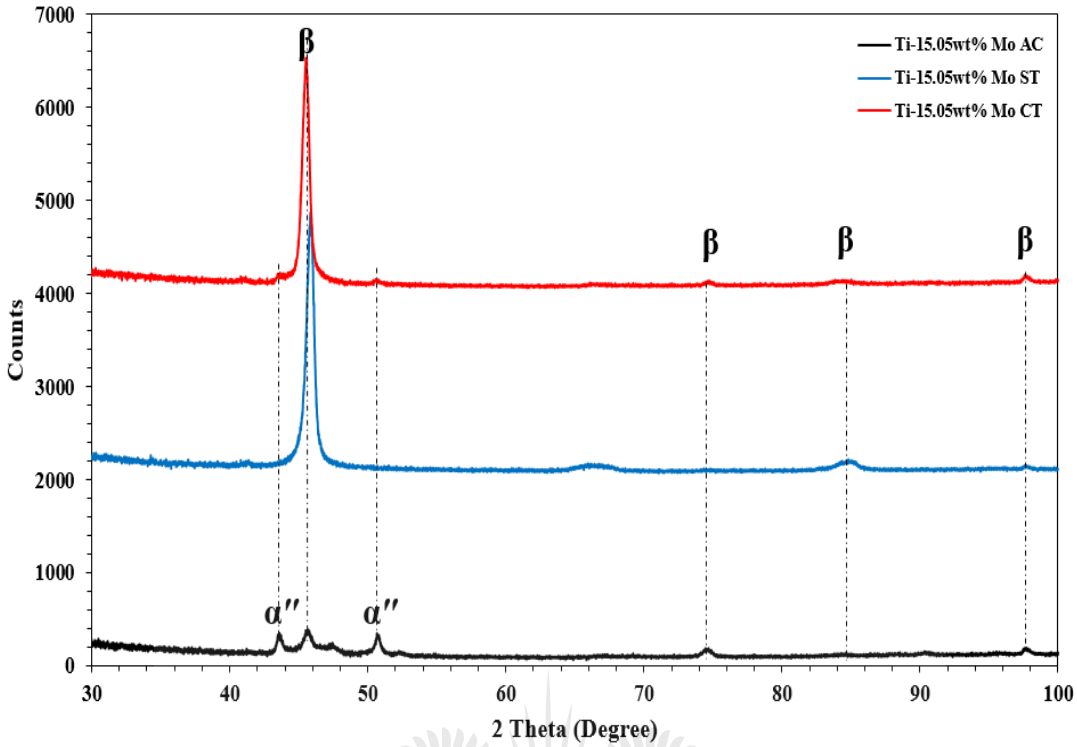

Figure 4. 5:XRD profile of Ti-15.05wt% Mo alloy in AC, ST and CT condition.

Table 4. 2: X-ray diffraction structures of all the studied Ti-Mo alloys vs those reported in literature.

	XRD Phase Identifications	
Alloy Composition (wt%)	**As-cast (AC)**	**Solution treatment (ST)**
Ti-10.02Mo	α+β	α+β
Ti-10.83Mo	α+β	α+β
Ti-12.89Mo	α+β	α+β
Ti-15.05Mo	α+β	β
Ti-10Mo [(Ho, *et al* (1999), Chen *et al* (2006); Oliveira (2008) and Martins *et al.(* 2011)]	β	-
Ti-12Mo [Ho,*et al* (1999) and Oliveira and Guastaldi, (2008)]	β	-
Ti-15Mo[(Ho *et al* (1999), Chen *et al* (2006) and Oliveira and Guastaldi, (2008)]	β	-

Ti-10Mo [Cardoso *et al.*, (2014),Wang *et al.*, (2016)]	-	β
Ti-15Mo[Zhao *et al.*,(2012), Cardoso *et al.*, (2014) and Wang *et al.*, (2016)]	-	β

4.2.2 Optical and scanning electron micrographs of Ti-Mo alloys in as-cast and solution treated conditions.

Figure 4. 6 to Figure 4. 9. depict the optical and SEM images of a series of Ti-Mo alloys in as-cast and solution treated condition. Figure 4. 6 (a) and (b) shows the OM micrographs of AC and ST respectively, it was evident that both images are comprised of equi-axed grains of β with sub-boundaries of different sizes. The sub-grain boundaries were concluded to be those of α″ structure. The SEM micrographs of Ti-10.02Mo alloy are displayed in Figure 4. 6 (c) and (d) showed the same structure as the as-cast alloys which is the β grains and needle like structure of orthorhombic martensitic α″ within the grains. The OM and SEM results of AC and ST showed that the Ms Temperature was higher during casting and quenching and they were consistent with the XRD in Figure 4. 2. An increase in the Mo content to Ti-10.83Mo is illustrated in Figure 4. 7 (a-d). The OM micrographs of As-cast and after solution treatment are shown in Figure 4. 7 (a) and (b) respectively. The as-cast OM micrographs and the SEM micrographs of Ti-10.83Mo after casting (Figure 4. 7 (a) and (c)) comprised β grains and needle like structure of orthorhombic martensitic α″ inside the grains. The needle like structure were observed to be nucleating from the grain boundary and their volume fraction after casting (AC) decreased as compared to Ti-10.02Mo. The decrease in the needle-like plate were due to the lower martensitic start temperature during casting as comparable to Ti-10.02Mo. The as-cast SEM and OM micrographs results were consistent with the XRD results in Figure 4. 3. The OM and SEM micrographs of Ti-10.83Mo after solution treatment (Figure 4. 7 b and d) show β grains only and this implies that the martensitic start temperature during quenching was below room temperature that was able to supress the α″ structure as compared to the Ms temperature found by the XRD technique.

Increasing the Mo content to Ti-12.89Mo as displayed in Figure 4. 8 shows that the OM and SEM micrographs after casting (AC) shows β grains and sub-grain of various size, the sub-grain structures were those of orthorhombic martensitic α″. It was evident that the martensitic α″ needles decreased as the Mo content increased due to the Ms Temperature during casting being significantly lower than in Ti-10.83Mo alloy hence the OM and SEM micrograph after casting (AC) were in agreement with the XRD results in Figure 4. 4. As the Mo content was further increased to Ti-15.05Mo showed that the OM and SEM micrographs after casting (AC) showed a two-phase morphology consisting of β equi-axed grains and needle like structure of orthorhombic martensitic α″ phase precipitated in the β matrix and nucleating from the grain boundaries. The martensitic start temperature was significantly lower as compare to the 3 alloys as the needle like structure significantly decreased in Ti-15.05Mo. The OM and SEM micrographs after solution treatment displayed the β grains structure only. The exceptional suppression in the α″ showed that the martensitic start temperature was below room temperature. The OM and SEM results after casting (AC) and after solution treatment (ST) were in agreement with the XRD depicted in Figure 4. 5.

It is evident from the OM and SEM images that when the Mo content increase in as-cast (AC) condition from Ti-10.02Mo-Ti-15.05Mo, the needle-like structure of orthorhombic martensitic α″ structure decreased and the equi-axed β grains became more dominant. The decrease in the needle-like structure was attributed not only to the increase in the β stabilizer but to the decrease in the martensitic start temperature during casting. The as-cast micrographs were consistent with the XRD results. The OM and SEM micrographs after solution treatment show that the needle-like structures decreased significantly as compared to as-cast. This significant decrease was characteristic of the significant decrease in the martensitic start temperature as the Mo content increased that suppressed the α″ phase and chemically stabilize the β phase.

The designed Ti-Mo alloys microstructural results were in disagreement with the work reported by Ho *et al* (1999) and Chen *et a*l (2006). However, the Ti-10.02Mo (AC) alloy was in agreement with the microstructures found by Chen *et al* (2006). The presence of martensitic phase was also reported in other studies as an evidence of martensitic transformation from β to α″ phase Mantani, (2006). The micrographs analyzed using the OM and SEM techniques in Ti-10.02Mo (ST) were in agreement

with those found by Wang *et al.*, (2016) but contradicting the ones reported by Cardoso *et al.*(2014). However, the Ti-15.05Mo (ST) alloy were consisted with experimental results reported by Zhao *et al.*, (2012), Cardoso *et al.*, (2014) and Wang *et al.*, (2016). Due to less work reported on the solution treated of Ti-10.83Mo (ST) and Ti-12.89Mo (ST) it was challenging to compare the experimental results with those reported in literature.

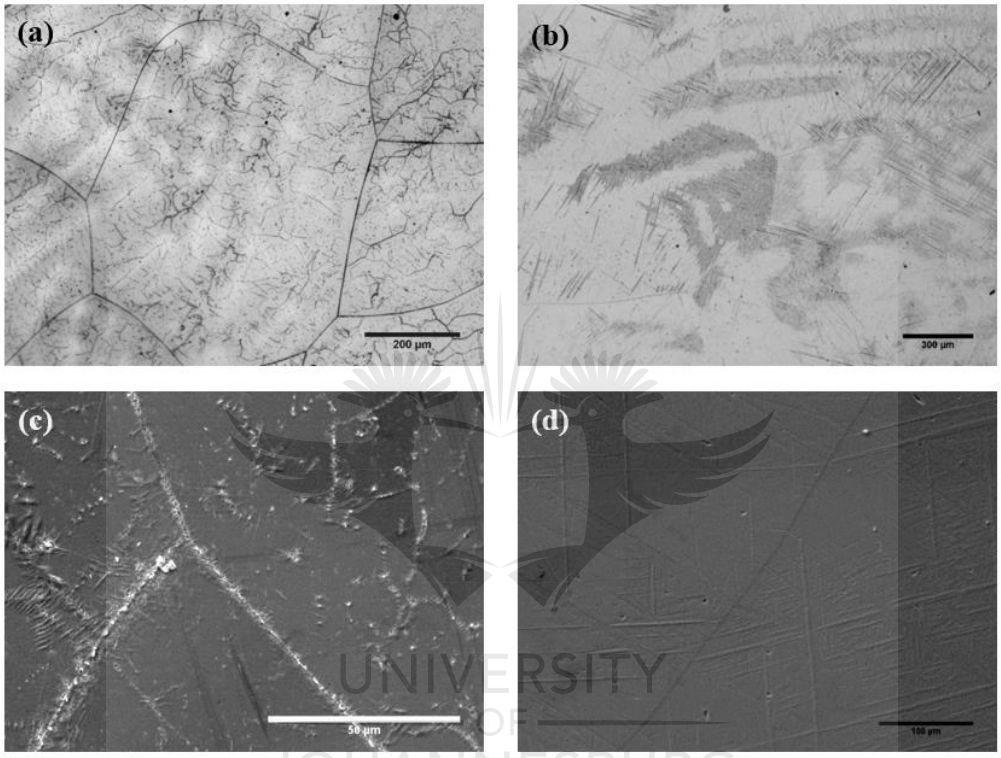

Figure 4. 6: Optical Micrographs of Ti-10.02wt% Mo in (a) AC and (b) ST conditions and the SEM micrographs of Ti-10.02wt% Mo in (c) AC and (d) ST conditions.

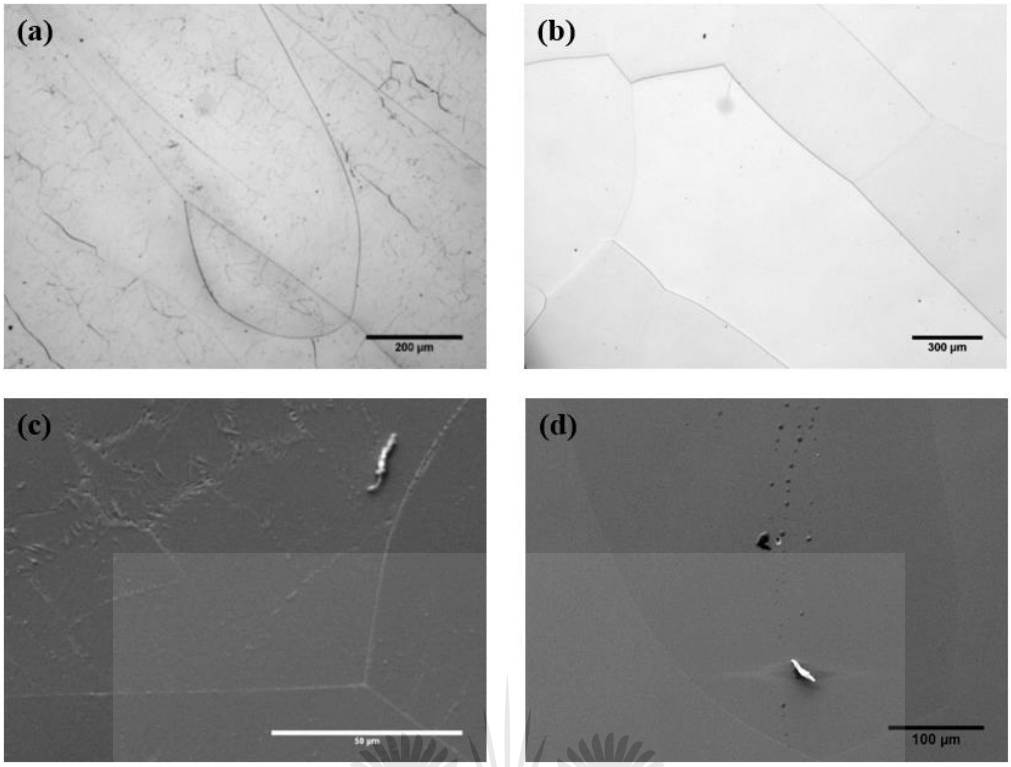

Figure 4. 7: Optical Micrographs of Ti-10.83wt% Mo in (a) AC and (b) ST conditions and the SEM micrographs of Ti-10.83wt% Mo in (c) AC and (d) ST conditions.

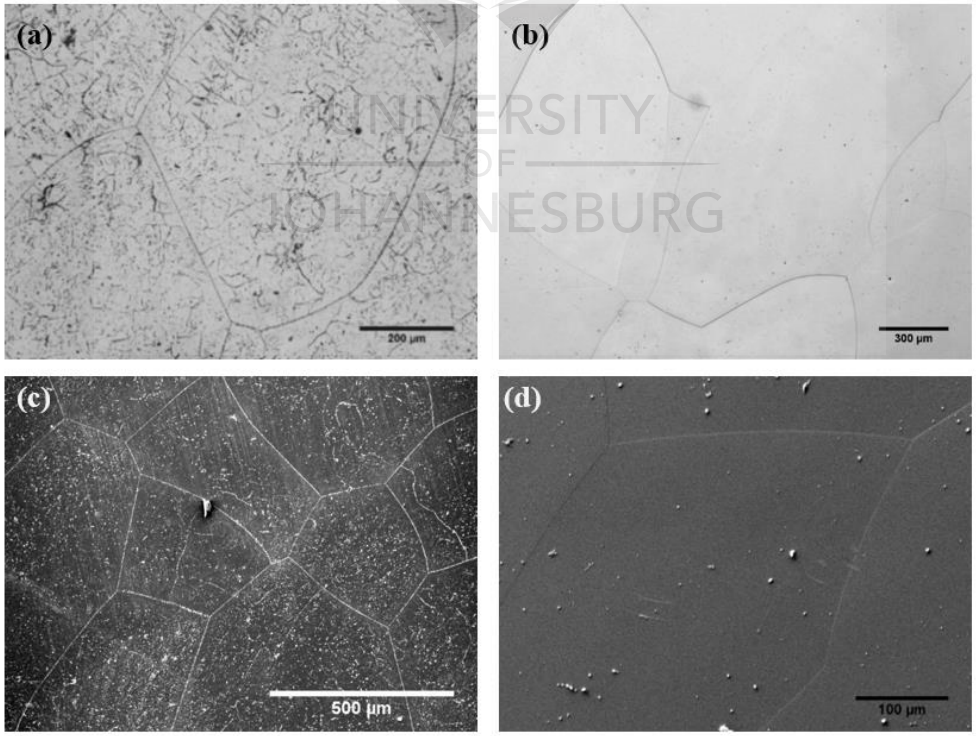

Figure 4. 8: Optical Micrographs of Ti-12.89 wt% Mo in (a) AC and (b) ST conditions and the SEM micrographs of Ti-12.89 wt% Mo in (c) AC and (d) ST conditions.

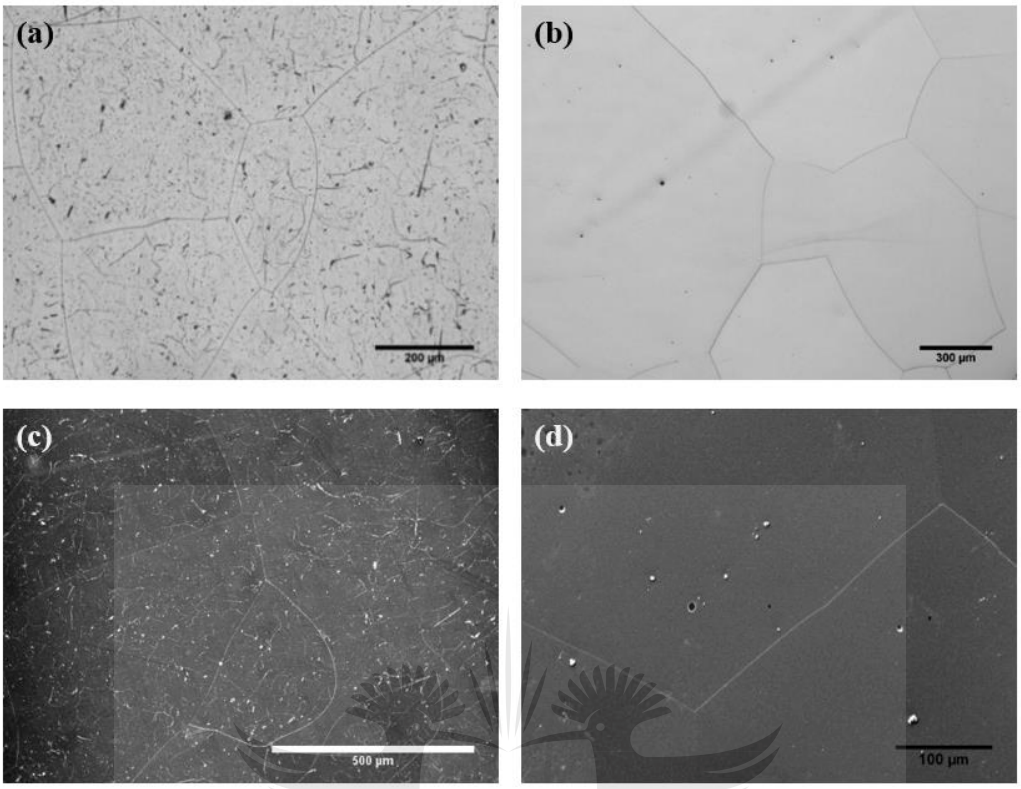

Figure 4. 9: Optical Micrographs of Ti-15.05wt% Mo in (a) AC and (b) ST conditions and the SEM micrographs of Ti-15.05wt% Mo in (c) AC and (d) ST conditions.

4.2.3. EBSD images of Ti-Mo alloys in as-cast and solution treated conditions.

The EBSD technique was utilized to further characterize the phase constituents and microstructural evolution of the designed Ti-Mo alloys after casting and solution treatment. The EBSD band contrast, IPF and phase maps for the as-cast Ti-Mo alloys are presented in Figure 4. 10 to Figure 4. 13. The band contrast of all the alloys displayed a clear β equiaxed grain boundary without needle like structure within the grain boundaries. The IPF maps at different direction showed the grain boundaries and small grains of different colours with particles inside the grains. The EBSD phase maps were analysed at different magnification in-order to illustrate the distributions of the particles within the alloys.

The analysed regions in the as-cast condition of Ti-10.02Mo and Ti-15.05Mo alloys (Figure 4. 10 and Figure 4. 13, respectively. They were identified as the matrix bcc β phase in red, the orthorhombic martensitic α″ in yellow, and the omega phase ω in yellow. The analysed regions in the as-cast condition of Ti-10.83Mo and Ti-12.89Mo

alloys in Figure 4. 11 and Figure 4. 12, respectively were also characterized wherein the orthorhombic martensitic α″ phase was presented in blue and the omega phase particles in yellow. The characterized regions in solution treated Ti-10.02Mo, Ti-10.83Mo, Ti-12.89Mo and Ti-15.05Mo (see Figure 4. 10-Figure 4. 12 (b)) were also identified as the bcc β phase in red, the orthorhombic martensitic α″ in blue, and the omega phase ω in a yellow.

As observered visually in Figure 4. 10 the as-cast and solution treated Ti-10.02Mo alloy showed the highest volume fraction of the omega and orthorhombic martensitic phase. As the Mo content increased to Ti-10.83Mo, it was evident that the volume fraction of the omega and martensitic in as-cast decreased significantly and this was illustrated in Figure 4. 11 . After solution treatment the EBSD map for Ti-10.83Mo alloy (Figure 4. 11) showed that the increase in the Mo content attributed to the high/increase in the volume fraction of the orthorhombic martensitic α″ phase and the omega phase (HCP hexagonal). Further increase in the Mo content to Ti-12.89Mo illustrated that the volume fraction of the both the omega and martensitic phase continues to significantly decrease after casting (As-cast), as evident in Figure 4. 12(a), whereas Figure 4. 12 showed that after solution treatment (ST) the volume fraction of the orthorhombic and omega phases was significantly increasing within this alloy. The significant increase in the Mo content to Ti-15.05Mo, the quantity of the omega phase and the orthorhombic phase in as-cast condition (AC) significantly decreased as compared to those observed in Ti-10.02Mo alloy in Figure 4. 10 (a). Therefore, the increase in the Mo content after casting decrease the volume fraction of the omega and martensitic phases. The volume fraction of the omega phase increased significantly after solution treatment while the volume of the martensitic precipitate decreased. This indicated that with a composition of Ti-15.05Mo, quenching from above the beta transus temperature precipitated a significant amount of omega phase.

The occurrence of the omega phase in EBSD maps is not well reported in literature especially in as-cast and solution treatment condition for binary Ti-Mo alloys hence it was challenging to compare these experimental results with the ones reported in literature. More experimental work needs to be done in order to quantify the use of this technique in characterizing the omega phase. The EBSD results of the designed alloys after casting and solution treatment were not in agreement with the XRD peaks and OM

and SEM micrographs reported in Figure 4. 6, Figure 4. 7,Figure 4. 8 and Figure 4. 9 respectively. This could be attributed to the segregation that could have occurred during casting.

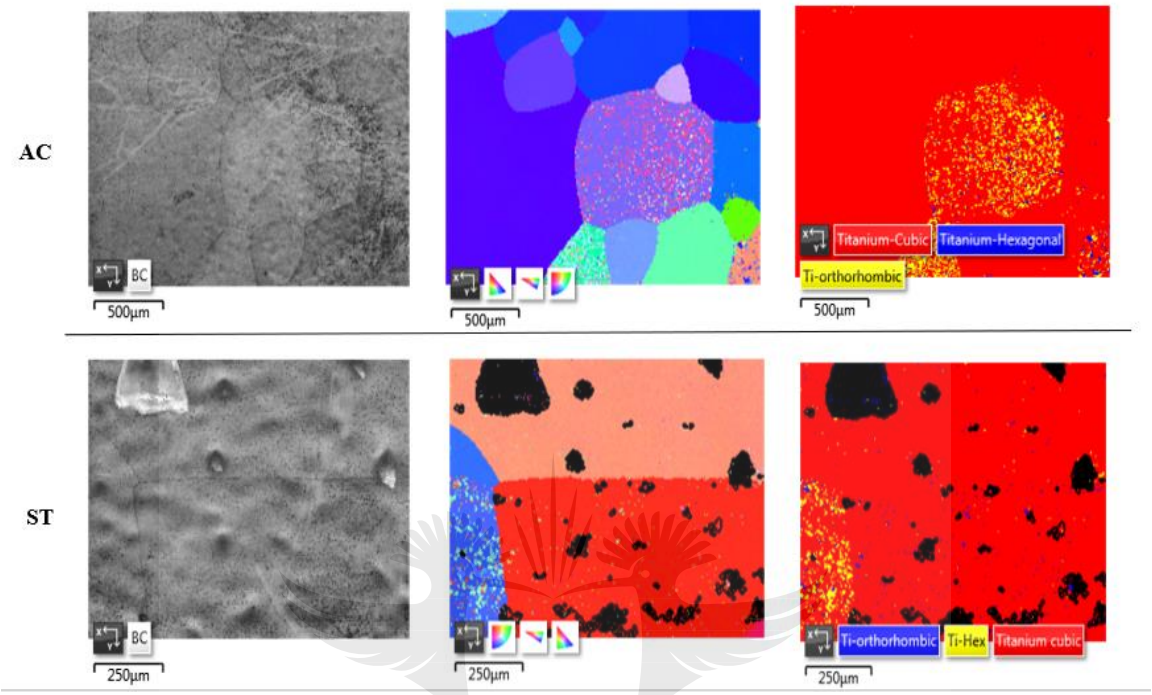

Figure 4. 10: EBSD maps of Ti-10Mo alloy in as-cast and solution treated condition.

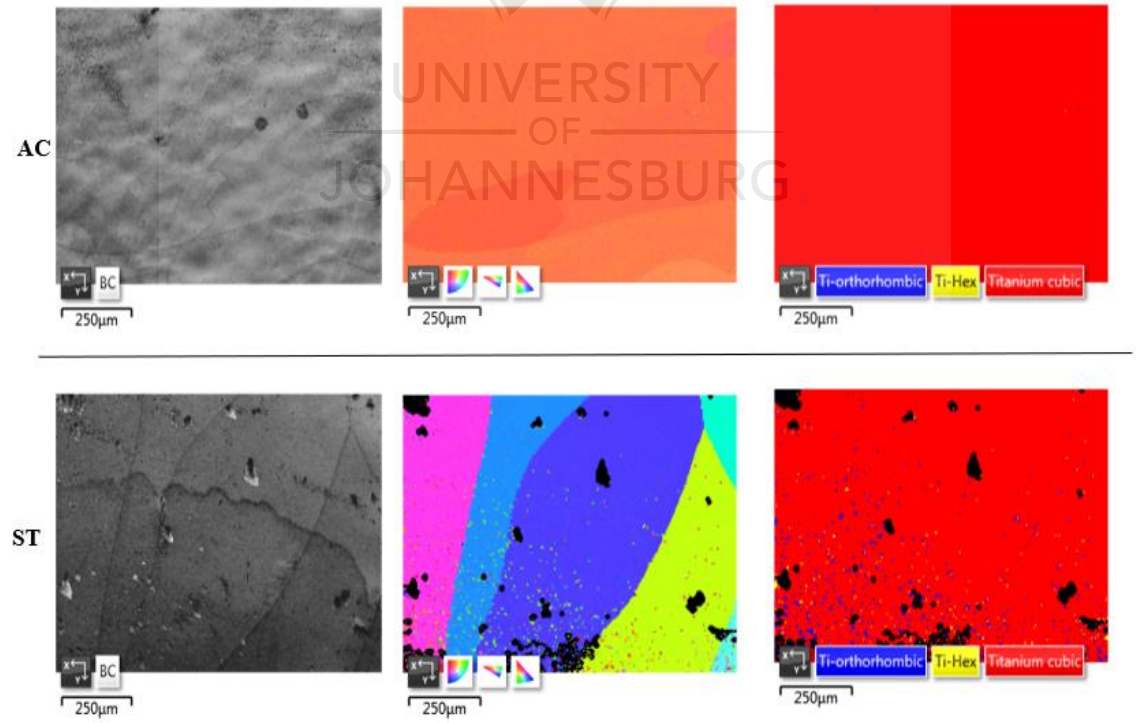

Figure 4. 11: EBSD maps of Ti-10.83Mo alloy in as-cast and solution treated

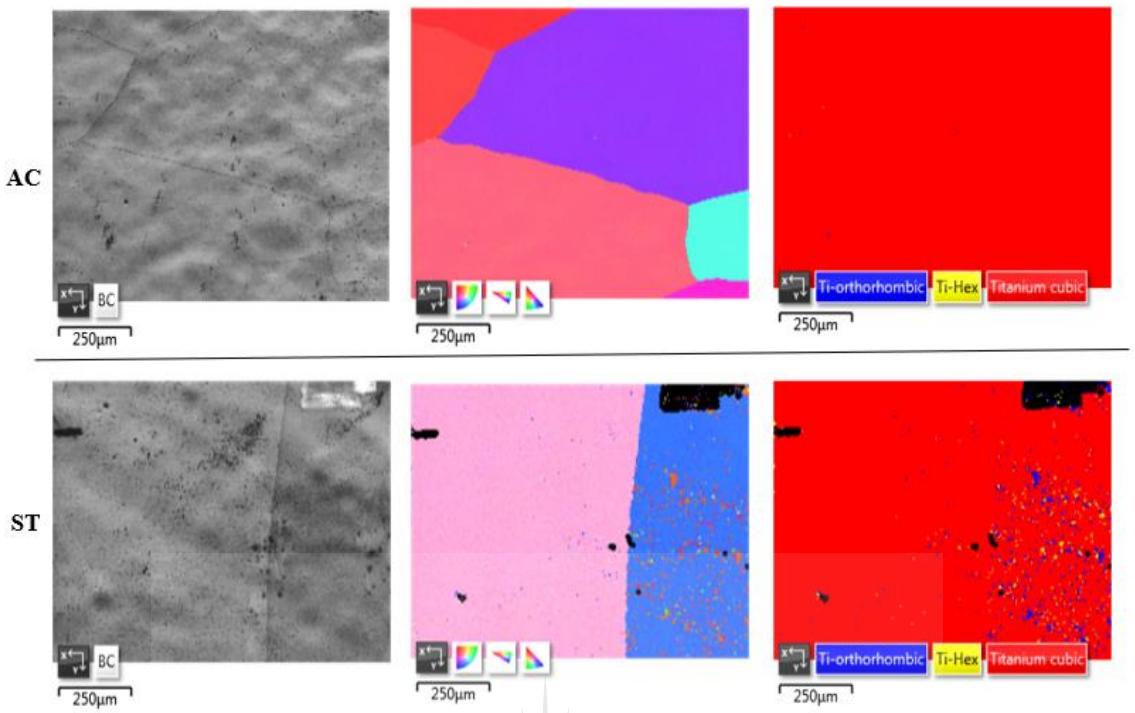

Figure 4. 12: EBSD maps of Ti-12.89Mo alloy in as-cast and solution treated condition

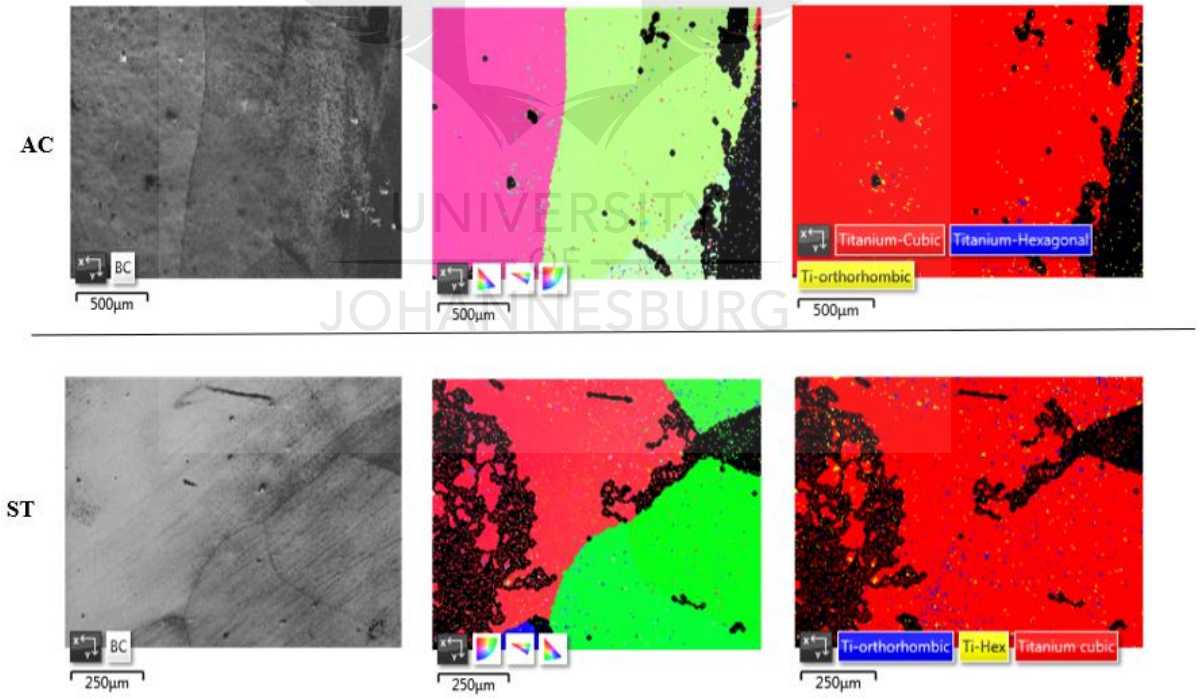

Figure 4. 13: EBSD maps of Ti-15.05Mo alloy in as-cast and solution treated condition

Table 4. 3 compares the theoretical finding and experimental findings of the designed alloys in as-cast conditions. According to the experimental findings analysed using different techniques it was shown that the results of the designed alloys analysed using

XRD, OM and SEM techniques were not in agreement with the all the predictions methods. The Moeq, the Kβ and e/a ratio predicted the stability of the β phase from a composition of Ti-10.02Mo, whereas the Bo and Md stability map only predicted the β stability when the Mo content was 12.89wt% and 15.05wt%. The Bo and Md stability map predicted the presence of the omega phase at a composition of Ti-10.02Mo and Ti-10.83Mo alloys but experimentally different characterization techniques (XRD, OM & SEM) could not detect the omega phase due to its low volume fraction or low detection limit.

The experimental results analysed by the EBSD techniques were not in agreement with the Moeq, Kβ and e/a ratio prediction methods but because they could not detect the α″ and ω phase. However, the EBSD results agreed with the predictions made by the average Bo and Md stability map for Ti-10.02Mo and Ti-10.83Mo alloys but they were not in agreement with alloy Ti-12.89Mo and Ti-15.05Mo because the EBSD technique analysed the orthorhombic martensitic α″ phase and the athermal omega (ω) phase. In conclusion all the predictions methods did not work for the designed alloys when analysed using the XRD, OM and SEM techniques. The average Bo and Md method only worked for two alloys (Ti-10.02Mo and Ti-10.83Mo) when using the EBSD technique. The β phase could not be stabilized experimentally with the designed alloys. In conclusion, the discrepancies in the theoretical and experimental may be because of the following reasons: most of the theoretical modes were developed under the assumption of equilibrium conditions. The solidification of the alloys during casting often occur at cooling rates that are far from equilibrium condition, hence the phase detected from experiments may differ from those predicted theoretically.

Table 4. 3: Theoretical Findings vs Experimental Findings of the designed alloys

	Theoretical Findings				**Experimental findings**		
Mo Content (wt %)	Moeq (wt %)	K_β	e/a ratio	Bo and Md	**XRD**	**OM & SEM**	**EBSD**
Ti-10.02 Mo	β	β	β	β +α″ +ω	**β+α″**	**β+α″**	**β+α″+ω**
Ti-10.83 Mo	β	β	β	β +α″+ω	**β+α″**	**β+α″**	**β+α″+ω**
Ti-12.89 Mo	β	β	β	β	**β+α″**	**β+α″**	**β+α″+ω**
Ti-15.05 Mo	β	β	β	β	**β+α″**	**β+α″**	**β+α″+ω**

Table 4. 4 compares the theoretical findings and the experimental findings of the designed alloys after solution treatment. The experimental results of the designed alloys analyzed by the XRD technique for Ti-10.02Mo and Ti-10.83Mo alloys were found to be inconsistent with the Moeq, Kβ and e/a ratio methods because of the presence of the orthorhombic martensitic α″ phase, however the Ti-12.89Mo and Ti-15.05Mo alloys were in agreement with the predictions methods (Moeq, Kβ, e/a ratio and the Bo and Md). The findings found by OM and SEM techniques indicated that Ti-10.83 Mo, Ti-12.89Mo and Ti-15.05Mo alloys were in agreement with the Moeq, Kβ and e/a ratio predictions methods. Ti-10.83Mo alloy were found to be in disagreement with the average Bo and Md prediction method, whereas Ti-12.89 and Ti-15.05Mo alloys were in agreement with the methods. The experimental findings analyzed using the EBSD techniques for Ti-10.02Mo and Ti-10.83Mo were only in agreement with the predictions made by the Bo and Md stability map, however the other two alloys were not in agreement with the all the predictions methods.

In conclusion the β stabilizing prediction methods worked for the Ti-12.89Mo and Ti-15.05Mo alloys when using the XRD technique, Ti-10.83 Mo, Ti-12.89Mo and Ti-15.05Mo alloys when using the SEM and OM techniques and one prediction method worked for Ti-10.02Mo and Ti-10.83Mo alloys when characterized using the EBSD techniques. Therefore, the β phase of the designed alloys after solution treatment were stabilized using the XRD techniques for Ti-12.89Mo and Ti-15.05Mo alloys because of the presence of the β phase only with no precipitation of secondary phases and when using the OM and SEM techniques for Ti-10.83Mo, Ti-12.89Mo and Ti-15.05Mo alloys.

Table 4. 4: Theoretical Findings vs Experimental findings of the designed alloys

	Theoretical Findings				**Experimental findings**		
Mo Content (wt. %)	Moeq (wt. %)	K_β	e/a ratio	Bo and Md	**XRD**	**OM & SEM**	**EBSD**
Ti-10.02 Mo	β	β	β	β +α″ +ω	**β+α″**	**β+α″**	**β+α″+ω**
Ti-10.83 Mo	β	β	β	β +α″+ω	**β+α″**	**β**	**β+α″+ω**
Ti-12.89 Mo	β	β	β	β	**β**	**β**	**β+α″+ω**
Ti-15.05 Mo	β	β	β	β	**β**	**β**	**β+α″+ω**

4.3 Effects of microstructural evolution on the mechanical properties of as-Cast (AC) and Solution treated (ST) Ti-Mo Alloys

34.3.1. Vickers micro-hardness of Ti-Mo alloys as-cast condition

Figure 4. 14 shows the micro-Vickers hardness of the as-cast binary Ti-Mo alloys. As shown in the Figure the micro-hardness decreased significantly as the Moeq increased. The highest modulus in Ti-10.02wt% Mo was attributed to the dispersion-hardening effect of β phase by the formation of high volume fraction of the precipitation of the omega phase and the orthorhombic martensitic α″ phase during quenching as displayed in the EBSD phase maps results in Figure 4.10. Bagariatskii et al (1959) also indicated that the presence of the omega phase corresponded to a sharp maximum in the hardness. The decrease in the Vickers micro-hardness from 440.6 $HV_{0.5}$ (Ti-10.83Mo) to 350.0 $HV_{0.5}$ (Ti-15.05Mo) was attributed to decrease in the volume fraction in the omega and the orthorhombic martensitic phase as it was seen in the EBSD phase maps from Figure 4. 11 to Figure 4. 13. It was reported that the phase constituent affects the Vickers micro-hardness value of beta Ti alloys which decrease in the following manner as reported by Lee, (2002) ; $H_\omega > H_{\alpha'} > H_{\alpha''} > H_\beta > Hv_\alpha$. The hardness of the alloy containing a high-volume fraction of omega will have the highest hardness than all the alloys containing less. The decrease in the orthorhombic phase and omega phase is in agreement with the results analysed by the XRD, optical microscope, SEM and EBSD.

The micro-hardness values of the as-cast Ti-10.02Mo, Ti-12.89Mo and Ti-15.05Mo alloys (473.6 $HV_{0.5}$, 412.6 $HV_{0.5}$ and 350.0 $HV_{0.5}$ respectively) were higher as compared to those reported by Ho, *et al (*1999) in Ti-10Mo (350 $HV_{0.2}$) and Ti-15Mo (307 $HV_{0.2}$) alloys in as-cast condition and higher than the hardness of CP-Ti (156

$HV_{0.2}$) reported also reported by Ho,*et al* (1999). Severino Martins Junior, Jose Roberto *et al* (2011) also reported a lower hardness in Ti-15Mo alloy and CP-Ti alloy (330 $HV_{0.5}$ and 210 $HV_{0.5}$ respectively) as compared to the studied alloys. The micro-hardness of Ti-10.02Mo (451 $HV_{0.4}$) alloy was higher than the value reported by Chen Yu-yong *et al* (2006) in as cast condition. However, for Ti-15Mo (381 $HV_{0.4}$), Chen Yu-yong *et al* (2006) found out the micro-hardness was higher than the one reported in this study also in as-cast condition. Likewise, the micro-hardness value of Ti6Al4V was 294 $HV_{0.5}$.

Figure 4. 15 shows the micro-Vickers hardness of the designed binary Ti-Mo alloys after solution treatment. The micro-hardness decreases as the Mo content increase in Ti-10.02, and Ti-10.83Mo alloys and the same trend is observed in the as-cast Ti-Mo alloys in Figure 4. 14. The high micro-Vickers hardness in Ti-10.02Mo (333.5 $HV_{0.5}$) alloy was attributed to the high quantity of the precipitation of the omega phase that was more evident in EBSD phase maps in Figure 4. 10. Although the XRD, OM, SEM illustrated that this alloy was dominated with the orthorhombic martensitic phase and the bcc β phase, there were not enough to lower the elastic modulus due to the omega phase depicted in the EBSD phase map being harder than both of them. The reduction in the micro-hardness as the amount of β stabilizing element (Mo) increased in Ti-10.83Mo (320.4 $HV_{0.5}$) alloy was attributed to the decrease in the volume fraction of the orthorhombic martensitic α″ structure and the dominant β phase structure as seen in Figure 4. 7 (b and d) and it was also attributed by the low volume fraction of the omega precipitates as it was noticeable in the EBSD maps in Figure 4. 11. The significant increase in the micro-hardness at Ti-12.89Mo after solution treatment (still lower than the as-cast) was characterized by the omega precipitates as observed in Figure 4. 12. Although the alloy showed an increase in the volume fraction of the dominant β structure as illustrated in Figure 4. 8 (b and d), the structure didn't have much impact in lowering the hardness because the high content of the hardening phase (ω) had no effect on it. The highest micro-hardness value in Ti-15.05Mo alloy with the dominant β structure (as compared to the as-cast), was attributed by the increase in the volume fraction in the omega phase as seen in the EBSD phase maps and by the stronger solid solution strengthening effect as reported by Ho, et al (1999). The designed Ti-10.02Mo and Ti-15.05Mo (298 and 340 HV respectively) alloys were not in agreement with the results reported by Cardoso *et al.*,(2014). The other two designed alloys are incomparable since there is little work reported on those alloys.

In conclusion, the micro-Vickers hardness of the studied alloys were not comparable to the ones reported in literature and the difference in this micro-Vickers may be due to the different load that was used during analysis/ testing and the number of indentations that may have contributed the difference in the error bars.

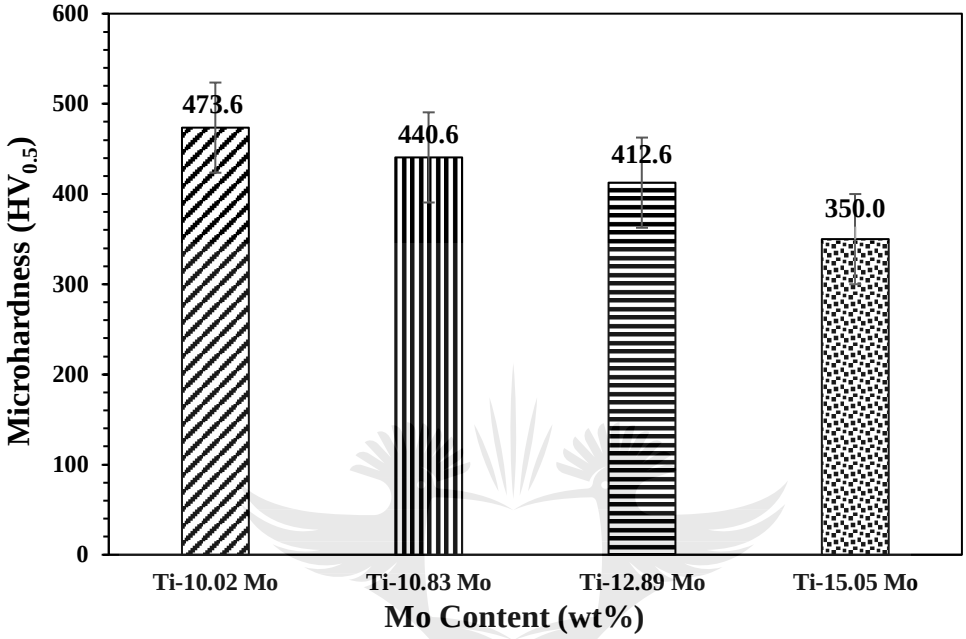

Figure 4. 14: Micro-hardness of as-cast Ti-Mo alloys

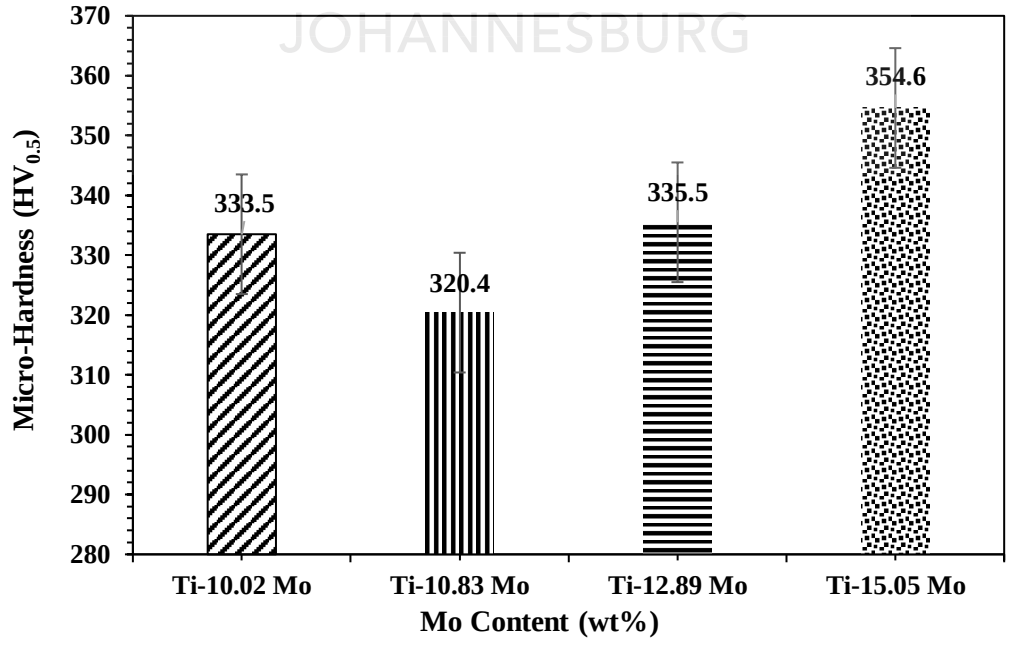

Figure 4. 15: Micro-Hardness values of solution treated Ti-Mo alloys.

4.3.2 Tensile properties of Ti-Mo alloys in as-cast and solution treated state

4.3.2.1 Stress strain curve and tensile properties of Ti-Mo alloys in as-cast and solution treated conditions.

Figure 4. 16 shows the stress-strain curve of as-cast Ti-Mo alloys after tensile test. The tensile test data of these designed alloys recorded before the extensometer was removed are presented in Table 4. 5. Amongst the designed alloys, Ti-10.83Mo alloy shows higher UTS followed by extensive work hardening, resulting in high elongation of 0.35%. Ti-15.05Mo alloys display the lowest yield strength and ultimate tensile strength with extensive work hardening but show low elongation of 0.14%. Ti-10.02Mo alloy displays a high yield strength and high UTS followed by less work hardening, resulting in a high elongation of 0.71% as compared to all other designed alloys. Ti-12.89Mo show no yield strength due to the removal of the extensometer with moderate UTS followed with the lowest work hardening effect and the lowest elongation of 0.09%. The Ti-10.83Mo alloy show a high yield strength and ultimate tensile strength with excellent ductility. It was considered to be suitable for biomedical application.

The high yield strength and UTS found in Ti-10.02Mo alloy as compared to Ti-12.89Mo may be attributed to the high-volume fraction of the omega phase as it was evident in the EBSD maps. The Ti-10.83Mo alloy show the highest UTS with no yield and this may be attributed to the solution strengthening effect, because the EBSD maps did show a low volume fraction of the omega phase as compared to Ti-10.02Mo alloy. The ultimate tensile strength of as-cast Ti-10.83Mo alloys were found to be higher as compared to commercially available Ti6Al4V alloy reported by Niinomi, (2008). It was challenging to compare the as-cast Ti-Mo alloys with the ones found in literature as there are limited research on the tensile properties of Ti-Mo alloys in as-cast conditions. It is also noticeable that it will be difficult to compare the mechanical properties of Ti-Mo alloys after tensile with the other binary alloy such as Ti-Sn due to less published work in literature.

The elastic admissible strain defined by Song et al, (1999) and Ozan *et al.*, (2015) as the ratio of yield strength or tensile strength over elastic modulus. It a useful parameter in the design of biomedical implants material. The higher the elastic admissible strain the more desirable the material is for biomedical application. Out of the as-cast Ti-Mo alloys, Ti-10.83Mo and Ti-15.05Mo alloys showed the highest elastic admissible strain

than all the alloys and also it was higher than the commercially available Ti6Al4V alloy, this implied that the developed and designed Ti-10.83Mo and Ti-15.05Mo alloys showed potential use in the biomedical implants materials as compared to other alloys.

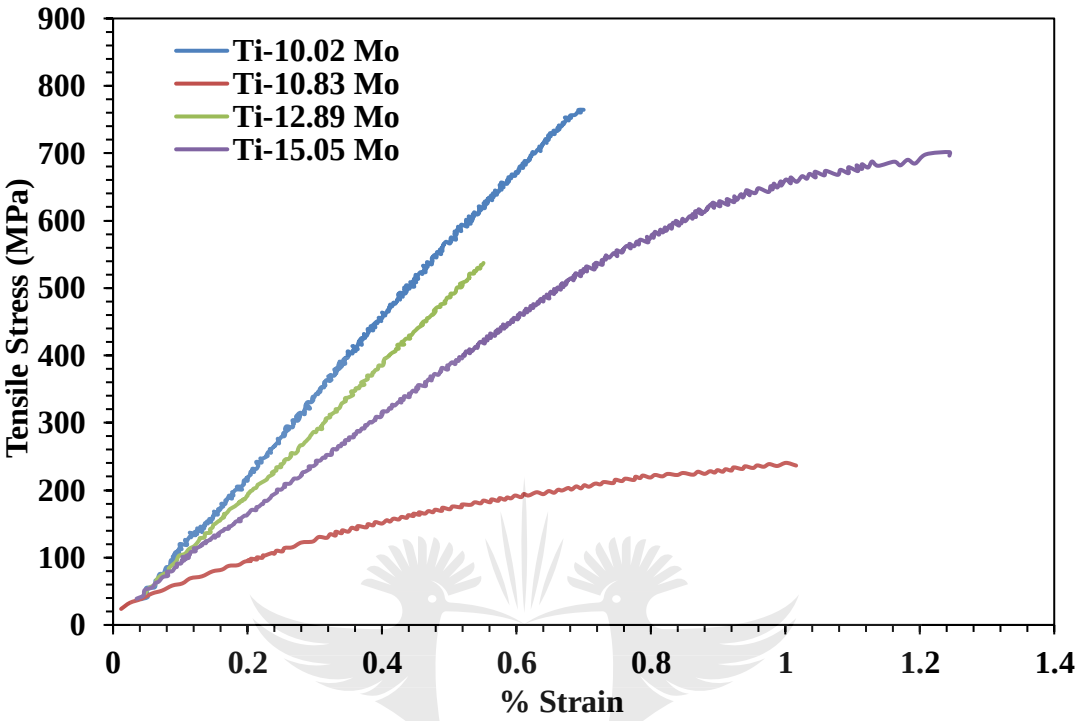

Figure 4. 16: Tensile stress vs % Strain graph of as-cast Ti- Mo alloys.

Table 4. 5: Tensile test data of as-cast Ti-Mo alloys

Alloy Name	Y.S (MPa)	UTS (MPa)	% Elongation	Elastic Modulus (GPa)	Elastic Admissible strain
Ti-10.02 Mo	741.07	662.99	0.71	113.0	0.586 %
Ti-10.83 Mo	-	885.45	0.35	105.17	0.842 %
Ti-12.89 Mo	-	643.10	0.09	104.47	0.616 %
Ti-15.05 Mo	542.47	593.48	0.14	70.48	0.842 %
Ti6Al4V (Niinomi, (2008)	**-**	**869**	**-**	**124**	**0.700%**

Figure 4. 17 shows the stress-strain curve of the solution treated alloys after tensile test. The tensile test data of these designed alloys recorded before the extensometer was removed are presented in Table 4. 6. Amongst the designed alloys, Ti-10.83Mo alloy shows a higher yield strength and UTS followed by extensive work hardening, resulting in higher elongation of 26.17%, Ti-10.02Mo alloy displays a high yield strength and lower UTS followed by extensive work hardening, resulting in a high elongation of 20.71% as compared to Ti-12.89Mo and Ti-15.05Mo alloys. Ti-12.89Mo displayed the lowest yield strength with moderate elongation, whereas Ti-15.05Mo was characterized with the lowest elongation of 6.95%.

The increase in the ultimate tensile strength and decrease in the ductility as the Mo content increase was attributed by the solid solution strengthening effect Hanada and Izumi, (1986). The yield strength of the designed Ti-10.02Mo and Ti-15.05Mo alloys were significantly higher than the ones reported by Wang *et al.*, (2016), however their ultimate tensile strength and elongation were lower than those reported by the same authors. The Ti-10.83Mo alloy show a high yield strength and ultimate tensile strength with excellent ductility, these properties are suitable for biomedical application however the alloy exhibited a higher elastic modulus as compared to Ti-15.05Mo.

The elastic admissible strain defined by Song et al, (1999) and Ozan *et al.*,(2015) as the ratio of yield strength over elastic modulus. It a useful parameter in the design of biomedical implants material. The higher the elastic admissible strain the more desirable the material is for biomedical application. The solution treated Ti-10.02, Ti-10.83 and Ti-.15.05Mo show high elastic admissible as compared to Ti-12.89Mo alloy, however Ti-15,05Mo proved to be a potential alloy to be used in the biomedical implants than the other alloys. As compared to the commercially available Ti6Al4V, CP-Ti and other work reported by different authors, the designed Ti-15.05Mo alloy show the highest elastic admissible strain in solution treated condition, implying that the developed and designed Ti-15.05Mo alloy can be suitable for biomedical application as compared to other alloys owing to its low elastic modulus after quenching.

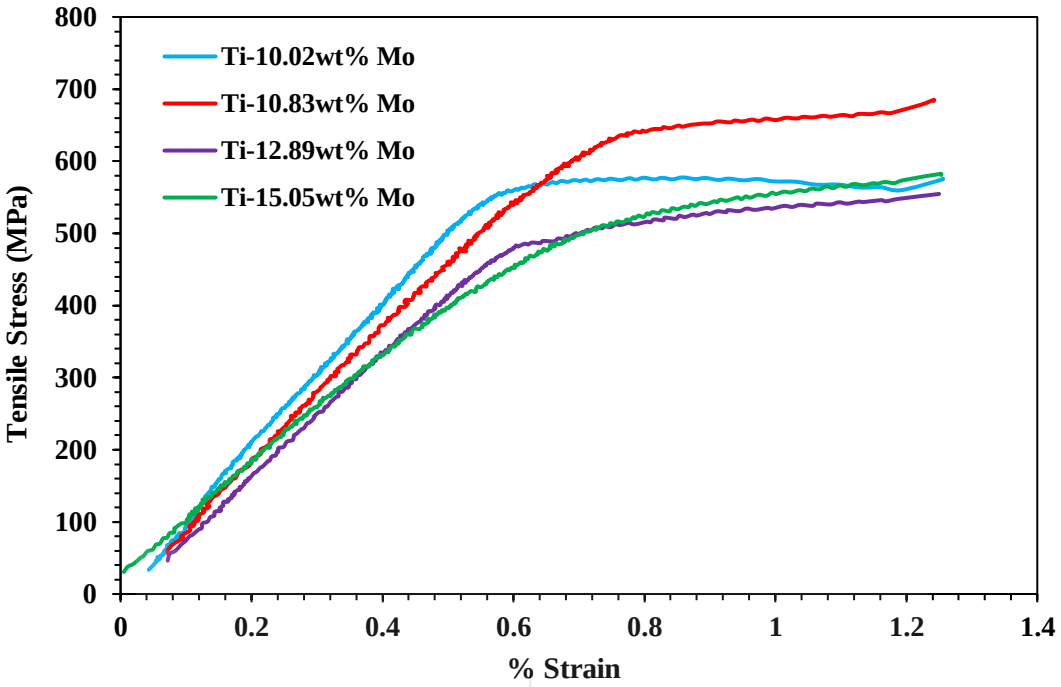

Figure 4. 17: Tensile stress vs % strain curve of solution treated Ti-Mo alloys.

Table 4. 6: Tensile test data of Solution treated Ti-Mo alloys.

Alloy Name	Y.S (MPa)	UTS (MPa)	% Elongation	E (GPa)	Elastic Admissible strain
Ti-10.02wt% Mo	594.31	684.65	20.71	95.17	0.719%
Ti-10.83wt% Mo	642.40	764.22	26.15	93.19	0.820%
Ti-12.89wt% Mo	515.37	718.23	16.60	110.25	0.651%
Ti-15.05wt% Mo	546.34	705.91	6.95	72.59	0.972%
Ti6Al4V(Niinomi, (1998)	**825**	**-**	**6**	**114**	**0.723%**
CP-Ti (Niinomi, 1998)	**485**	**-**	**24**	**103**	**0.471%**
Ti-10Mo (Wang *et al* 2016)	**420.31**	**756.17**	**24.02**	**97.03**	**0.779%**
Ti-15 Mo (Wang *et al.*, 2016)	**302.18**	**739.38**	**29.02**	**104.06**	**0.711%**
Ti-15 Mo (Zhao *et al.*, 2012)	**410**	**680**	**49**	**79**	**0.861%**

4.3.2.2 Elastic modulus of as-cast and solution treated Ti-Mo alloys

The elastic modulus of the as-cast binary Ti-Mo alloys are illustrated in Figure 4. 18. As it could be seen, the elastic modulus decreased when the Moeq/ Mo content increases. The highest elastic modulus seen in Ti-10.02Mo alloy was attributed to the high volume fraction of the omega phase as observed in the EBSD phase maps as seen in Figure 4. 10. It was reported by Hao *et al.,* (2006) that a small volume fraction of the omega phase can have a detrimental effect on the mechanical properties especially the elastic modulus. Graft (1957) also indicated that the ω phase had an unusually high elastic modulus. The decrease in the elastic modulus in Ti-10.83Mo, Ti-12.89Mo and Ti-15.05Mo alloys were attributed to the decrease in the precipitation omega phase as seen in the EBSD results In Figure 4. 11, Figure 4. 12 and Figure 4. 13.

The phases influence the elastic modulus in the following manner as reported by $E_{\omega} > E_{\alpha'} > E_{\alpha''} > E_{\beta}$, Lee *et al* (2002). The elastic modulus of the omega phase is higher than the elastic modulus of martensitic phase and generally the β alloys have the lowest elastic modulus. The elastic modulus of the as-cast Ti-Mo alloys were lower than commercially available Ti6Al4V as reported by Niinomi, (2008). It was hard to compare the elastic modulus with the Ti-Mo alloys reported by Ho, *et al* (1999) in as-cast conditions and Ti-Sn alloys because they reported on the bending modulus only and the elastic modulus results were obtained from tensile test. This study was able to design and developed binary Ti-Mo alloys, Ti-15.05Mo alloy possess grater chances of being used for biomedical application owing to its low elastic modulus after casting.

The elastic modulus of solution treated binary Ti-Mo alloys are illustrated in Figure 4. 19. As shown in the Figure 4. 19, the elastic modulus fluctuates as the amount of the β stabilizing element increases, it begins as being high at Ti-10.02Mo (95.17 GPa), it decreases at Ti-10.83Mo (93.19 GPa), it significantly increases at Ti-12.89Mo alloy (110.25 GPa) and it cardinally decrease when the Mo content rises to Ti-15.05Mo (72.59 GPa). The high elastic modulus in Ti-10.02Mo alloy was reference to the amount of precipitation of the omega phase as evident on the EBSD maps in Figure 4. 10, the omega phase is reported by Hao *et al.,* (2006) to be deleterious and harmful to the mechanical properties as it increase the elastic modulus. It's been reported by Lee (2002) that the ω phase have a higher elastic modulus than β and martensitic α″ phase.

The decrease in the elastic modulus in Ti-10.83Mo may be ascribed by the low volume fraction of the omega (ω) phase precipitates as observed in the EBSD maps in Figure 4. 11 implying that the stability of the β phase and suppression of the precipitation of other phases was more pronounced. The escalated elastic modulus when the Mo content was increased in Ti-12.89Mo was attributed to the high quantity of the omega (ω) phase particles as displayed in the EBSD maps in Figure 4. 12. It is well known that the omega phase has a significant effect on the mechanical properties of Ti alloys and it is likely to increase the elastic modulus Akahoria *et al* (2005). The decrease in the elastic modulus as the Mo content increased was ascribed by the stability of the β and the suppression of the orthorhombic martensitic α″ phase and this is evident in the XRD patterns, OM and SEM images in Figure 4. 2-Figure 4. 5, and Figure 4. 6-Figure 4. 9 respectively.

The elastic modulus of the designed alloys after solution treatment were found to be lower than the commercially available Ti6Al4V alloy reported by Niinomi M, (1986). The elastic modulus of the designed Ti-10.02Mo and Ti-15.05Mo alloys were found to be lower than those reported by Zhou and Luo, (2011), Zhao *et al.*, (2012), Cardoso *et al.*, (2014) and Wang *et al.*, (2016) in solution treatment conditions. This study was able to design and developed binary Ti-Mo alloys, Ti-15.05Mo alloy which possess grater chances of being used for biomedical application owing to its low elastic modulus after solution treated conditions.

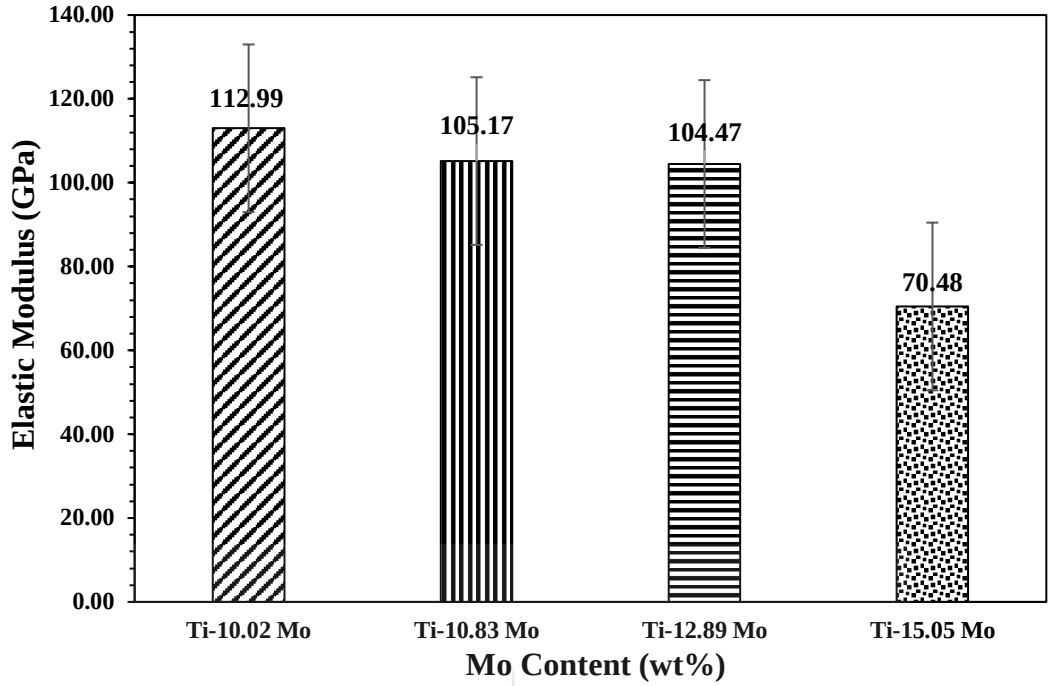

Figure 4. 18: Elastic Modulus of Ti-Mo alloys in as-cast conditions.

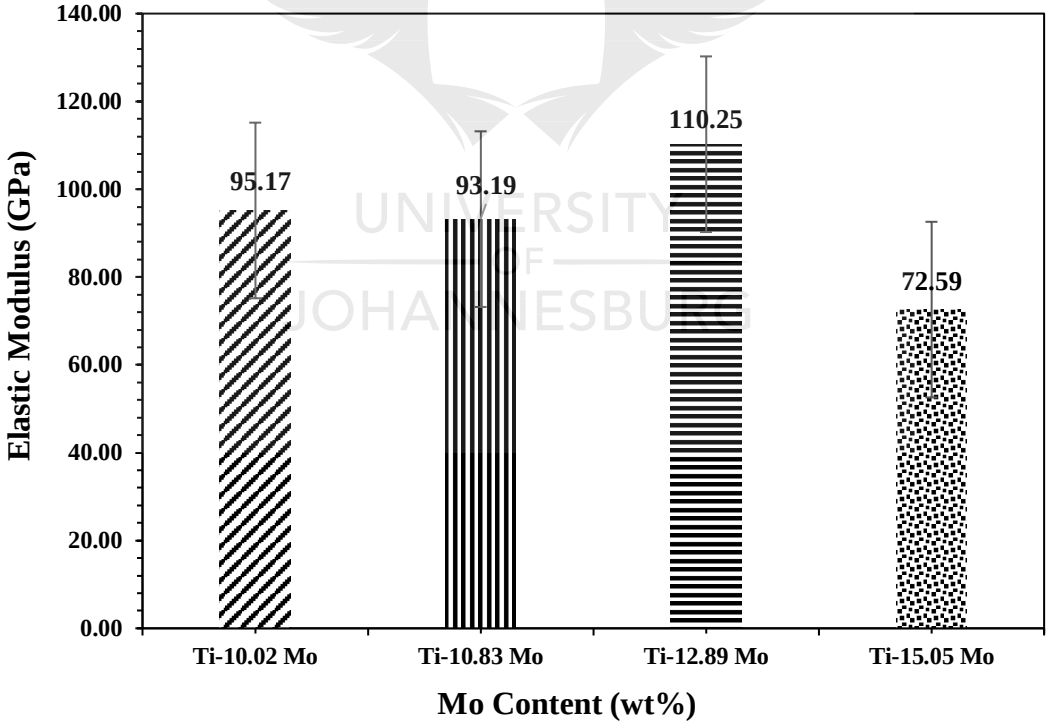

Figure 4. 19: Elastic Modulus of solution treated Ti-Mo alloys.

4.3.2.3 Fracture Surfaces of As-Cast and solution treated alloys after Tensile Test

Figure 4. 20 displays the SEM fracture surface of the as-cast Ti-Mo alloys after tensile test. Ti-10.02Mo illustrate both dimples features and cleavage facets but apart from the dimple features, cleavage facets are more pronounced which indicates that Ti-10.02Mo alloy experienced both brittle and ductile fracture however due to pronounced cleavage facet brittle fracture was more dominant than ductile fracture and it is also evident in the tensile stress-strain curve. Ti-10.83Mo alloy showed small dimples features without the presence of cleavage facets implying ductile fracture and it was noticeable in the tensile stress-strain curve in figure 4.17. Ti-12.89Mo and Ti-15.05Mo alloys showed more cleavage features with small dimple feature.

Figure 4. 21 (a-d) displays SEM micrographs of the fractured surface of the solution treated of the designed Ti-Mo specimens after tensile test. As displayed by the Figure 4. 20 the designed alloys were characterized by both cleavage facets and dimples ruptures. The Ti-10.02Mo alloy in Figure 4. 21 (a) was represented by a high amount of smooth cleavage facets than dimples ruptures in the fractured surface which is an indicative of a typical brittle fracture. The Ti-10.83Mo alloy was comprised of small dimples ruptures and cleavage facets in the fractured surface but the small dimples were more definite and that was prophecy of high ductility and ductile fracture.

The Ti-12.89Mo alloys was composed of medium dimples features with cleavage facets in the SEM fractography indicative of both ductile and brittle fracture. The Ti-15.05Mo alloy was characterized by large dimples features with less cleavage facets, even though the ductility of this alloy decreased this alloy indicated a ductile fracture. The fracture surface of the designed Ti-10.02Mo and Ti-15.05Mo alloys were not in agreement with those found by (Wang *et al.*, 2016), as the author reported that the alloys were characterized by ductile fracture only

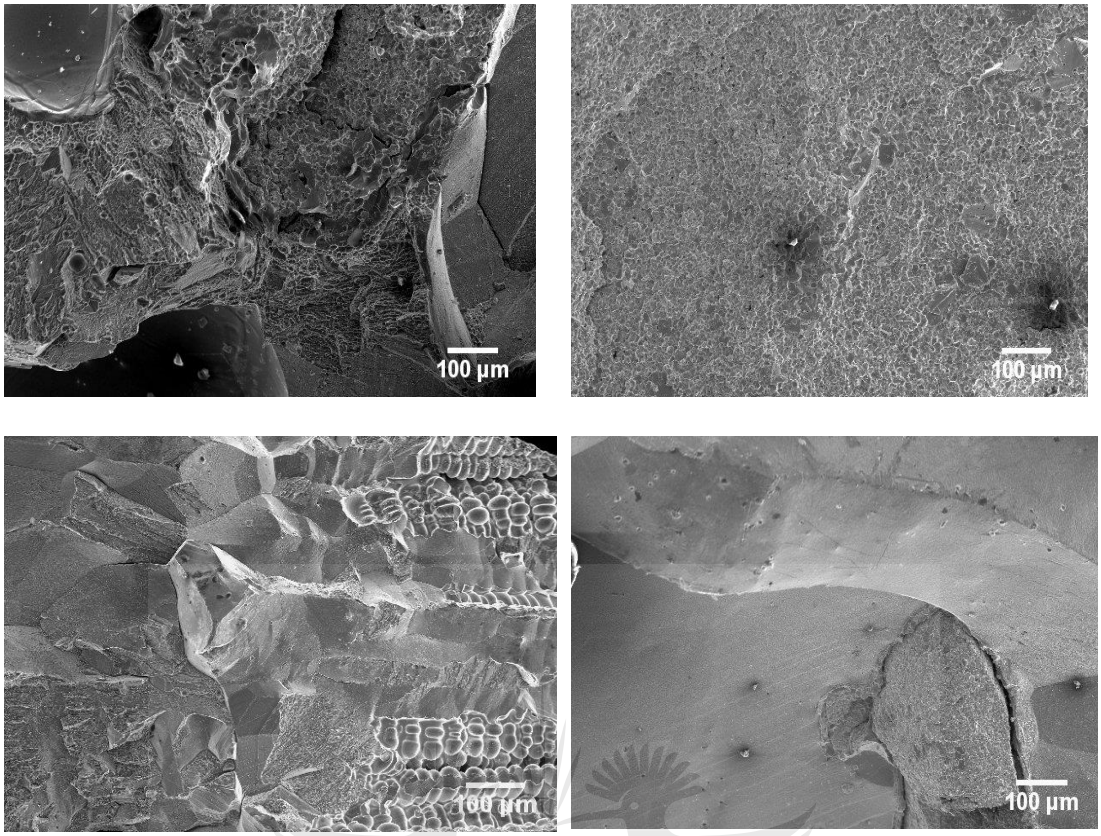

Figure 4. 20 : Tensile fracture surfaces of as-cast (a) Ti-10.02 Mo,(b) Ti-10.83 Mo, (c) Ti-12.89 Mo and Ti-15.05 Mo alloys.

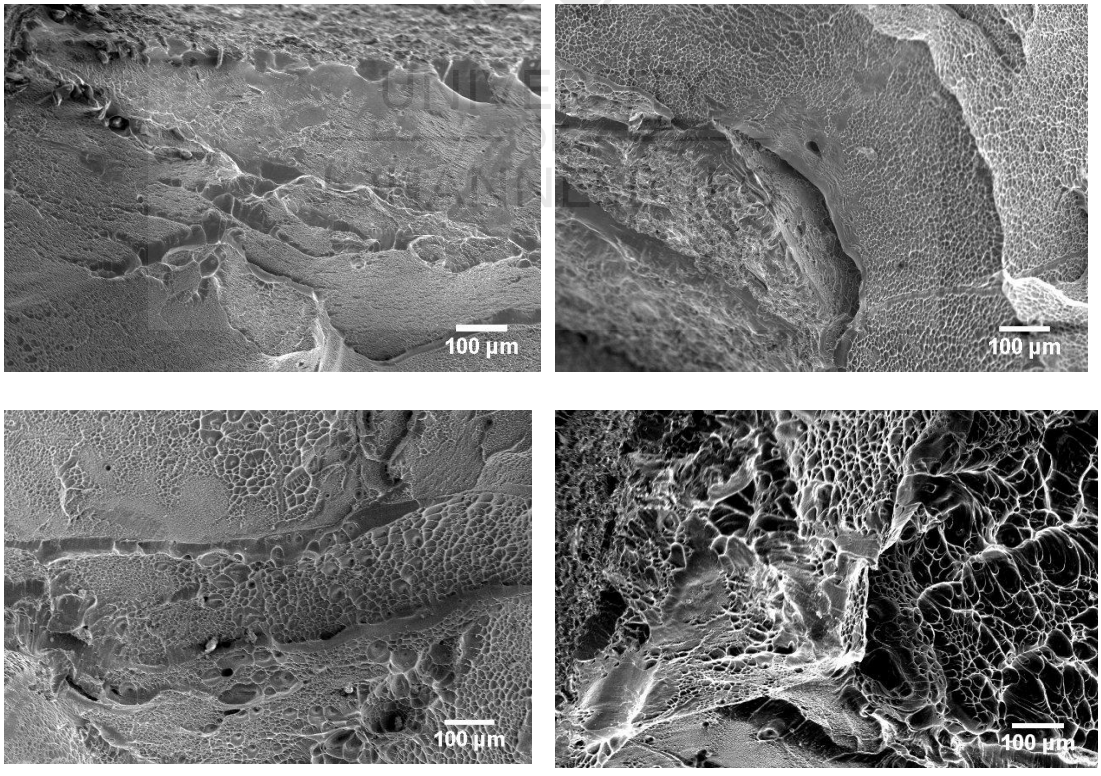

Figure 4. 21: Tensile Fracture Surfaces of solution treated (a) Ti-10.02 Mo, (b) Ti-10.83 Mo, (c) Ti-12.89 Mo and (d) Ti-15.05 Mo alloys.

4.3.3 Bending properties of as-cast and solution treated Ti-Mo alloys

4.3.3.1 Bending Strength and flexural stress vs extension curve of as-cast Ti-Mo alloys

The bending strength and the flexural stress vs extension curve of as-cast Ti-Mo alloys are illustrated in Figure 4. 22 and Figure 4. 23 respectively. As it can be seen in the Figure 4. 22, the bending strengths of the as-cast Ti-Mo alloys are fluctuating, the lowest bending strength is found in Ti-12.89Mo alloy whereas the highest bending strength is seen in Ti-10.83Mo alloy. According to the flexural stress vs extension, Ti-10.83Mo and Ti-15.05Mo alloy show the highest strengths with the largest extension as compared to Ti-10.02Mo and Ti-12.89Mo which show lower strength with low flexural extension. It was important to note that despite the strong hardening effect of the omega phase in Ti-10.02Mo, the bending strength was low as compared to those alloys that didn't have a high fraction of the omega phase e.g. Ti-15.05Mo alloy. The high bending strength in Ti-10.83Mo and Ti-15.05Mo was characterized by the premature brittle fracture that occurred in this alloy but not in Ti-10.02Mo and Ti-12.89Mo. The omega induced embrittlement of the β phase was considered by Williams and Paton, (1973). The high bending strength in those alloys may be due to the brittle fracture as this alloy didn't show a high-volume fraction of omega phase precipitates as shown in the EBSD maps in Figure 4. 11 (a) and Figure 4. 13 (b).

The bending strength of the Ti-10.02Mo alloy, the Ti-12.89Mo alloy is lower but the Ti-15.05 Mo alloy is higher as compared to the ones reported by (Ho, 2008) in as-cast conditions (1752 MPa in Ti-10Mo, 1440 MPa in Ti-12.5Mo and 1348 MPa in Ti-15Mo). The bending strength of commercially available Ti6Al4V alloy was found to be higher than that of the studied alloys except for Ti-10.83Mo. When comparing Ti-10.02Mo alloy with other binary alloys such as Ti-10Cr alloy Ho *et al*, (2009) and Ti-10Sn Hsu *et al*,(2009), it was found that Ti-10.02 Mo show the lowest bending strength.

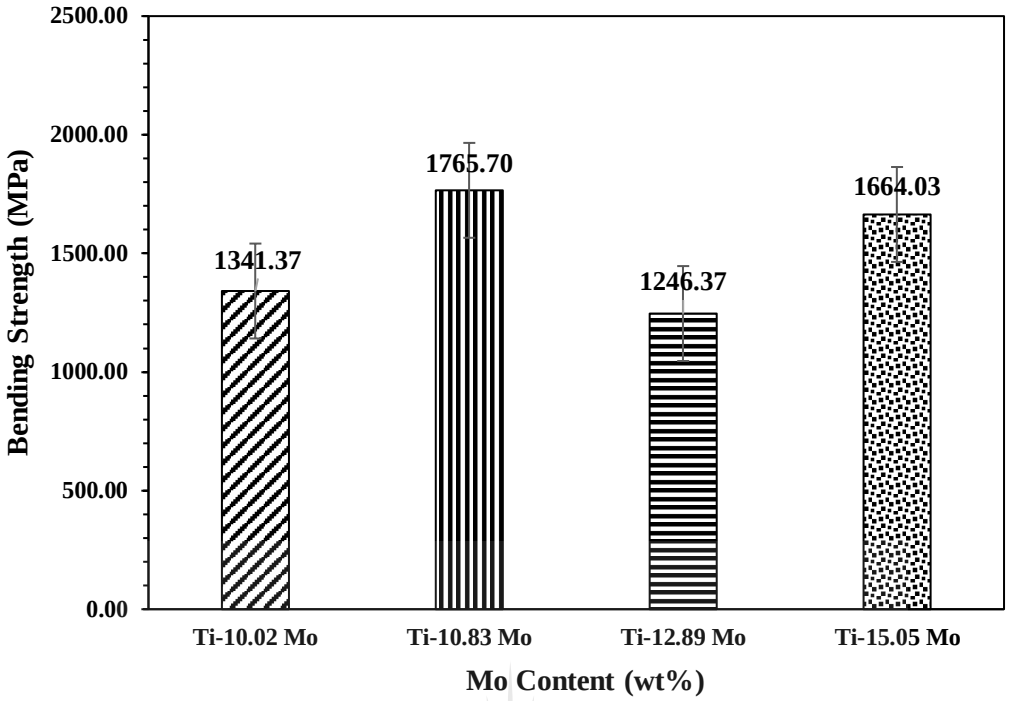

Figure 4. 22: Bending Strength of Ti-Mo alloys in as-cast condition.

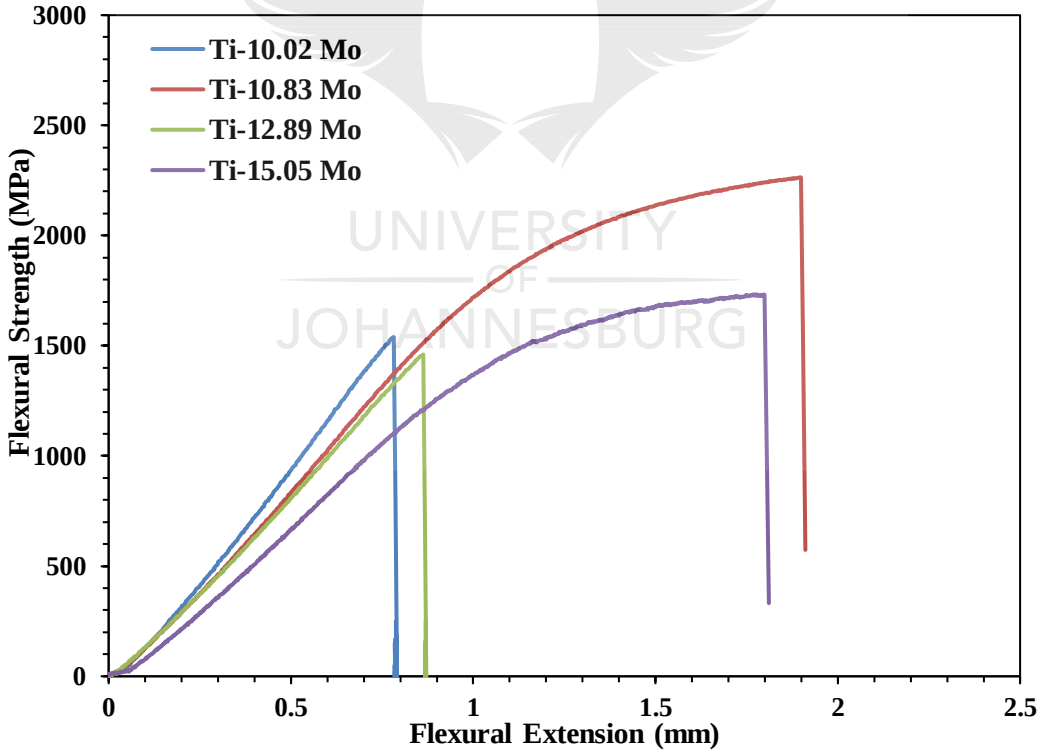

Figure 4. 23: Flexural stress vs extension curve for as-cast Ti-Mo alloys.

4.3.3.2 Bending Strength and flexural stress vs extension of Solution Treated Alloys.

The bending strength and the typical flexural stress vs extension profiles of the series of Ti-Mo alloys are illustrated in Figure 4. 24 and Figure 4. 25 respectively. The designed Ti-10.02Mo alloy shows low strength of 1529.30 MPa with extensive work hardening effect and flexural extension of above 8mm. The Ti-10.83Mo alloy displayed the highest bending strength followed by moderate work hardening and a flexural extension of above 7 mm, while the Ti-12.89Mo alloy illustrated the lowest bending strength with weak work hardening and a flexural extension of above 6mm and Ti-15.05Mo alloy showed a high bending strength followed by low work hardening with flexural extension of above 4mm.

The high bending strength in Ti-10.83Mo and Ti-15.05Mo was attributed to the higher volume fraction of the omega phase [refs]. It can be assumed that the omega phase induced embrittlement of the β phase as proposed prior by Williams and Paton, (1973). Despite the strong hardening effect of the omega phase in Ti-10.02Mo and Ti-12.89Mo, as also evident in the EBSD maps in Figure 4. 10 and Figure 4. 12, findings from this study show that it did not cause an increase in the bending strength (particularly in Ti-10.02Mo and Ti-12.89Mo alloys).

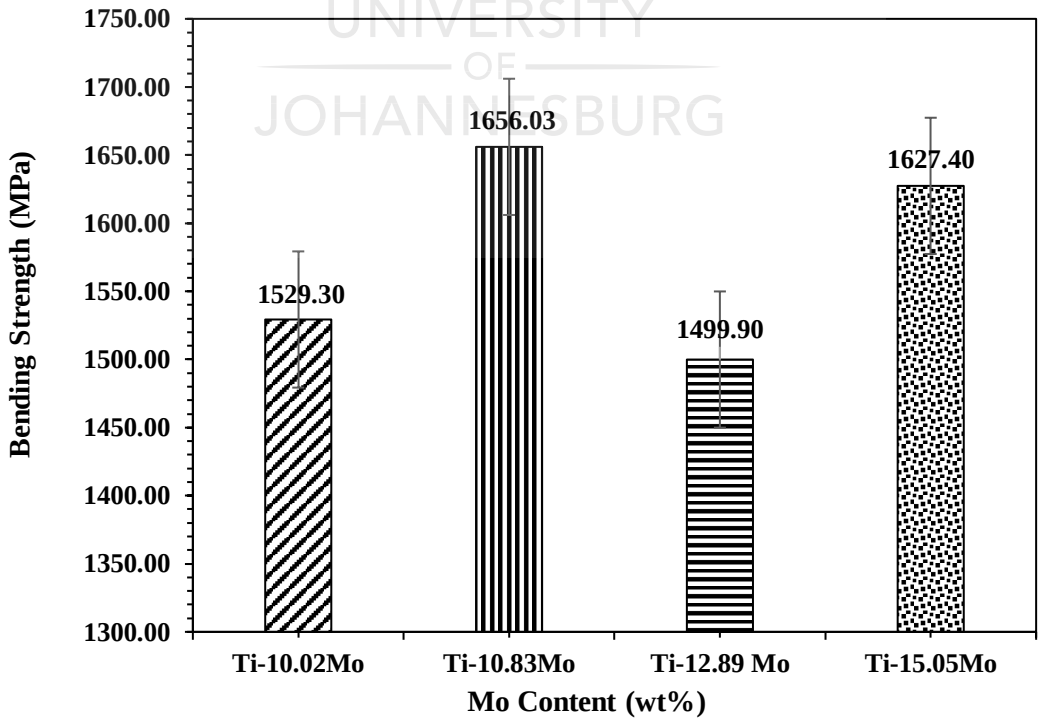

Figure 4. 24: Bending Strength of solution treated of Ti-Mo alloys.

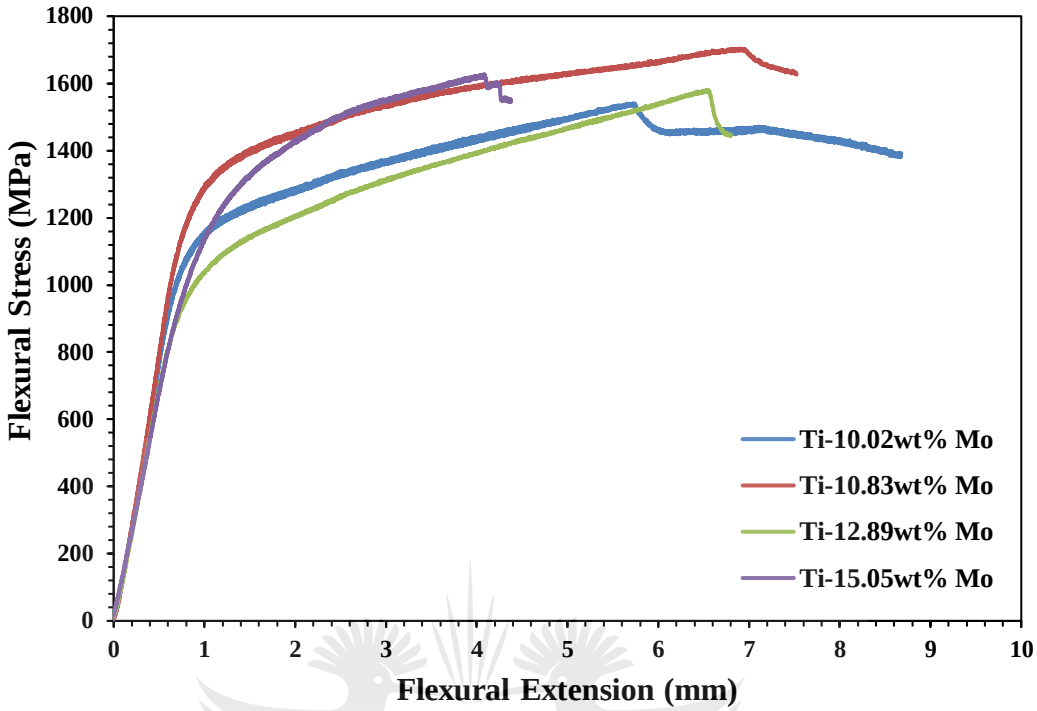

Figure 4. 25: Flexural stress vs extension of solution treated Ti-Mo alloys

4.3.3.3 Fracture surfaces of as-cast alloys after 3-point Bend Test

The fracture surfaces analyzed using the SEM technique were illustrated in Figure 4. 26. Ti-10.02Mo and Ti-10.83Mo alloys (Figure 4. 26 (a) and (b)) show small dimple features and cleavage facets with some small gas holes. Even though the alloys show small dimples the cleavage facets were more pronounced implying that the alloys deformed in a brittle fracture and ductile fracture manner. Ti-12.89Mo and Ti-15.05Mo alloys show only cleavage facets which implied that the alloy experienced brittle fracture.

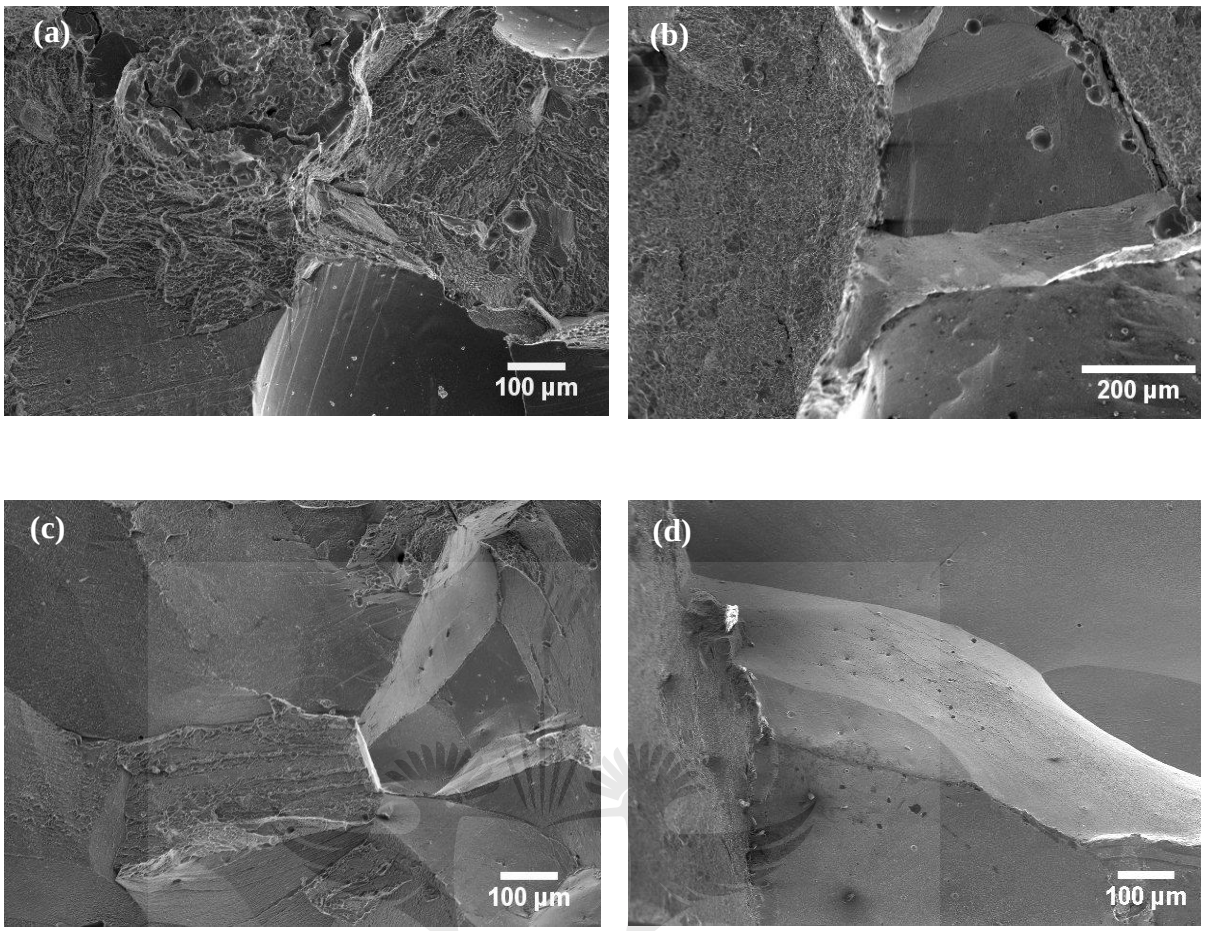

Figure 4. 26: Fracture surfaces of as-cast Ti-10.02Mo (a), Ti-10.83Mo (b), Ti-12.89Mo (c) and Ti-15.05Mo (d) after bending test.

4.3.4 Compression Properties of Solution treated Ti-Mo alloys.

4.3.4.1 Micro-hardness of compressed Ti-Mo alloys

The micro-Vickers hardness of the solution treated alloys after compression test are illustrated in Figure 4. 27. The graphs showed an increase in hardness as the Mo content increased until the Mo content was at Ti-12.89Mo alloy and then it significantly decreased. The designed Ti-12.89Mo alloy displayed the highest micro-hardness after compression and this may be attributed to the high-volume fraction of the omega phase as it was evident in the EBSD maps in Figure 4. 12. The decrease in the micro-hardness in Ti-15.05Mo alloy may be attributed by the stability of the β phase as it was observed in the XRD, SEM and OM results. It was difficult to conclude on the decrease in the micro-hardness in Ti-15.05Mo alloy using the EBSD results due to the miss indexing that occurred during analysis of this alloy. The micro-hardness of the designed Ti-

15.05Mo alloy after compression test was discovered to be higher than the micro-hardness reported by Zhang *et al.*,(2015).

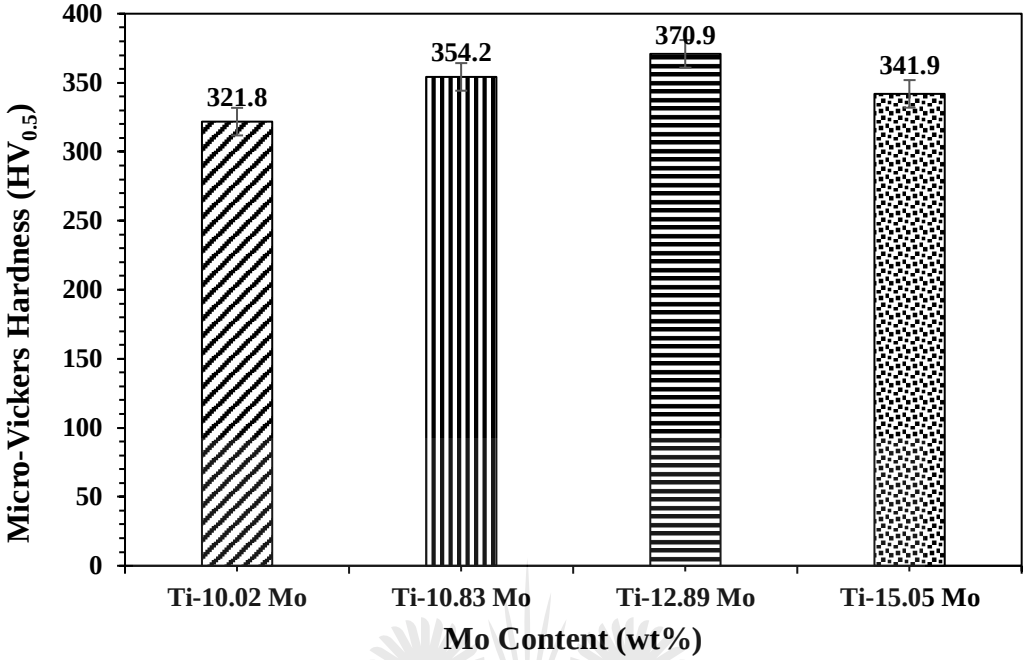

Figure 4. 27: Micro-Hardness of compressed Ti-Mo alloys.

4.3.4.2 Compressive Strength of the designed Ti-Mo alloys after solution treatment

Figure 4. 28 shows the compressive strength of the solution treated Ti-Mo binary alloys. The compressive strength of the designed Ti-15.05Mo alloy possessed the highest strength, whereas Ti-12.89Mo alloy show the lowest compressive strength. The compressive strength of the designed alloys is inversely proportional to the micro Vickers hardness. The compressive strength of Ti-15.05Mo alloy was higher whereas it displayed the lowest hardness value. The high compressive strength may be attributed by the solid solution strengthening effect. The high strength could not be attributed by the premature brittle fracture because the samples didn't fracture or break. The compressive strength for Ti-12.89Mo alloy was lower whereas it showed the highest hardness value. The low compressive strength in Ti-12.89Mo alloy is still under investigation. The compressive strength of the designed Ti-15.05Mo alloy was found to be lower than the one reported by Zhang *et al.*, (2015).

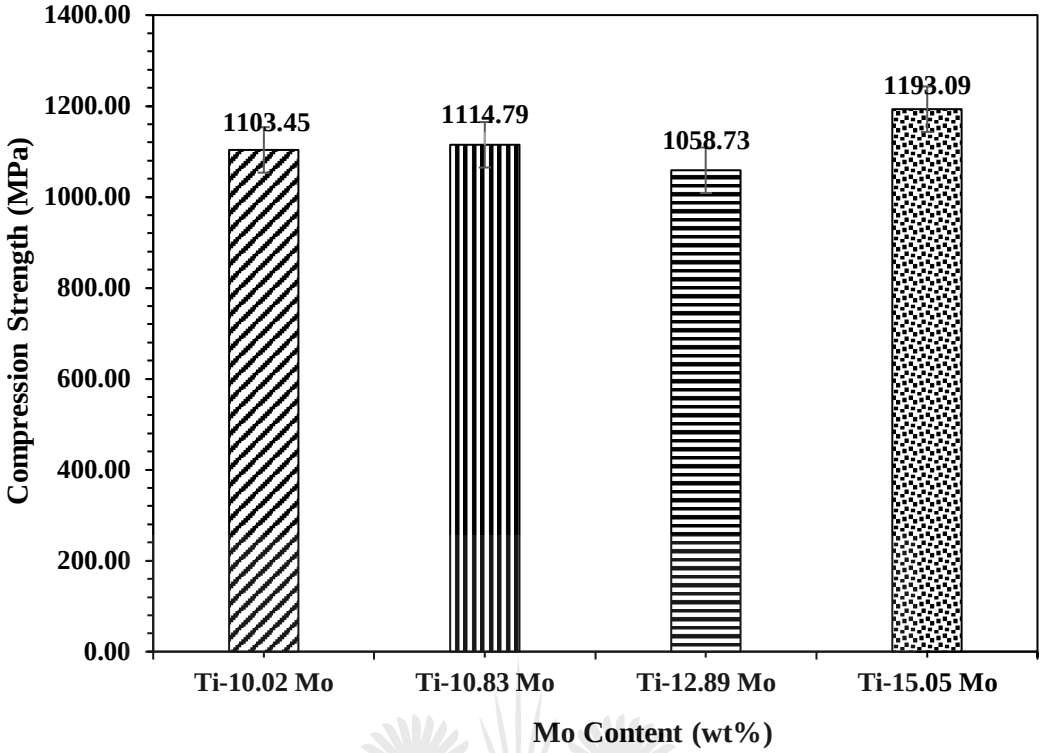

Figure 4. 28: Compression strength of binary Ti-Mo alloys.

The compressive stress-extension curves of the designed Ti-Mo alloys are depicted in Figure 4. 29. All the designed alloys exhibited an extensive plastic deformation behavior. The compressive stress –extension curves are comprised of two characteristic regions i.e. (I) the linear elastic region and (II) the plastic and yielding region Xu and Cai, (2017). The linear elastic region occurs due to the bending unit cell and when the compressive load continues to impose on material then a collapse of unit cell occur which is governed by the plastic yielding region. The plastic region occurs when stress intensity reduces when the samples is been loaded for a long period of time at a constant strain rate. It occurs due to the formation of shear bands Kusano *et al* (2010).

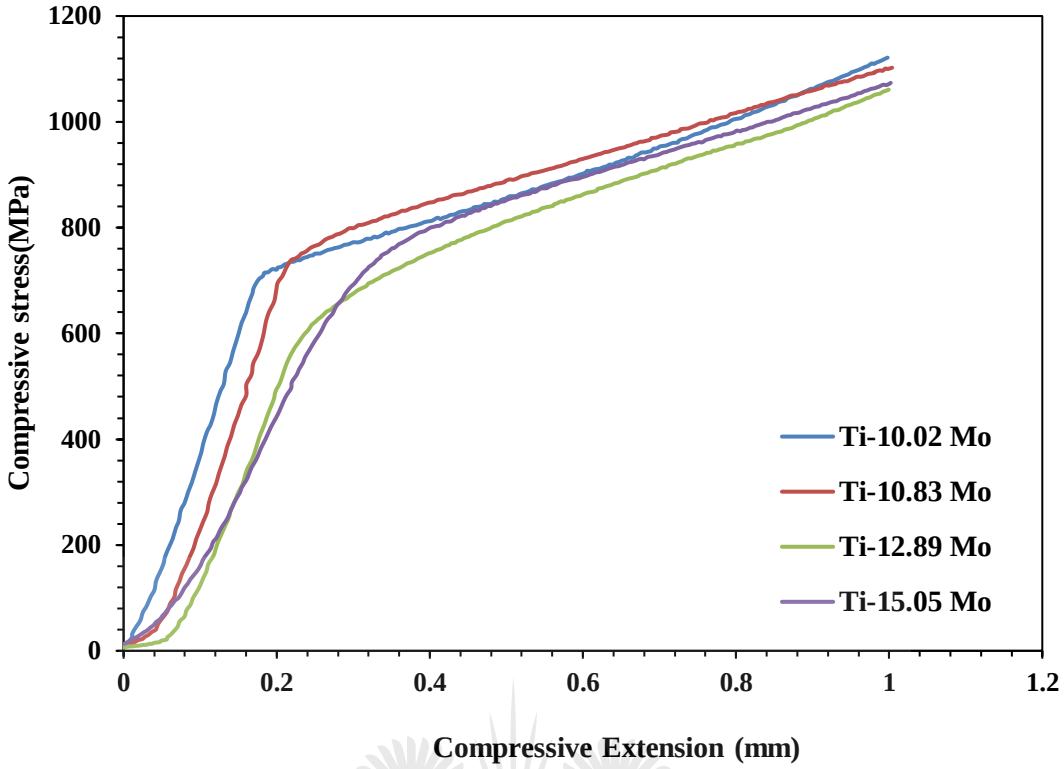

Figure 4. 29: Compressive stress vs extension curve for the designed alloys.

4.4 The Deformation behaviour of solution treated Ti-Mo alloys after compression Test.

The section of the experimental results is based on the deformation behavior explained by the Bo and Md phase stability maps. The calculated average Bo and Md parameters of the designed alloys are presented in Table 3.1 and they are superimposed on the stability map in Figure 3.2 in chapter 3.

4.4.1 Deformation Behaviors

4.4.1.1 Optical Microstructures after compression test.

In order to understand the deformation mechanism of the designed alloys, compression test was performed. Figure 4. 30 displays the optical microstructure of the designed alloys after deformation. It was observed that deformation induced products were present in all the designed alloys. Three types of deformation products were identified as: thin parallel plates, wide bands and wavy thin lines. The parallel plates were described as those related to the stress induced martensite and according to previous studies by Hanada and Izumi, (1986) on β Ti alloys, such wide deformation bands were

probably mechanical twins and the thinner deformation bands were described as those of slip.

The micrographs of the designed Ti-10.02Mo alloy was comprised with β gains and inside of those grains there were thin parallel plates, wider deformation bands, which implied that Ti-10.02Mo alloy undergo deformation by SIM and twinning. The Ti-10.83Mo alloy was comprised of wider β grains with parallel plates and wide deformation bands inside the grains and in addition to the parallel and wide band, there existed the thin deformation bands and this implied that this alloy undergo deformation by SIM+ twinning+ slip. As the Mo content increased (Moeq) the volume fraction of the parallel deformation plate decrease and wider deformation bands becomes more pronounced and this is more evident in the designed Ti-12.89Mo alloy which was comprised of wider bands and wavy thin deformation bands and this show that the alloy deformed by twinning and slip only. Further increase in the Mo content shows a decrease in the volume fraction of the wider deformation bands and the high quantity of the wavy thin deformation bands and this was show in the designed Ti-15.05Mo alloy as it consisted of β grains that exhibited thin wavy deformation bands illustrating deformation by twinning and slip, with slip mechanism being the dominant.
Sadeghpour *et al.*, (2018) reported similar micrographs in their research study Ti-4733, Ti-3573 and Ti-3873 alloys after different process such as hot rolling and compression test and also Xiang *et al.*, (2018) reported on the similar micrographs on the Ti-15.05Mo alloy after solution treatment and cold rolling.

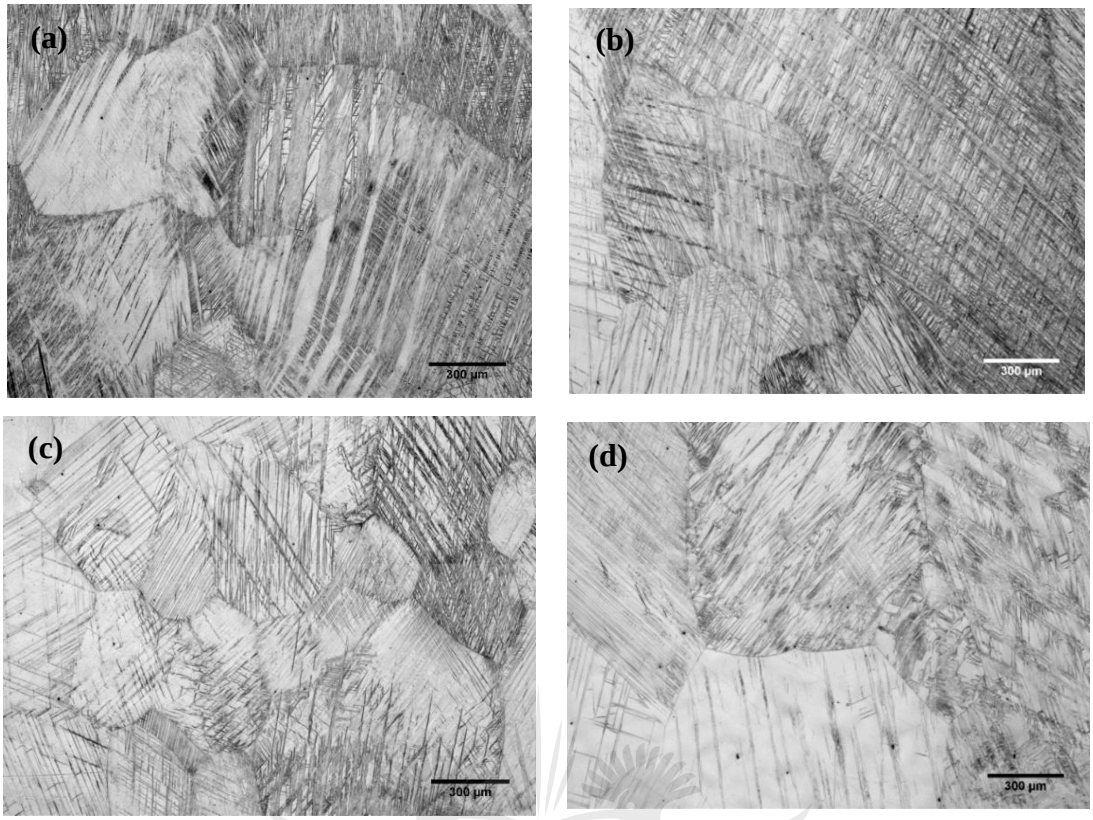

Figure 4. 30: Optical Micrographs of (a)Ti-10wt% Mo,(b) Ti-11wt% Mo, (c) Ti-13wt% Mo and (d) Ti-15wt% Mo alloys after compression test.

4.4.1.2 EBSD Maps after Compressed Samples:

EBSD analysis was used to identify the deformation mechanism on the designed Ti-Mo alloys. The EBSD band contrast and IPF maps of Ti-10.02Mo illustrated in Figure 4. 31 (a) and (b) respectively. The band contrast map shows the parallel deformation plates and wider deformation bands. The IPF map of Ti-10.02Mo displayed bigger β grains that exhibited parallel plates of orthorhombic martensitic and wider deformation bands. The occurrence of the orthorhombic martensitic was confirmed by the XRD peaks in Figure 4. 2. Therefore, this alloy is said to undergo SIM plus twinning transformation during deformation. The phase maps of Ti-10.02Mo alloy taken at low and high magnification are illustrated in Figure 4. 31 (c and d), they showed the presence of orthorhombic martensitic phase in a blue color, the athermal hexagonal omega phase in a red yellow and the matrix in a red color. According to the phase maps the parallel deformation plates and the wider deformation bands were comprised of high-volume fraction of the omega phase and high-volume fraction of orthorhombic martensitic α″ phase precipitated along the parallel and wider deformation bands. The high magnification phase map shows that the wider deformation bands was mostly

comprised of the bcc β phase, whereas the matrix was comprised of the omega phase with a high-volume fraction of the orthorhombic martensitic α″ phase. The EBSD results implied that this alloy was predicted to undergo deformation by SIM +stress induced hexagonal +twinning and Slip mechanism.

The EBSD band contrast and IPF maps of the designed Ti-10.83Mo alloy are displayed in Figure 4. 32 (a) and (b). The band contrast map showed wider deformation bands, with parallel plates and wavy thin deformation bands. The IPF maps illustrated wider β grains and thin deformation bands and particles inside the grains. The IPF also showed a lot of dark spots which are black marks or artifacts that may occurred during electropolishing. The phase maps at low and high magnification in figure Figure 4. 32 (c) and (d) showed that the particles were that of orthorhombic martensitic α" represented in a blue color, the athermal hexagonal omega phase in a yellow color and the bcc beta matric in a red color. A higher volume fraction of the omega phase was seen to be precipitated along the parallel plates and the wavy thin deformation bands. The volume fraction of the omega phase was observed to be lower as the one perceived in Ti-10.02Mo alloy. The EBSD characteristics indicated that the designed Ti-10.83Mo alloy undergo deformation by SIM + Twinning + Slip mechanism.

The EBSD band contrast and IPF maps of the designed Ti-12.89Mo alloy are demonstrated in Figure 4. 33 (a) and (b). The band contrast map exemplified parallel plates, wider bands and thin deformation bands. The IPF maps showed a lot of artifacts that may occurred during electropolishing, large β grains with parallel bands inside the grains and particles. The phase maps at low and high magnification illuminated in Figure 4. 33 (c) and (d) were characterized as those of orthorhombic martensitic α" represented in a blue color, the athermal hexagonal omega phase in a yellow color and the bcc beta matric in a red color. The phase maps also indicated a higher volume fraction of artifacts (dark spots) from electro-polishing. The phase maps at low magnification displayed a higher segment of orthorhombic martensitic precipitated inside the beta grains, whereas the higher magnification phase map characterized a higher content of the athermal hexagonal omega phase precipitated along the parallel bands. The fraction of the omega phase decreased as the Mo content increased. The EBSD results indicate that Ti-12.89Mo alloy undergo SIM + Twinning + Slip.

The EBSD band contrast and IPF maps of the designed Ti-15.05Mo alloy are illustrated in Figure 4. 34 (a) and (b). The band contrast map shows large β grains and within the grains there were wider deformation bands with less thin wavy deformation bands. The IPF maps displayed wider β grains and within the grains were particles shown with different colors. The phase map analyzed at high and low magnification in Figure 4. 34 (c and d) show that the particles were that of orthorhombic martensitic α″ phase represented in a blue color, the athermal hexagonal omega phase in yellow and the bcc beta matrix in red. A high-volume fraction of the omega and orthorhombic martensitic phase were seen to be distributed along the wider deformation bands. The volume fraction of the omega phase was observed to decrease at higher magnification within the designed Ti-15.05Mo alloy. In conclusion the volume fraction of the omega phase decreased as the Mo content increased. The EBSD analysis implied that the designed Ti-15.05Mo alloy undergo deformation by stress induced hexagonal + twinning and slip mechanism.

There is few literature that explain the detection of the omega phase using the EBSD technique especially for binary Ti-Mo alloys, however in their research study based on Ti-5Al-5V-5Mo-3Cr-0.5Fe alloy after solution treatment and compression test, Tayyeb *et al* (2019) observed the presence of the stress induced transformation omega phase using the EBSD technique. G.S.Dyakonovabe. *et al* (2015) also reported on the presence of the omega phase in the EBSD maps.

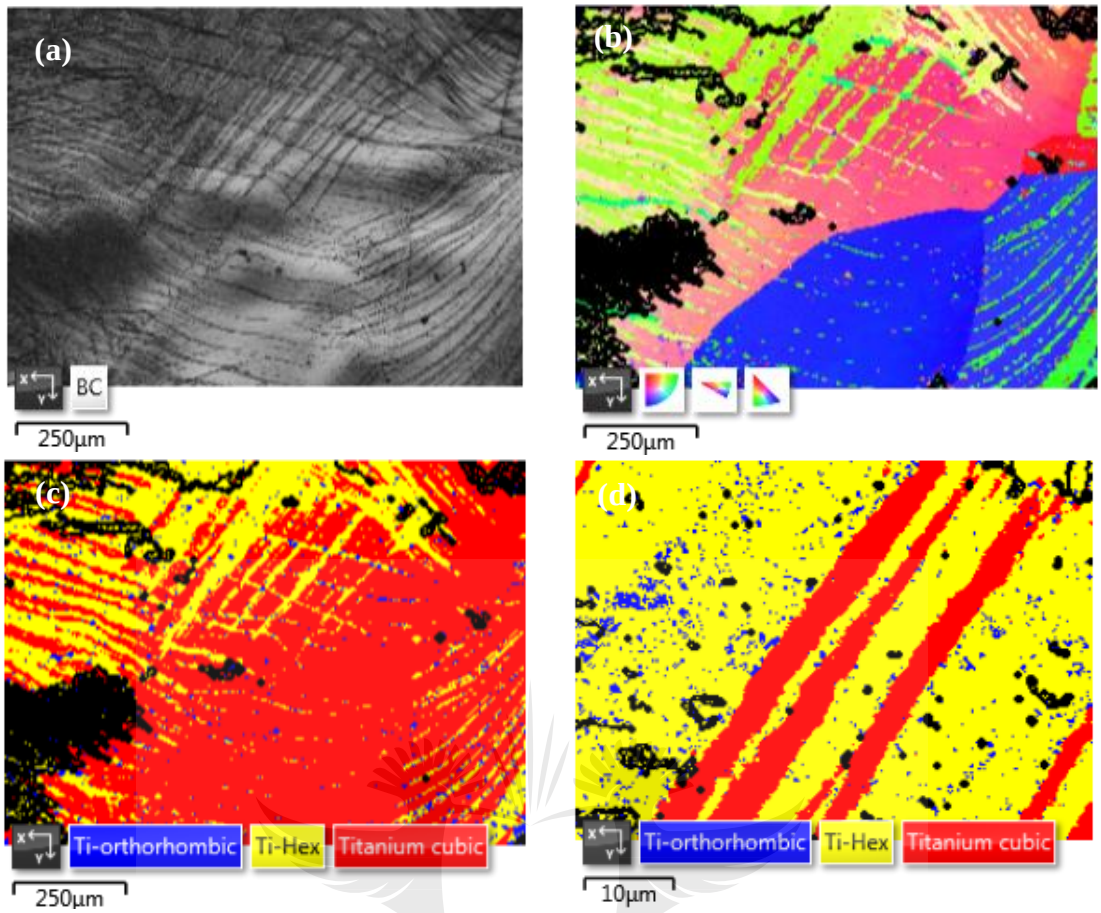

Figure 4. 31: EBSD band contrast, IPF maps and Phase maps of deformed Ti-10.02wt% Mo alloy.

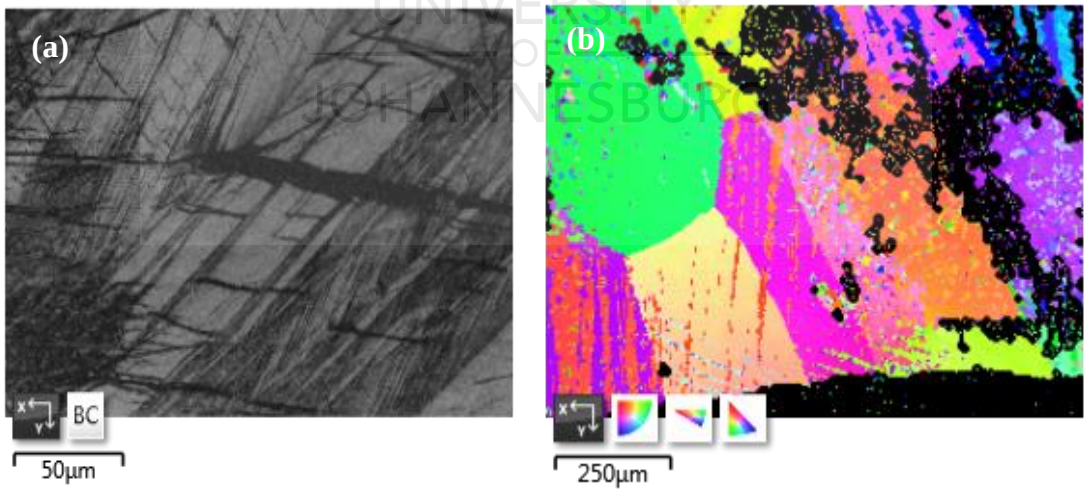

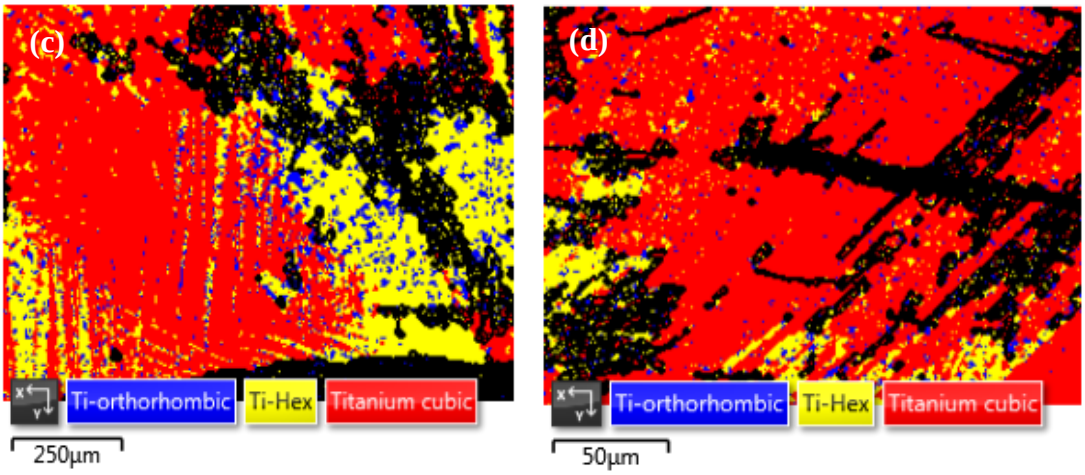

Figure 4. 32 : EBSD band contrast, IPF maps and Phase maps of deformed Ti-10.83wt% Mo alloy

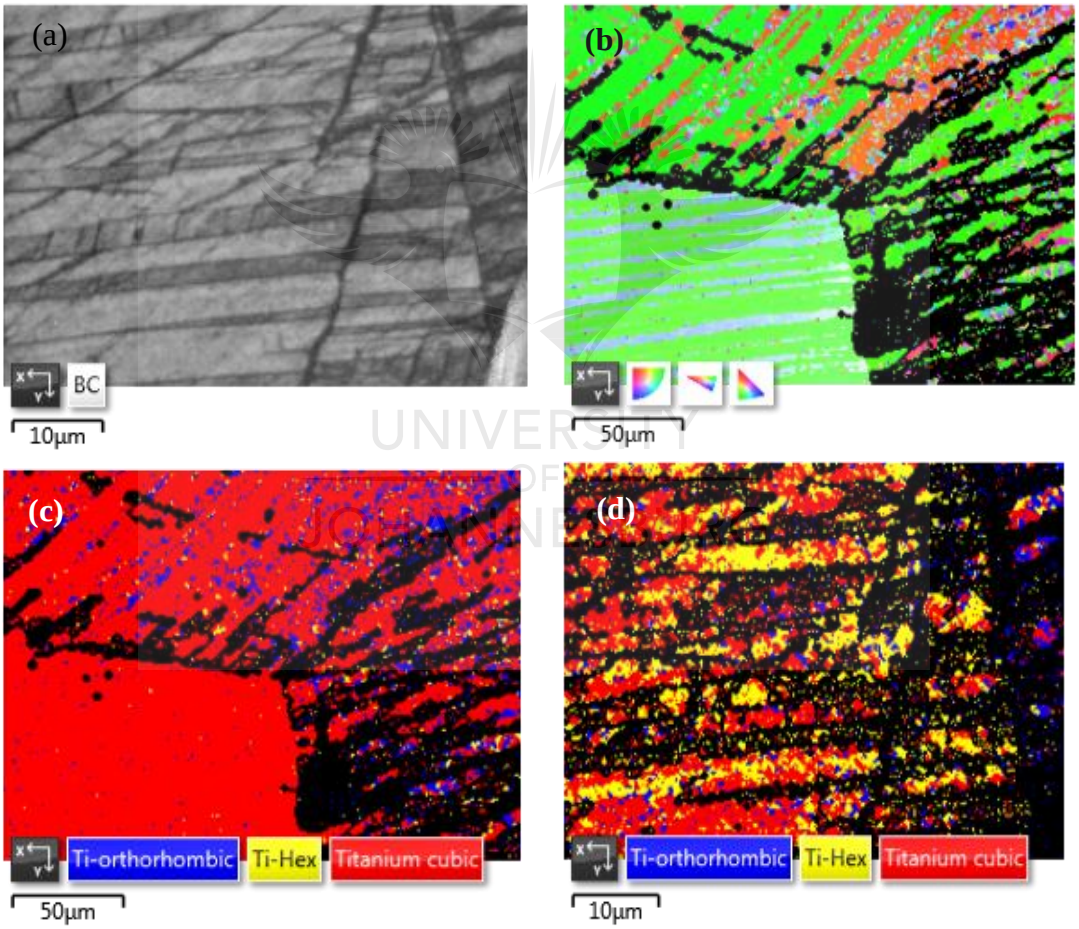

Figure 4. 33 :EBSD band contrast, IPF maps and Phase maps of deformed Ti-12.89wt% Mo alloy

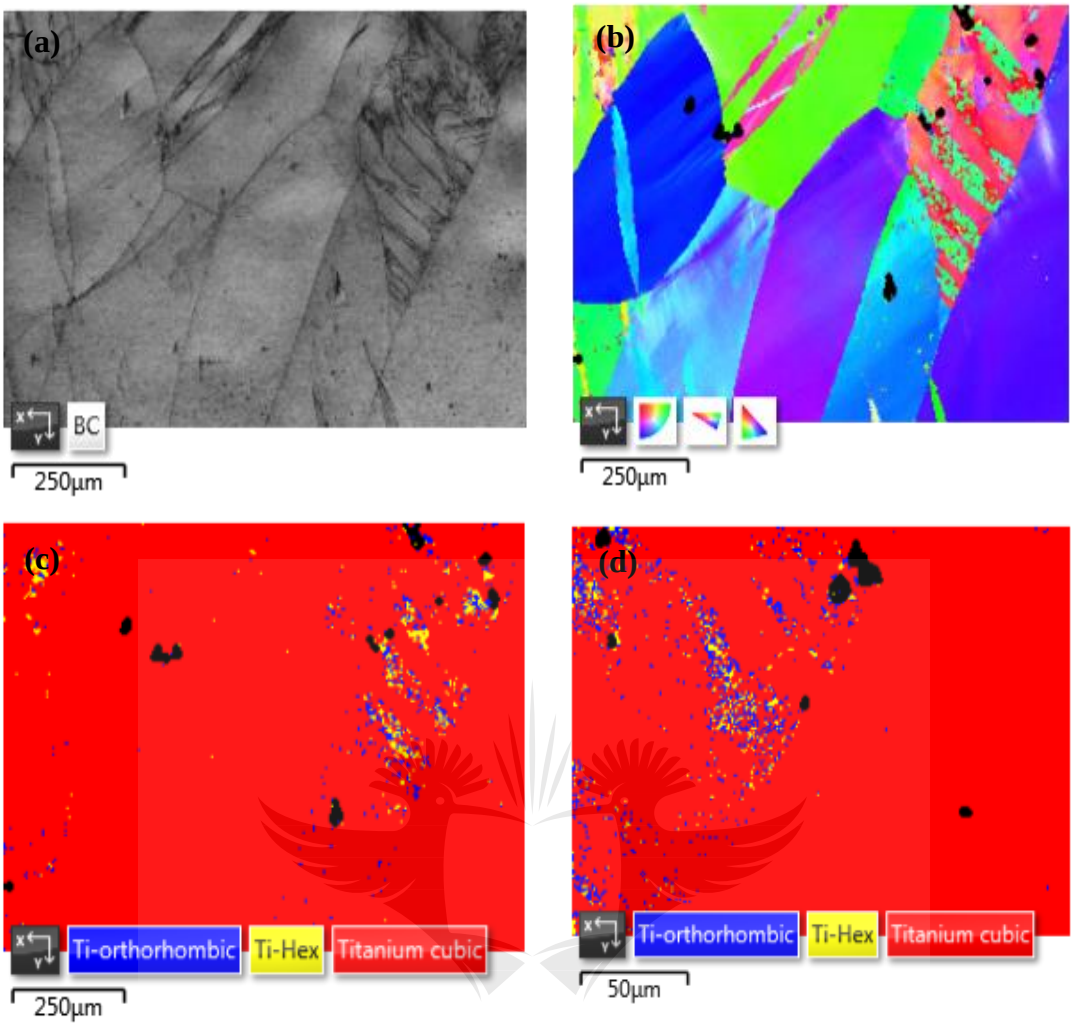

Figure 4. 34: EBSD band contrast, IPF maps and Phase maps of Ti-15.05wt% Mo alloy

4.6.2.3 SEM micrographs of Micro-Vickers Indents.

Deformation behavior can it analyzed using the micro Vickers indents Figure 4. 33 present the SEM micrographs captured in the vicinity of the micro-hardness indentation for all the designed Ti-Mo alloys. No crack was found on the corners of an indenter for all the investigated alloys as all of them display significant plasticity after compression test. In β type Ti alloys, the occurrence of twin and slip mechanism during deformation highly depends on the β stability of an alloy. The low β stability alloys exhibit twin mechanism while slip mechanism is found to be dominant in alloys high in β phase stability. The straight or thick deformation bands are indicative of twin mechanism, while the wavy or thin deformation bands are indicative of slip mechanism, M, (2018).

The designed Ti-10.02 Mo and Ti-10.83 Mo alloys were comprised of straight twin bands which demonstrated that twin mechanism was the dominant deformation. As the Mo content increased the amount of straight twin bands decreased and wavy slip bands were observed in the Ti-12.89Mo alloy and this implied that this alloy experienced twining plus slip deformation mechanism. The higher the Mo content the more the straight twins bands decreased and few deformation bands were observed around the indents and this is evident in alloy Ti-15.05Mo alloy, this implied that this alloy displayed deformation by slip mechanism only.

It was challenging to compare the deformation of the designed alloys with those found in literature because there is less work on the deformation behavior of binary Ti-Mo alloys but were able to just compare it with the deformation behavior of those multicomponent alloys reported in literature for example: in their research study Haghighi, and Ehtemam, (2015) evaluated the deformation behavior of Ti-Fe-Ta alloys with different content of Fe and Ta in as-cast condition. They discovered that all the alloys were comprised of shear bands except for Ti-8Fe and Ti-9Fe-2Ta alloys. Jawed *et al.*, (2019) reported similar deformation behavior obtained from the micro-Vickers indents in their research alloy Ti-25Nb-8Zr-xCr (x=2, 4, 6 & 8), which was arc melted, homogenized and quenched in water. They recorded that as the content of Cr increased the straight twin bands decreased and the wavy slip bands were pronounced around the indents. Jawed *et al.*, (2019) also studied the deformation behavior of Ti-25Nb-xSn (x=1, 3, 5)–xCr (x=2, 4) wt% alloys using the micro-Vickers indent in as-cast condition. Their results illustrated that as the composition of Sn and Cr increase the straight twin bands diminish and the wavy slip bands becomes more pronounced.

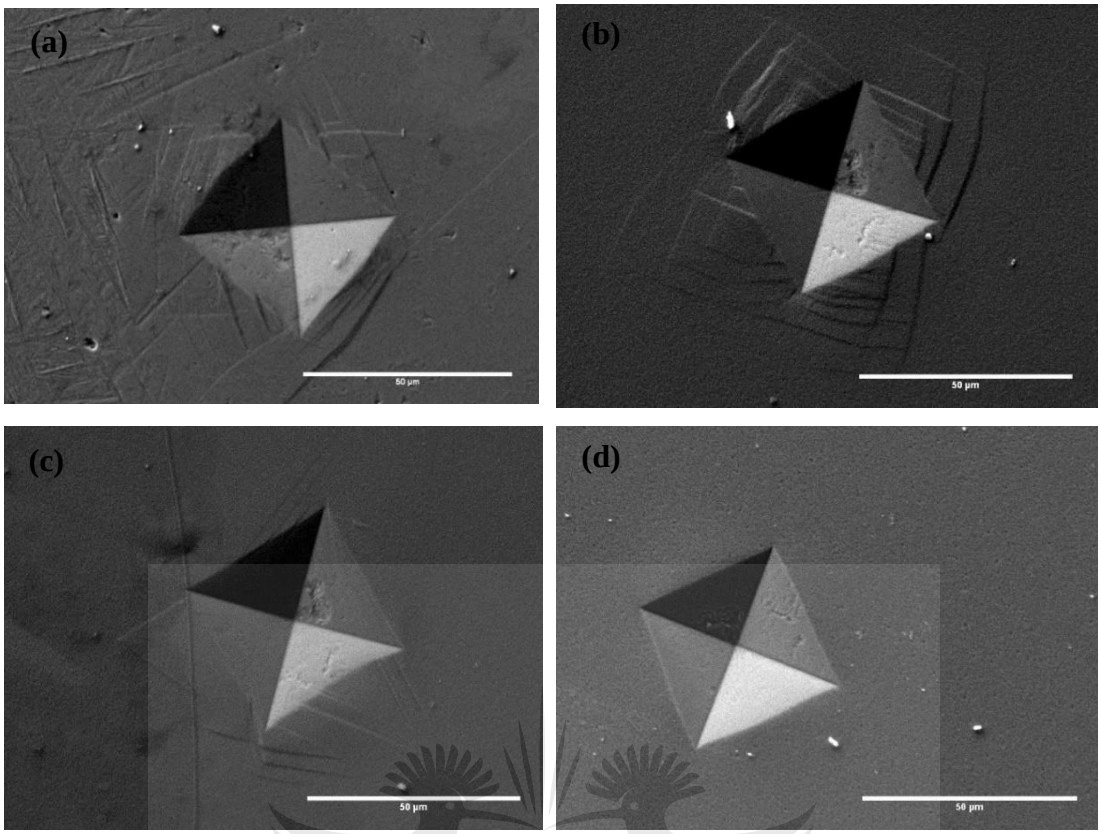

Figure 4. 35: SEM micro-graphs around the Micro-Vickers hardness indentation captured for the designed Ti-Mo alloys.

4.6.4 Tensile properties of solution treated alloys

The yield strength and elongation obtained from the tensile test results can determine the deformation behavior of Ti alloys. Min *et al.*, (2010), stated that alloys with low yield strength and high ductility deform by twinning, whereas alloys with high yield strength and low ductility deform by slip only. It is also been shown that SIM in metastable β Ti alloys can result in an improved combination of strength and ductility and this was stated by Paradkara *et al* (2009).

The deformation behavior according to the tensile properties of the designed alloys are summarized in Table 4. 7. As it can be seen in the table, Ti-10.02Mo and Ti-10.83Mo alloys show the highest yield strength with high %elongation than Ti-12.89Mo and Ti-15.05Mo alloys, and it was implied that they deform by twinning and slip. Ti-12.89Mo alloy displayed a high %elongation and low yield strength as compared to Ti-15.05 Mo alloy and it implied that it deforms by twinning only. The Ti-15.05Mo alloy exhibited high yield strength and low %elongation that Ti-12.89Mo alloy and it was implied that

it will deform by slip only. The results of the research alloys were compared to those reported by Jawed *et al.*, (2019) due to less research work reported on the binaries.

Table 4. 7: Yield strength and Elongation of solution treated Ti-Mo alloys

Mo Content (wt %)	Y.S (Mpa)	% Elongation	Deformation mechanism
Ti-10.02 Mo	594.31	20.71	Twinning + Slip
Ti-10.83 Mo	642.40	26.15	Twinning + Slip
Ti-12.89 Mo	515.37	16.60	Twining
Ti-15.05 Mo	546.34	6.95	Slip

Table 4. 8 shows the results predicted by the Bo and Md stability map and the experimental findings. According to the theoretical findings, the Bo and Md stability map predicted that as the Moeq increase (same as the Mo content) the deformation mechanism changes from stress induced transformation and twinning to slip. The experimental findings illustrated that the deformation behavior of the designed alloys analyzed using the OM technique were in agreement with the theoretical finding for Ti-10.02Mo alloy only and the rest of the designed alloys were inconsistent with the theoretical findings. The EBSD analysis for Ti-10.02Mo,Ti-10.83Mo alloys were in agreement with the prediction made by the Bo and Md stability map, the Ti-15.05Mo and Ti-12.89Mo alloys was not in agreement with the theoretical results because of the deformation by twinning mechanism that wasn't predicted by the Bo and Md stability map.

The experimental results characterized after tensile test for Ti-10.83 and Ti-15.05Mo alloys were in agreement with the predictions made by the Bo and Md stability map, whereas Ti-10.02Mo and Ti-12.89Mo alloy disagreed with the prediction method because the Bo and Md stability map predicted the SIM mechanism in Ti-10.02Mo alloy and deformation by Slip mechanism in Ti-12.89Mo alloy. The experimental results characterized using the micro-Vickers hardness indents for Ti-10.02 Mo, Ti-10.83Mo and Ti-12.89Mo alloys displayed deformation by Twinning, twinning and twinning plus slip respectively which in disagreement with those predicted by the Bo

and Md stability map, while Ti-15.05Mo alloy was consistence with the predictions made by the Bo and Md stability map.

Table 4. 8: Theoretical vs Experimental findings of the designed Ti-Mo alloys.

Theoretical Findings			Experimental Findings		
Mo Content (wt %)	Moeq (wt %)	Bo and Md	OM	EBSD	Deformation by tensile
Ti-10.02 Mo	10.02	SIM +Twin	SIM+ Twin	SIM+ Twin	Twinning + Slip
Ti-10.83 Mo	10.83	Twin+ Slip	SIM+ Twin+ Slip	SIM+Twin+Slip	Twinning + Slip
Ti-12.89 Mo	12.89	Slip	Twin + Slip	SIM+Twin+Slip	Twining
Ti-15.05 Mo	15.05	Slip	Twin + Slip	Twin +Slip	Slip

CHAPTER 5: CONCLUSION AND RECOMMENDATIONS

5.0 CONCLUSIONS

In this study, four binary Ti-Mo alloys were designed using the cluster plus glue atom model. β stabilizing prediction methods were used to predict the stability of the β phase in those four alloys and to evaluate the relationship between the stability of the β phase and low E - for their use in biomedical applications. The alloys were fabricated by an arc melting process, the ingots were solution treated at 1100˚C for 1 h and then water quenched, and compression test was done on the solution treated alloys. All the as-cast and solution treated alloys were characterized for phase and microstructural evolution using the OM, SEM, XRD and EBSD techniques and for mechanical properties using the tensile test, three-point bend test, micro-Vickers hardness and for deformation using the compression test. The microstructural behavior of the deformed alloys was investigated using the OM, EBSD, micro-hardness indents and tensile properties. Based on the experimental results the following conclusions can be drawn:

- The β stabilizing predictions methods such as Moeq, e/a ratio and the Kβ predicted that all the designed alloy were comprised of the β phase only after quenching from the beta field region, whereas the Bo and Md stability map predicted that Ti-10.02Mo and Ti-10.83Mo alloy will comprise of three phase: β, α″ and ω phase, whereas Ti-12.89Mo and Ti-15.05Mo alloys were predicted to exhibit the β phase only.. The Bo and Md stability map was also used to predict the deformation behavior of the designed alloys and the predictions were as follows: Ti-10.02Mo alloy was predicted to undergo deformation by SIM and twinning, the Ti-10.83Mo alloy was predicted to deform by twining and slip, while the Ti-12.89Mo and Ti-15.05Mo alloys were predicted to deform by slip mechanism only. The theoretical results indicated that designed and developed Ti-12.89 and Ti-15.05Mo alloy possess greater chances of being used in the biomedical application as they can stabilize the β phase which can lower the elastic modulus
- The phase and microstructural evolution of the as-cast Ti-Mo alloys studied by XRD, OM and SEM characterization techniques illustrated that all the designed alloys were not in agreement with the predictions methods because they consist of the bcc β phase and orthorhombic martensitic α″ phase only. The three characterization techniques were not able to detect the ω phase due to its

detection limit. The EBSD technique that was used to further characterize the microstructural evolution present revealed the presence of the omega phase in addition to the orthorhombic martensitic α″ phase and the bcc β phase, the Ti-10.02Mo and Ti-10.83Mo alloys were consistent with the predictions methods and all the designed alloys in as-cast condition could not stabilize the β phase. The designed and developed alloys in as-cast conditions characterized using different techniques showed that they possess low chances of being used in biomedical application as they presented secondary phases that affect the mechanical properties negatively.

- The effect of phase and microstructural evolution on the mechanical properties showed that the elastic modulus and the Vickers microhardness decreased significantly when the Mo content increased. The lowest elastic modulus was found to be 70.48GPa in Ti-15.05Mo alloy while the highest was found in Ti-10.02Mo (112.99GPa). The highest modulus in Ti-10.02Mo was attributed to the high-volume fraction of the omega phase. The highest bending strength was found in the as-cast Ti-10.83Mo alloy to be 1765.70 MPa. The mechanical properties of the designed alloys in as-cast condition showed that only Ti-15.05Mo alloy have potential to be used in biomedical application as it posses a lower elastic modulus, even though it had low strength which was a disadvantage.
- The effect of solution treatment on the phase and microstructural evolution of the as-cast alloys characterized using the XRD technique show that the designed alloys Ti-10.02Mo and Ti-10.83Mo were not in agreement with the prediction methods as they could not retain the β phase because of the presence of the omega and α″ phase, while Ti-12.89Mo and Ti-15.05Mo alloys were consistence with the prediction methods and were able to stabilize the β phase. The designed Ti-10.83, Ti-12.89 and Ti-15.05Mo alloys studied using OM and SEM techniques were able to stabilize the β phase and agreed with the prediction's methods. The EBSD technique illustrated that all the designed alloys could not stabilize the β phase, however, Ti-10.02Mo and Ti-10.83Mo alloys were in agreement with the prediction methods. The developed and designed Ti-10.83Mo,Ti-12.89Mo and Ti-15.05Mo alloys after solution treatment investigated using the OM were able to retain the β phase, indicating

that the alloys can have potential use in biomedical application but the EBSD technique proved otherwise.

- The influence of phase and microstructural evolution on the mechanical properties of solution treated alloys investigated using the Vickers microhardness and elastic modulus illustrated that the Vickers microhardness significantly increased as the Mo content increased, the highest hardness was obtained at a composition Ti-15.05Mo (354.6 HV) and this increase was attributed to the solid solution strengthening effect and the high content of the omega phase. The lowest elastic modulus after solution treatment was obtained at a composition of Ti-15.05Mo (72.59GPa) and this was attributed to the low volume fraction of the omega phase. The highest bending strength after solution treatment was found at Ti-15.05Mo alloy (1627.40 MPa) and the highest compression strength found in Ti-15.05Mo alloy was found to be 1193.09 Mpa. The mechanical properties of the designed alloys indicated that Ti-15.05Mo alloy in solution treated possess great potential for the use in biomedical application because of its lowest elastic modulus, elastic admissible strain, even though its strength its still moderate, the elastic modulus is lower than Ti6Al4V alloy.
- The microstructural evolution during deformation of the solution treated alloys after compression test characterized using the OM and EBSD techniques illustrated that Ti-10.02wt% Mo alloy was in agreement with the prediction methods made by the Bo and Md stability map while Ti-10.83Mo Ti-12.89Mo and Ti-15.05Mo alloys were not because they deformed by SIM and Twin mechanism but by twinning plus slip mechanism respectively. Further characterization of the deformation behavior using the yield strength vs elongation methods showed that the designed alloys Ti-10.83Mo and Ti-15.05Mo were in agreement with the predictions made by the Bo and Md stability map. Ti-15.05Mo alloy was able to deform by slip while Ti-10.02Mo and Ti-12.89Mo alloy were inconsistence with the Bo and Md stability map predictions.

5.1 RECOMMENDATIONS

Binary β–Ti alloys with composition of 15.05Mo content show a significant improvement in the elastic modulus after solution treatment. Apart from the high elastic modulus and the release of toxic ions, Ti6Al4V has shown merit in various implant applications due to its outstanding properties. Alloying Ti with Mo is thus showing great promise in addressing the current drawbacks of Ti6Al4V alloy. This study will thus form basis for further investigations to determine the viability of this material for manufacturing of orthopedic implants.

Future works will include (i) the investigation of adding more compositions of Mo and other stabilizing elements such as Nb or Ta to further stabilize the beta phase, suppress the omega and martensitic phase, and lower the elastic modulus so it matches that close to the bone. Future works will involve the investigation of the effects of thermomechanical processing (cold rolling, hot rolling or hot forging) of the mechanical properties especially the elastic modulus with hope of lowering it. Further studies will also include the introduction of pore into the binary alloys to further reduce the elastic modulus. The Bio-corrosion and Tribo-corrosion behavior of the developed Ti-Mo alloys in simulated body fluids should also be considered.

REFERENCES

Abdel-hady, M., Hinoshita, K. and Morinaga, M. (2006) 'General approach to phase stability and elastic properties of b -type Ti-alloys using electronic parameters', 55, pp. 477–480. doi: 10.1016/j.scriptamat.2006.04.022.

American, N., Corporation, R. and Oaks, T. (1969) 'The Formation of Omega Phase in Titanium and Zirconium Alloys : A Review', 4, pp. 554–563.

Ankem, S. and Greene, C. A. (1999) 'Recent developments in microstructure / property relationships of beta titanium alloys', 263, pp. 127–131.

Ankem, Z. W. S. (2010) 'The effect of metastability on room temperature deformation behavior of b and a + b titanium alloys', pp. 5022–5031. doi: 10.1007/s10853-009-4178-0.

AV, D. (2001) 'Martensitic transformation and metastable β-phase in binary titanium alloys with d-metals of 4-6 periods', *Scripta Materialia*, 44, pp. 905–910.

Banerjee, D. and Williams, J. C. (2013) 'Perspectives on Titanium Science and Technology', *Acta Materialia*. Acta Materialia Inc., 61(3), pp. 844–879. doi: 10.1016/j.actamat.2012.10.043.

Banerjee S, S. S. (2006) 'Quality of life in dementia: more than just cognition. An analysis of associations with quality of life in dementia', 77(2).

Bania, P. J. (1994) 'Beta Titanium Alloys and Their Role in the Titanium Industry J', (July), pp. 16–19.

Bania, P. J. and Parris, W. M. (1990) 'High strength alpha-beta titanium-base alloy'. Google Patents.

Bennett, J. M. (2018) 'Data Descriptor : GlobTherm , a global database on thermal tolerances for aquatic and terrestrial organisms', pp. 1–7. doi: 10.1038/sdata.2018.22.

Bhattacharjee, S. (2005) 'Reactive oxygen species and oxidative burst : Roles in stress , senescence and signal transduction in plants', 89(7).

Britton, T. B. *et al.* (2016) 'Materials Characterization Tutorial : Crystal orientations and EBSD — Or which way is up ?', *Materials Characterization*. The Authors, 117, pp. 113–126. doi: 10.1016/j.matchar.2016.04.008.

Brozek, C. *et al.* (2016) 'Scripta Materialia A β -titanium alloy with extra high strain-hardening rate : Design and mechanical properties', *SMM*. Elsevier Ltd, 114, pp. 60–64. doi: 10.1016/j.scriptamat.2015.11.020.

Buzatu, M. *et al.* (no date) 'Obtaining and Characterization of the Ti15Mo5W Alloy

for Biomedical Applications', pp. 596–600.

C, L. (2003) 'Titanium and Alloys'.

CA, E. (1988) 'The influence of stem size and extent of porous coating on femoral bone resorption after primary cementless hip arthroplasty.', *231*, 231, pp. 7–28.

Cardoso, F. F. *et al.* (2014) 'Ti – Mo alloys employed as biomaterials : Effects of composition and aging heat treatment on microstructure and mechanical behavior', *Journal of the Mechanical Behavior of Biomedical Materials*. Elsevier, 32, pp. 31–38. doi: 10.1016/j.jmbbm.2013.11.021.

Chen, Q. and Thouas, G. A. (2015) 'Metallic implant biomaterials', *Materials Science and Engineering R: Reports*. Elsevier B.V., 87, pp. 1–57. doi: 10.1016/j.mser.2014.10.001.

Chen Yu-yong, Xu, Li-juan, LIU, Zhi-gaung, KONG, Fan-tao, CHEN, Z. (2006) 'Microstructures and properties of titanium alloys Ti-Mo for dental use', *Transactions of Nonferrous Metals Society of China*, 16, pp. 824–828. doi: https://doi.org/10.1016/S1003-6326(06)60308-7.

Chen Yunhui, Jessica Ellen Frith, Ali Dehghan-Manshadi, Hooyar Attar, Damon Kent, Nicolas Dominique Mathieu Soro, Michael J Bermingham, M. S. D. (2017) 'Mechanical properties and biocompatibility of porous titanium scaffolds for bone tissue engineering', *Journal of the Mechanical Behavior of Biomedical Materials*, 75, pp. 169–174. doi: https://doi.org/10.1016/j.jmbbm.2017.07.015.

Davis, R., Flower, H. M. and West, D. R. F. (1979) 'Martensitic transformations in Ti-Mo alloys', *Journal of Materials Science*, 14(3), pp. 712–722. doi: 10.1007/BF00772735.

Devaraj, A. *et al.* (2012) 'Experimental evidence of concurrent compositional and structural instabilities leading to x precipitation in titanium – molybdenum alloys', *Acta Materialia*. Acta Materialia Inc., 60(2), pp. 596–609. doi: 10.1016/j.actamat.2011.10.008.

EJ, E. (1986) 'The in vitro toxicity of cobalt-chrome-molybdenum alloy and its constituent metals', *Biomaterials*, volume 7(1), pp. 25–29.

G.S.DyakonovabE.ZemtsovabcS.MironovdI.P.SemenovaaR.Z.ValievbS.L.Semiatine (2015) 'An EBSD investigation of ultrafine-grain titanium for biomedical applications', *material Science and Engineering: A*, 648, pp. 305–310. doi: https://doi.org/10.1016/j.msea.2015.09.080.

G, W. (1993) *Materials properties handbook:titanium alloys*.

Geetha, M. *et al.* (2009) 'Ti based biomaterials, the ultimate choice for orthopaedic implants–a review', *Progress in materials science*. Elsevier, 54(3), pp. 397–425.

Gerd, L. J. (2003) 'Titanium Based Intermetallics', *Springer Series in Biomaterials Science and Engineering*, pp. 289–312.

Gordin, D. M. *et al.* (2004) 'Development of a b -type Ti ± 12Mo ± 5Ta alloy for biomedical applications : cytocompatibility and metallurgical aspects', 5, pp. 885–891.

Graft WH, L. D. and R. W. (1957) 'The influence of alloying on the elastic modulus of titanium alloys', *ASM Trans*, pp. 263–279.

Grosdidier, T. *et al.* (2000) 'Effect of Microstructure Variations on the Formation of Deformation-Induced Martensite and Associated Tensile Properties in a Metastable Ti Alloy', 31(April).

Haghighi, S. Ehtemam, et al. (2015) 'Effect of α ″martensite on the microstructure and mechanical properties of beta-type Ti–Fe–Ta alloys.', *Materials and Design*, 76, pp. 47–54.

Hanada, S. and Izumi, O. (1986) 'Transmission Electron Microscopic Observations of Mechanical Twinning in Metastable Beta Titanium Alloys', 17(August).

Hanada, S. and Izumi, O. (1987) 'Correlation of Tensile Properties , Deformation Modes , and Phase Stability in Commercial / 3-Phase Titanium Alloys', 18(February), pp. 265–271.

Hao, C. and Wu, C. (2011) 'Dynamic behavior of a rigid , perfectly plastic free-free beam subjected to a local uniformly distributed impulsive load at one end', pp. 2103–2108. doi: 10.4028/www.scientific.net/AMM.66-68.2103.

Hao, Y. L. *et al.* (2006) 'Effect of Zr and Sn on Young ' s modulus and superelasticity of Ti – Nb-based alloys', 441, pp. 112–118. doi: 10.1016/j.msea.2006.09.051.

HE, C. (1973) 'On the nature of the omega transformation', *Acta Metallurgica Sinica (English Letters)*, 21(10), pp. 1445–1449. doi: 0001-6160(73)900.

Ho, W. (2008) 'Effect of omega phase on mechanical properties of Ti-Mo alloys for biomedical applications', *Journal of Medical and Biological Engineering*. WALTER H CHANG, 28(1), p. 47.

Ho, W. *et al.* (2009) 'Mechanical properties and deformation behavior of cast binary Ti – Cr alloys', 468, pp. 533–538. doi: 10.1016/j.jallcom.2008.01.046.

Ho, W. F., Ju, C. P. and Lin, J. H. C. (1999) 'Structure and properties of cast binary Ti } Mo alloys', 20(May), pp. 2115–2122.

Hsu, H. *et al.* (2009) 'The structure and mechanical properties of as-cast Zr – Ti alloys',

488, pp. 279–283. doi: 10.1016/j.jallcom.2009.08.105.

Humphreys, F. J. (2004) ‘Characterisation of fine-scale microstructures by electron backscatter diffraction (EBSD)’, 51, pp. 771–776. doi: 10.1016/j.scriptamat.2004.05.016.

Ikehata, H. *et al.* (2004) ‘First-principles calculations for development of low elastic modulus Ti alloys’, *Physical Review B.* APS, 70(17), p. 174113.

Jawed, S. F. *et al.* (2019) ‘Beta-type Ti-Nb-Zr-Cr alloys with large plasticity and signi fi cant strain hardening’, 181, pp. 0–10. doi: 10.1016/j.matdes.2019.108064.

Karase, O. P. *et al.* (2003) ‘Deformation beha v ior of beta-titanium alloys’, 354, pp. 121–132. doi: 10.1016/S0921-5093(02)00935-8.

Keda, Y. M. *et al.* (2002) ‘Antibodies to pituitary surface antigens during various pituitary disease states’, pp. 417–423.

Kim, H. Y. (2006) ‘Martensitic transformation , shape memory effect and superelasticity of Ti – Nb binary alloys’, 54, pp. 2419–2429. doi: 10.1016/j.actamat.2006.01.019.

Kolli, R. P. (2018) ‘A Review of Metastable Beta Titanium Alloys’, pp. 1–41. doi: 10.3390/met8070506.

Kuroda, D. *et al.* (1998) ‘Design and mechanical properties of new i type titanium alloys for implant materials’, 243, pp. 244–249.

Kusano, Y., Inamura, T. and Kanetaka, H. (2010) ‘Phase Constitution and Mechanical Properties of Ti (Cr , Mn) Sn Biomedical Phase Constitution and Mechanical Properties of Ti- (Cr , Mn) -Sn Biomedical Alloys’, (October 2015). doi: 10.4028/www.scientific.net/MSF.654-656.2118.

Laheurte, P. *et al.* (2010) ‘Mechanical properties of low modulus β titanium alloys designed from the electronic approach’, *Journal of the Mechanical Behavior of Biomedical Materials*. Elsevier Ltd, 3(8), pp. 565–573. doi: 10.1016/j.jmbbm.2010.07.001.

Landolt, D. (2018) ‘Fundamental aspects of electropolishing’, 4686(January 1987). doi: 10.1016/0013-4686(87)87001-9.

Lee CM, Ju CP, C. L. J. (2002) ‘Structure-property relstionship of cast Ti-Nb alloys’, *journal of oral rahabilitation.* doi: https://doi.org/10.1046/j.1365-2842.2002.00825.x.

Liu, L. H. *et al.* (2015) ‘Ultrafine grained Ti-based composites with ultrahigh strength and ductility achieved by equiaxing microstructure’, 79, pp. 1–5. doi: 10.1016/j.matdes.2015.04.032.

Long, M. and Rack, H. J. (1998) ‘Titanium alloys in total joint replacement — a materials science perspective’, 19.

Lu, J. *et al.* (2013) ‘ScienceDirect Microstructure and beta grain growth behavior of Ti – Mo alloys solution treated’, *Materials Characterization*. Elsevier Inc., 84(96), pp. 105–111. doi: 10.1016/j.matchar.2013.07.014.

M, M. (2018) ‘1.3 - The molecular orbital approach and its application to biomedical titanium alloy design’, *woodhead publishing series in biomaterials*, pp. 39–64. doi: https://doi.org/10.1016/B978-0-12-812456-7.00003-2.

Mantani Y, T. M. (2006) ‘Phase transformation of quenched α″ martensite by aging in Ti–Nb alloys’, *material Science and Engineering: A*, 438–440, pp. 315–319. doi: https://doi.org/10.1016/j.msea.2006.02.180.

Manuscript, A. and Implants, S. (2008) ‘NIH Public Access’, 28(32), pp. 4845–4869.

Marker, C. *et al.* (2018) ‘Effects of alloying elements on the elastic properties of bcc Ti-X alloys from first-principles calculations’, *Computational Materials Science*. Elsevier B.V., 142, pp. 215–226. doi: 10.1016/j.commatsci.2017.10.016.

Marteleur, M. *et al.* (2012) ‘On the design of new b -metastable titanium alloys with improved work hardening rate thanks to simultaneous TRIP and TWIP effects’, 66, pp. 749–752. doi: 10.1016/j.scriptamat.2012.01.049.

Martins, J. R. S. *et al.* (2011) ‘Preparation and characterization of Ti-15Mo alloy used as biomaterial’, *Materials Research*, 14(1), pp. 107–112. doi: 10.1590/S1516-14392011005000013.

Metallurgy, I. and Technology, J. (2000) ‘© 2000 ASM International. All Rights Reserved. Titanium: A Technical Guide, 2nd Edition (#06112G) www.asminternational.org’.

Min, X. H. *et al.* (2010) ‘Effects of ⌴ phase precipitation on crevice corrosion and tensile strength in Ti – 15Mo alloy’, 527, pp. 1480–1488. doi: 10.1016/j.msea.2009.10.033.

Min, X. H. *et al.* (2012) ‘Heterogeneous twin formation and its effect on tensile properties in Ti – Mo based titanium alloys’, *Materials Science & Engineering A*. Elsevier B.V., 554, pp. 53–60. doi: 10.1016/j.msea.2012.06.009.

Min, X. H. *et al.* (2014) ‘Materials Science & Engineering A Transition of multi-deformation modes in Ti – 10Mo alloy with oxygen addition’, *Materials Science & Engineering A*. Elsevier, 590, pp. 88–96. doi: 10.1016/j.msea.2013.10.010.

Mitragotri, S. (2015) 'NIH Public Access', (February 2009). doi: 10.1038/nmat2344.

Moffat, D. L. and Larbalestier, D. C. (1988) 'The Competition between Martensite and Omega in Quenched Ti-Nb Alloys', 19(July).

Mohamed Abdel-Hady Gepreel and Mitsuo Niinomi (2012) 'Biocompatibility of Ti-alloys for long-term implantation', *Journal of the Mechanical Behavior of Biomedical Materials*, 20, pp. 407–415. doi: https://doi.org/10.1016/j.jmbbm.2012.11.014.

Moiseev, V. N. and Antipov, A. I. (1995) 'Aluminium effect on beta-phase stability in beta-titanium alloys', *Metallovedenie i Termicheskaya Obrabotka Metallov*, pp. 30–35.

Morinaga M, Yukawa N, Maya T, S. K. and A. H. (1988) 'Theoretical design of titanium alloys', pp. 1601–1606.

Morinaga, M. (2016) 'Alloy Design Based on Molecular Orbital Method + 1', 57(3).

Morinaga, M. and Yukawa, H. (1997) 'Alloy design with the aid of molecular orbital method', *Bulletin of Materials Science*, 20(6), pp. 805–815. doi: 10.1007/BF02747420.

Morinaga M, Y. N. and A. H. (1985) 'Alloying effect on the electronic structure of BCC Fe', *IOP Conference Series: Materials Science and Engineering*, 15.

MP, G. (2002) 'Fundamentals of modern manufacturing'.

Nabeel, M. *et al.* (2012) 'Privacy Preserving Policy Based Content Sharing in Public Clouds'.

Navarro, M., Michiardi, A. and Castan, O. (2008) 'Biomaterials in orthopaedics', (January 2014). doi: 10.1098/rsif.2008.0151.

Niinomi, M. (1998) 'Mechanical properties of biomedical titanium alloys', 243, pp. 231–236.

Niinomi, M. (2008a) 'Mechanical biocompatibilities of titanium alloys for biomedical applications', *Journal of the Mechanical Behavior of Biomedical Materials*, 1(1), pp. 30–42. doi: 10.1016/j.jmbbm.2007.07.001.

Niinomi, M. (2008b) 'Mechanical biocompatibilities of titanium alloys for biomedical applications', *Journal of the mechanical behavior of biomedical materials*. Elsevier, 1(1), pp. 30–42.

Niinomi, M. and Nakai, M. (2011) 'Titanium-Based Biomaterials for Preventing Stress Shielding between Implant Devices and Bone', 2011. doi: 10.1155/2011/836587.

Niinomi M, A. M. and K. T. (1986) 'Evaluation of toughness in 7075 alloy by R Curve Method', 159.

Nyakana, S. L. *et al.* (2005) 'Quick Reference Guide for Titanium Alloys in the 00s', 14(December), pp. 799–811. doi: 10.1361/105994905X75646.

Okazaki, Y. (1996) ‘Corrosion resistance and corrosion fatigue strength of new titanium alloys for medical implants without V and A1’, 213, pp. 138–147.

Okazaki, Y. and Gotoh, E. (2005) ‘Comparison of metal release from various metallic biomaterials in vitro’, 26, pp. 11–21. doi: 10.1016/j.biomaterials.2004.02.005.

Oliveira, N. T. C. *et al.* (2007) ‘Development of Ti – Mo alloys for biomedical applications : Microstructure and electrochemical characterization’, 453, pp. 727–731. doi: 10.1016/j.msea.2006.11.061.

Oliveira, N. T. C. and Guastaldi, A. C. (2008) ‘Electrochemical behavior of Ti-Mo alloys applied as biomaterial’, *Corrosion Science*, 50(4), pp. 938–945. doi: 10.1016/j.corsci.2007.09.009.

Ozan, S. *et al.* (2015) ‘Acta Biomaterialia Development of Ti – Nb – Zr alloys with high elastic admissible strain for temporary orthopedic devices’, *Acta Biomaterialia*. Acta Materialia Inc., 20, pp. 176–187. doi: 10.1016/j.actbio.2015.03.023.

ParadkaraS.V.KamataA.K.GogiaaB.P.Kashyapb (2009) ‘On the validity of Hall–Petch equation for single-phase β Ti–Al–Nb alloys undergoing stress-induced martensitic transformation’, *material Science and Engineering: A*, 520(1–2), pp. 168–173. doi: https://doi.org/10.1016/j.msea.2009.05.041.

PD, F. (1954) ‘Isothermal transformation of titanium chromium alloys’, *Transactions of Nonferrous Metals Society of China*, 46, pp. 231–256.

Polmear IJ (2006) ‘Light Alloys: From Traditional Alloys to Nanocrystals’, 4, p. 421.

Ren, Y. *et al.* (2013) ‘Magnetic EDTA-modified chitosan / SiO 2 / Fe 3 O 4 adsorbent : Preparation , characterization , and application in heavy metal adsorption’, *Chemical Engineering Journal*. Elsevier B.V., 226, pp. 300–311. doi: 10.1016/j.cej.2013.04.059.

Sabeena, M. *et al.* (2013) ‘Thermodynamic basis of non-equilibrium phase transformations of bcc β-phase in Ti-Mo system’, *Transactions of the Indian Institute of Metals*, 66(4), pp. 401–407. doi: 10.1007/s12666-013-0272-8.

Sadeghpour, S. *et al.* (2018) ‘On the compressive deformation behavior of new beta titanium alloys designed by d-electron method’, *Journal of Alloys and Compounds*. Elsevier B.V, 746, pp. 206–217. doi: 10.1016/j.jallcom.2018.02.212.

Severino Martins Junior, Jose Roberto [1] ; Nogueira, Renata Abdallah [1] ; de Araujo, Raul Oliveira [1] ; Goto Donato, Tatiani Ayako [2] ; Arana-Chavez, Vitor Elias [2] ; Rosifini Alves Claro, Ana Paula [3] ; Silos Moraes, Joao Carlos [4] ; Rabelo Buzala, C. R. [1] (2011) ‘Preparation and Characterization of Ti-15Mo Alloy used as Biomaterial’.

Shetty, S., Kusminski, C. M. and Scherer, P. E. (2009) ‘Adiponectin in health and

disease : evaluation of adiponectin-targeted drug development strategies', (April). doi: 10.1016/j.tips.2009.02.004.

Sidambe, A. T. (2014) 'Biocompatibility of Advanced Manufactured Titanium Implants—A Review', (December). doi: 10.3390/ma7128168.

Sikka SK, V. Y. (1982) 'Omega phase in materials', *Progress in materials science*, 27(3–4), pp. 245–310. doi: 10.1016/0079-6425(82)90002-0.

Singh, J., et al. "Strain field due to substitutional transition-metal impurities in bcc metals: A. to dilute vanadium alloys. . P. R. B. 49. . (1994): 932. (1994) 'No Title Strain field due to substitutional trasnsition metal impurities in bcc metals: Application to dilute Vanadium alloys', 49.2, p. 932.

Song Y et al (1999) 'No Title Theoretical Study of the effects of alloying elements on the strength and modulus of beta-type bio titaniium alloys', 260, pp. 269–274.

Sukedai, E. *et al.* (2011) 'Nucleation Behaviour of to ! Phase Transformations in -Type Ti-Mo Alloys', 52(3), pp. 324–330. doi: 10.2320/matertrans.MB201017.

Sumner, D. R. *et al.* (1998) 'Functional adaptation and ingrowth of bone vary as a function of hip implant stiffness', 31.

TayyebAli, LinWangXingwangCheng, AnjinLiu, X. (2019) 'Omega phase formation and deformation mechanism in heat treated Ti-5553 alloy under high strain rate compression', *Material Letters*, 236, pp. 163–166.

ToshikazuAkahoriaMitsuoNiinomiaHisaoFukuibMichiharuOgawacHiroyukiTodaa (2005) 'Improvement in fatigue characteristics of newly developed beta type titanium alloy for biomedical applications by thermo-mechanical treatments', *Material Science and Engineering :C*, 25(3), pp. 248–254.

Viceconti, M. *et al.* (2000) 'Large-sliding contact elements accurately predict levels of bone } implant micromotion relevant to osseointegration', 33, pp. 1611–1618.

Wang, C. H. *et al.* (2016) 'Martensitic microstructures and mechanical properties of as-quenched metastable b -type Ti – Mo alloys', pp. 6886–6896. doi: 10.1007/s10853-016-9976-6.

Wang, Q. *et al.* (2013) 'β-Ti alloys with low young's moduli interpreted by cluster-plus-glue-atom model', *Metallurgical and Materials Transactions A: Physical Metallurgy and Materials Science*, 44(4), pp. 1872–1879. doi: 10.1007/s11661-012-1523-8.

Wang, Q. *et al.* (2015) 'Microstructures and Stability Origins of β-(Ti,Zr)-(Mo,Sn)-Nb Alloys with Low Young's Modulus', *Metallurgical and Materials Transactions A:*

Physical Metallurgy and Materials Science. Springer US, 46(9), pp. 3924–3931. doi: 10.1007/s11661-015-3011-4.

Welsch, G. (1993) *Materials properties handbook*.

Williams, J. C. and Paton, N. E. (1973) 'The 0 ., -Phase as an Example of an Unusual Shear Transformation o', 4(December).

Xiang, L. *et al.* (2018) 'Effect of Pre-cold Rolling-Induced Twins and Subsequent Precipitated x -Phase on Mechanical Properties in a b -Type Ti – Mo Alloy', *Acta Metallurgica Sinica (English Letters)*. The Chinese Society for Metals, 31(6), pp. 604–614. doi: 10.1007/s40195-017-0687-z.

Xu, Y. H. and Cai, M. (2017) 'Influence of Loading System Stiffness on Post-peak Stress – Strain Curve of Stable Rock Failures', pp. 2255–2275. doi: 10.1007/s00603-017-1231-1.

Yong, L. I. U. *et al.* (2003) 'Microstructures and mechanical behavior of PM Ti-Mo alloy', 10(2), pp. 81–86.

Yu, L. *et al.* (1993) 'Agaricus bisporus'.

Zhang, J. *et al.* (2018) 'Materials Characterization Fabrication and characterization of a novel β metastable Ti-Mo-Zr alloy with large ductility and improved yield strength', *Materials Characterization*. Elsevier, 139(September 2017), pp. 421–427. doi: 10.1016/j.matchar.2018.03.031.

Zhang, L. *et al.* (2015) 'Effect of Nb addition on microstructure , mechanical properties and castability of ù -type TiíMo alloys', *Transactions of Nonferrous Metals Society of China*. The Nonferrous Metals Society of China, 25(7), pp. 2214–2220. doi: 10.1016/S1003-6326(15)63834-1.

Zhang, L. C. *et al.* (2005) 'Nucleation of stress-induced martensites in a Ti / Mo-based alloy', 0, pp. 2833–2836.

Zhang, L. C. *et al.* (2011) 'Manufacture by selective laser melting and mechanical behavior of a biomedical Ti – 24Nb – 4Zr – 8Sn alloy', *Scripta Materialia*. Acta Materialia Inc., 65(1), pp. 21–24. doi: 10.1016/j.scriptamat.2011.03.024.

Zhao, X. *et al.* (2012) 'Acta Biomaterialia Beta type Ti – Mo alloys with changeable Young ' s modulus for spinal fixation applications', *Acta Biomaterialia*. Acta Materialia Inc., 8(5), pp. 1990–1997. doi: 10.1016/j.actbio.2012.02.004.

Zheng, Y. (2013) 'Nucleation Mechanisms of Refined Alpha Microstructure in Beta Titanium Alloys', (May 2013), p. 211. doi: osu1366296464.

Zhou, Y. and Luo, D. (2011) 'Microstructures and mechanical properties of Ti – Mo

alloys cold-rolled and heat treated', *Materials Characterization*. Elsevier Inc., 62(10), pp. 931–937. doi: 10.1016/j.matchar.2011.07.010.

Zhou, Y. and Niinomi, M. (2009) 'Ti – 25Ta alloy with the best mechanical compatibility in Ti – Ta alloys for biomedical applications', *Materials Science & Engineering C*. Elsevier B.V., 29(3), pp. 1061–1065. doi: 10.1016/j.msec.2008.09.012.

Zhou YB (2000) 'No Title', *Titanium Alloys*.

Abdel-hady, M., Hinoshita, K. and Morinaga, M. (2006) 'General approach to phase stability and elastic properties of b -type Ti-alloys using electronic parameters', 55, pp. 477–480. doi: 10.1016/j.scriptamat.2006.04.022.

American, N., Corporation, R. and Oaks, T. (1969) 'The Formation of Omega Phase in Titanium and Zirconium Alloys : A Review', 4, pp. 554–563.

Ankem, S. and Greene, C. A. (1999) 'Recent developments in microstructure / property relationships of beta titanium alloys', 263, pp. 127–131.

Ankem, Z. W. S. (2010) 'The effect of metastability on room temperature deformation behavior of b and a + b titanium alloys', pp. 5022–5031. doi: 10.1007/s10853-009-4178-0.

AV, D. (2001) 'Martensitic transformation and metastable β-phase in binary titanium alloys with d-metals of 4-6 periods', *Scripta Materialia*, 44, pp. 905–910.

Banerjee, D. and Williams, J. C. (2013) 'Perspectives on Titanium Science and Technology', *Acta Materialia*. Acta Materialia Inc., 61(3), pp. 844–879. doi: 10.1016/j.actamat.2012.10.043.

Banerjee S, S. S. (2006) 'Quality of life in dementia: more than just cognition. An analysis of associations with quality of life in dementia', 77(2).

Bania, P. J. (1994) 'Beta Titanium Alloys and Their Role in the Titanium Industry ====== J', (July), pp. 16–19.

Bania, P. J. and Parris, W. M. (1990) 'High strength alpha-beta titanium-base alloy'. Google Patents.

Bennett, J. M. (2018) 'Data Descriptor : GlobTherm , a global database on thermal tolerances for aquatic and terrestrial organisms', pp. 1–7. doi: 10.1038/sdata.2018.22.

Bhattacharjee, S. (2005) 'Reactive oxygen species and oxidative burst : Roles in stress , senescence and signal transduction in plants', 89(7).

Britton, T. B. *et al.* (2016) 'Materials Characterization Tutorial : Crystal orientations and EBSD — Or which way is up ?', *Materials Characterization*. The Authors, 117, pp. 113–126. doi: 10.1016/j.matchar.2016.04.008.

Brozek, C. *et al.* (2016) 'Scripta Materialia A β -titanium alloy with extra high strain-hardening rate : Design and mechanical properties', *SMM*. Elsevier Ltd, 114, pp. 60–64. doi: 10.1016/j.scriptamat.2015.11.020.

Buzatu, M. *et al.* (no date) 'Obtaining and Characterization of the Ti15Mo5W Alloy for Biomedical Applications', pp. 596–600.

C, L. (2003) 'Titanium and Alloys'.

CA, E. (1988) 'The influence of stem size and extent of porous coating on femoral bone resorption after primary cementless hip arthroplasty.', *231*, 231, pp. 7–28.

Cardoso, F. F. *et al.* (2014) 'Ti – Mo alloys employed as biomaterials : Effects of composition and aging heat treatment on microstructure and mechanical behavior', *Journal of the Mechanical Behavior of Biomedical Materials*. Elsevier, 32, pp. 31–38. doi: 10.1016/j.jmbbm.2013.11.021.

Chen, Q. and Thouas, G. A. (2015) 'Metallic implant biomaterials', *Materials Science and Engineering R: Reports*. Elsevier B.V., 87, pp. 1–57. doi: 10.1016/j.mser.2014.10.001.

Chen Yu-yong, Xu, Li-juan, LIU, Zhi-gaung, KONG, Fan-tao, CHEN, Z. (2006) 'Microstructures and properties of titanium alloys Ti-Mo for dental use', *Transactions of Nonferrous Metals Society of China*, 16, pp. 824–828. doi: https://doi.org/10.1016/S1003-6326(06)60308-7.

Chen Yunhui, Jessica Ellen Frith, Ali Dehghan-Manshadi, Hooyar Attar, Damon Kent, Nicolas Dominique Mathieu Soro, Michael J Bermingham, M. S. D. (2017) 'Mechanical properties and biocompatibility of porous titanium scaffolds for bone tissue engineering', *Journal of the Mechanical Behavior of Biomedical Materials*, 75, pp. 169–174. doi: https://doi.org/10.1016/j.jmbbm.2017.07.015.

Davis, R., Flower, H. M. and West, D. R. F. (1979) 'Martensitic transformations in Ti-Mo alloys', *Journal of Materials Science*, 14(3), pp. 712–722. doi: 10.1007/BF00772735.

Devaraj, A. *et al.* (2012) 'Experimental evidence of concurrent compositional and structural instabilities leading to x precipitation in titanium – molybdenum alloys', *Acta Materialia*. Acta Materialia Inc., 60(2), pp. 596–609. doi: 10.1016/j.actamat.2011.10.008.

EJ, E. (1986) 'The in vitro toxicity of cobalt-chrome-molybdenum alloy and its constituent metals', *Biomaterials*, volume 7(1), pp. 25–29.

G.S.DyakonovabE.ZemtsovabcS.MironovdI.P.SemenovaaR.Z.ValievbS.L.Semiatine

(2015) ‘An EBSD investigation of ultrafine-grain titanium for biomedical applications’, *material Science and Engineering: A*, 648, pp. 305–310. doi: https://doi.org/10.1016/j.msea.2015.09.080.

G, W. (1993) *Materials properties handbook:titanium alloys*.

Geetha, M. *et al.* (2009) ‘Ti based biomaterials, the ultimate choice for orthopaedic implants–a review’, *Progress in materials science*. Elsevier, 54(3), pp. 397–425.

Gerd, L. J. (2003) ‘Titanium Based Intermetallics’, *Springer Series in Biomaterials Science and Engineering*, pp. 289–312.

Gordin, D. M. *et al.* (2004) ‘Development of a b -type Ti ± 12Mo ± 5Ta alloy for biomedical applications : cytocompatibility and metallurgical aspects’, 5, pp. 885–891.

Graft WH, L. D. and R. W. (1957) ‘The influence of alloying on the elastic modulus of titanium alloys’, *ASM Trans*, pp. 263–279.

Grosdidier, T. *et al.* (2000) ‘Effect of Microstructure Variations on the Formation of Deformation-Induced Martensite and Associated Tensile Properties in a Metastable Ti Alloy’, 31(April).

Haghighi, S. Ehtemam, et al. (2015) ‘Effect of α ″martensite on the microstructure and mechanical properties of beta-type Ti–Fe–Ta alloys.’, *Materials and Design*, 76, pp. 47–54.

Hanada, S. and Izumi, O. (1986) ‘Transmission Electron Microscopic Observations of Mechanical Twinning in Metastable Beta Titanium Alloys’, 17(August).

Hanada, S. and Izumi, O. (1987) ‘Correlation of Tensile Properties , Deformation Modes , and Phase Stability in Commercial / 3-Phase Titanium Alloys’, 18(February), pp. 265–271.

Hao, C. and Wu, C. (2011) ‘Dynamic behavior of a rigid , perfectly plastic free-free beam subjected to a local uniformly distributed impulsive load at one end’, pp. 2103–2108. doi: 10.4028/www.scientific.net/AMM.66-68.2103.

Hao, Y. L. *et al.* (2006) ‘Effect of Zr and Sn on Young ’ s modulus and superelasticity of Ti – Nb-based alloys’, 441, pp. 112–118. doi: 10.1016/j.msea.2006.09.051.

HE, C. (1973) ‘On the nature of the omega transformation’, *Acta Metallurgica Sinica (English Letters)*, 21(10), pp. 1445–1449. doi: 0001-6160(73)900.

Ho, W. (2008) ‘Effect of omega phase on mechanical properties of Ti-Mo alloys for biomedical applications’, *Journal of Medical and Biological Engineering*. WALTER H CHANG, 28(1), p. 47.

Ho, W. *et al.* (2009) ‘Mechanical properties and deformation behavior of cast binary Ti

– Cr alloys', 468, pp. 533–538. doi: 10.1016/j.jallcom.2008.01.046.

Ho, W. F., Ju, C. P. and Lin, J. H. C. (1999) 'Structure and properties of cast binary Ti } Mo alloys', 20(May), pp. 2115–2122.

Hsu, H. *et al.* (2009) 'The structure and mechanical properties of as-cast Zr – Ti alloys', 488, pp. 279–283. doi: 10.1016/j.jallcom.2009.08.105.

Humphreys, F. J. (2004) 'Characterisation of fine-scale microstructures by electron backscatter diffraction (EBSD)', 51, pp. 771–776. doi: 10.1016/j.scriptamat.2004.05.016.

Ikehata, H. *et al.* (2004) 'First-principles calculations for development of low elastic modulus Ti alloys', *Physical Review B.* APS, 70(17), p. 174113.

Jawed, S. F. *et al.* (2019) 'Beta-type Ti-Nb-Zr-Cr alloys with large plasticity and signi fi cant strain hardening', 181, pp. 0–10. doi: 10.1016/j.matdes.2019.108064.

Karase, O. P. *et al.* (2003) 'Deformation beha v ior of beta-titanium alloys', 354, pp. 121–132. doi: 10.1016/S0921-5093(02)00935-8.

Keda, Y. M. *et al.* (2002) 'Antibodies to pituitary surface antigens during various pituitary disease states', pp. 417–423.

Kim, H. Y. (2006) 'Martensitic transformation , shape memory effect and superelasticity of Ti – Nb binary alloys', 54, pp. 2419–2429. doi: 10.1016/j.actamat.2006.01.019.

Kolli, R. P. (2018) 'A Review of Metastable Beta Titanium Alloys', pp. 1–41. doi: 10.3390/met8070506.

Kuroda, D. *et al.* (1998) 'Design and mechanical properties of new i type titanium alloys for implant materials', 243, pp. 244–249.

Kusano, Y., Inamura, T. and Kanetaka, H. (2010) 'Phase Constitution and Mechanical Properties of Ti (Cr , Mn) Sn Biomedical Phase Constitution and Mechanical Properties of Ti- (Cr , Mn) -Sn Biomedical Alloys', (October 2015). doi: 10.4028/www.scientific.net/MSF.654-656.2118.

Laheurte, P. *et al.* (2010) 'Mechanical properties of low modulus β titanium alloys designed from the electronic approach', *Journal of the Mechanical Behavior of Biomedical Materials*. Elsevier Ltd, 3(8), pp. 565–573. doi: 10.1016/j.jmbbm.2010.07.001.

Landolt, D. (2018) 'Fundamental aspects of electropolishing', 4686(January 1987). doi: 10.1016/0013-4686(87)87001-9.

Lee CM, Ju CP, C. L. J. (2002) 'Structure-property relstionship of cast Ti-Nb alloys',

journal of oral rahabilitation. doi: https://doi.org/10.1046/j.1365-2842.2002.00825.x.

Liu, L. H. *et al.* (2015) 'Ultrafine grained Ti-based composites with ultrahigh strength and ductility achieved by equiaxing microstructure', 79, pp. 1–5. doi: 10.1016/j.matdes.2015.04.032.

Long, M. and Rack, H. J. (1998) 'Titanium alloys in total joint replacement — a materials science perspective', 19.

Lu, J. *et al.* (2013) 'ScienceDirect Microstructure and beta grain growth behavior of Ti – Mo alloys solution treated', *Materials Characterization*. Elsevier Inc., 84(96), pp. 105–111. doi: 10.1016/j.matchar.2013.07.014.

M, M. (2018) '1.3 - The molecular orbital approach and its application to biomedical titanium alloy design', *woodhead publishing series in biomaterials*, pp. 39–64. doi: https://doi.org/10.1016/B978-0-12-812456-7.00003-2.

Mantani Y, T. M. (2006) 'Phase transformation of quenched α″ martensite by aging in Ti–Nb alloys', *material Science and Engineering: A*, 438–440, pp. 315–319. doi: https://doi.org/10.1016/j.msea.2006.02.180.

Manuscript, A. and Implants, S. (2008) 'NIH Public Access', 28(32), pp. 4845–4869.

Marker, C. *et al.* (2018) 'Effects of alloying elements on the elastic properties of bcc Ti-X alloys from first-principles calculations', *Computational Materials Science*. Elsevier B.V., 142, pp. 215–226. doi: 10.1016/j.commatsci.2017.10.016.

Marteleur, M. *et al.* (2012) 'On the design of new b -metastable titanium alloys with improved work hardening rate thanks to simultaneous TRIP and TWIP effects', 66, pp. 749–752. doi: 10.1016/j.scriptamat.2012.01.049.

Martins, J. R. S. *et al.* (2011) 'Preparation and characterization of Ti-15Mo alloy used as biomaterial', *Materials Research*, 14(1), pp. 107–112. doi: 10.1590/S1516-14392011005000013.

Metallurgy, I. and Technology, J. (2000) '© 2000 ASM International. All Rights Reserved. Titanium: A Technical Guide, 2nd Edition (#06112G) www.asminternational.org'.

Min, X. H. *et al.* (2010) 'Effects of ⌴ phase precipitation on crevice corrosion and tensile strength in Ti – 15Mo alloy', 527, pp. 1480–1488. doi: 10.1016/j.msea.2009.10.033.

Min, X. H. *et al.* (2012) 'Heterogeneous twin formation and its effect on tensile properties in Ti – Mo based □ titanium alloys', *Materials Science & Engineering A*.

Elsevier B.V., 554, pp. 53–60. doi: 10.1016/j.msea.2012.06.009.

Min, X. H. *et al.* (2014) 'Materials Science & Engineering A Transition of multi-deformation modes in Ti – 10Mo alloy with oxygen addition', *Materials Science & Engineering A*. Elsevier, 590, pp. 88–96. doi: 10.1016/j.msea.2013.10.010.

Mitragotri, S. (2015) 'NIH Public Access', (February 2009). doi: 10.1038/nmat2344.

Moffat, D. L. and Larbalestier, D. C. (1988) 'The Competition between Martensite and Omega in Quenched Ti-Nb Alloys', 19(July).

Mohamed Abdel-Hady Gepreel and Mitsuo Niinomi (2012) 'Biocompatibility of Ti-alloys for long-term implantation', *Journal of the Mechanical Behavior of Biomedical Materials*, 20, pp. 407–415. doi: https://doi.org/10.1016/j.jmbbm.2012.11.014.

Moiseev, V. N. and Antipov, A. I. (1995) 'Aluminium effect on beta-phase stability in beta-titanium alloys', *Metallovedenie i Termicheskaya Obrabotka Metallov*, pp. 30–35.

Morinaga M, Yukawa N, Maya T, S. K. and A. H. (1988) 'Theoretical design of titanium alloys', pp. 1601–1606.

Morinaga, M. (2016) 'Alloy Design Based on Molecular Orbital Method + 1', 57(3).

Morinaga, M. and Yukawa, H. (1997) 'Alloy design with the aid of molecular orbital method', *Bulletin of Materials Science*, 20(6), pp. 805–815. doi: 10.1007/BF02747420.

Morinaga M, Y. N. and A. H. (1985) 'Alloying effect on the electronic structure of BCC Fe', *IOP Conference Series: Materials Science and Engineering*, 15.

MP, G. (2002) 'Fundamentals of modern manufacturing'.

Nabeel, M. *et al.* (2012) 'Privacy Preserving Policy Based Content Sharing in Public Clouds'.

Navarro, M., Michiardi, A. and Castan, O. (2008) 'Biomaterials in orthopaedics', (January 2014). doi: 10.1098/rsif.2008.0151.

Niinomi, M. (1998) 'Mechanical properties of biomedical titanium alloys', 243, pp. 231–236.

Niinomi, M. (2008a) 'Mechanical biocompatibilities of titanium alloys for biomedical applications', *Journal of the Mechanical Behavior of Biomedical Materials*, 1(1), pp. 30–42. doi: 10.1016/j.jmbbm.2007.07.001.

Niinomi, M. (2008b) 'Mechanical biocompatibilities of titanium alloys for biomedical applications', *Journal of the mechanical behavior of biomedical materials*. Elsevier, 1(1), pp. 30–42.

Niinomi, M. and Nakai, M. (2011) 'Titanium-Based Biomaterials for Preventing Stress Shielding between Implant Devices and Bone', 2011. doi: 10.1155/2011/836587.

Niinomi M, A. M. and K. T. (1986) ‘Evaluation of toughness in 7075 alloy by R Curve Method’, 159.

Nyakana, S. L. *et al.* (2005) ‘Quick Reference Guide for Titanium Alloys in the 00s’, 14(December), pp. 799–811. doi: 10.1361/105994905X75646.

Okazaki, Y. (1996) ‘Corrosion resistance and corrosion fatigue strength of new titanium alloys for medical implants without V and A1’, 213, pp. 138–147.

Okazaki, Y. and Gotoh, E. (2005) ‘Comparison of metal release from various metallic biomaterials in vitro’, 26, pp. 11–21. doi: 10.1016/j.biomaterials.2004.02.005.

Oliveira, N. T. C. *et al.* (2007) ‘Development of Ti – Mo alloys for biomedical applications : Microstructure and electrochemical characterization’, 453, pp. 727–731. doi: 10.1016/j.msea.2006.11.061.

Oliveira, N. T. C. and Guastaldi, A. C. (2008) ‘Electrochemical behavior of Ti-Mo alloys applied as biomaterial’, *Corrosion Science*, 50(4), pp. 938–945. doi: 10.1016/j.corsci.2007.09.009.

Ozan, S. *et al.* (2015) ‘Acta Biomaterialia Development of Ti – Nb – Zr alloys with high elastic admissible strain for temporary orthopedic devices’, *Acta Biomaterialia*. Acta Materialia Inc., 20, pp. 176–187. doi: 10.1016/j.actbio.2015.03.023.

ParadkaraS.V.KamataA.K.GogiaaB.P.Kashyapb (2009) ‘On the validity of Hall–Petch equation for single-phase β Ti–Al–Nb alloys undergoing stress-induced martensitic transformation’, *material Science and Engineering: A*, 520(1–2), pp. 168–173. doi: https://doi.org/10.1016/j.msea.2009.05.041.

PD, F. (1954) ‘Isothermal transformation of titanium chromium alloys’, *Transactions of Nonferrous Metals Society of China*, 46, pp. 231–256.

Polmear IJ (2006) ‘Light Alloys: From Traditional Alloys to Nanocrystals’, 4, p. 421.

Ren, Y. *et al.* (2013) ‘Magnetic EDTA-modified chitosan / SiO 2 / Fe 3 O 4 adsorbent : Preparation , characterization , and application in heavy metal adsorption’, *Chemical Engineering Journal*. Elsevier B.V., 226, pp. 300–311. doi: 10.1016/j.cej.2013.04.059.

Sabeena, M. *et al.* (2013) ‘Thermodynamic basis of non-equilibrium phase transformations of bcc β-phase in Ti-Mo system’, *Transactions of the Indian Institute of Metals*, 66(4), pp. 401–407. doi: 10.1007/s12666-013-0272-8.

Sadeghpour, S. *et al.* (2018) ‘On the compressive deformation behavior of new beta titanium alloys designed by d-electron method’, *Journal of Alloys and Compounds*. Elsevier B.V, 746, pp. 206–217. doi: 10.1016/j.jallcom.2018.02.212.

Severino Martins Junior, Jose Roberto [1] ; Nogueira, Renata Abdallah [1] ; de Araujo,

Raul Oliveira [1] ; Goto Donato, Tatiani Ayako [2] ; Arana-Chavez, Vitor Elias [2] ; Rosifini Alves Claro, Ana Paula [3] ; Silos Moraes, Joao Carlos [4] ; Rabelo Buzala, C. R. [1] (2011) 'Preparation and Characterization of Ti-15Mo Alloy used as Biomaterial'.

Shetty, S., Kusminski, C. M. and Scherer, P. E. (2009) 'Adiponectin in health and disease : evaluation of adiponectin-targeted drug development strategies', (April). doi: 10.1016/j.tips.2009.02.004.

Sidambe, A. T. (2014) 'Biocompatibility of Advanced Manufactured Titanium Implants—A Review', (December). doi: 10.3390/ma7128168.

Sikka SK, V. Y. (1982) 'Omega phase in materials', *Progress in materials science*, 27(3–4), pp. 245–310. doi: 10.1016/0079-6425(82)90002-0.

Singh, J., et al. "Strain field due to substitutional transition-metal impurities in bcc metals: A. to dilute vanadium alloys. . P. R. B. 49. . (1994): 932. (1994) 'No Title Strain field due to substitutional trasnsition metal impurities in bcc metals: Application to dilute Vanadium alloys', 49.2, p. 932.

Song Y et al (1999) 'No Title Theoretical Study of the effects of alloying elements on the strength and modulus of beta-type bio titaniium alloys', 260, pp. 269–274.

Sukedai, E. *et al.* (2011) 'Nucleation Behaviour of to ! Phase Transformations in -Type Ti-Mo Alloys', 52(3), pp. 324–330. doi: 10.2320/matertrans.MB201017.

Sumner, D. R. *et al.* (1998) 'Functional adaptation and ingrowth of bone vary as a function of hip implant stiffness', 31.

TayyebAli, LinWangXingwangCheng, AnjinLiu, X. (2019) 'Omega phase formation and deformation mechanism in heat treated Ti-5553 alloy under high strain rate compression', *Material Letters*, 236, pp. 163–166.

ToshikazuAkahoriaMitsuoNiinomiaHisaoFukuibMichiharuOgawacHiroyukiTodaa (2005) 'Improvement in fatigue characteristics of newly developed beta type titanium alloy for biomedical applications by thermo-mechanical treatments', *Material Science and Engineering :C*, 25(3), pp. 248–254.

Viceconti, M. *et al.* (2000) 'Large-sliding contact elements accurately predict levels of bone } implant micromotion relevant to osseointegration', 33, pp. 1611–1618.

Wang, C. H. *et al.* (2016) 'Martensitic microstructures and mechanical properties of as-quenched metastable b -type Ti – Mo alloys', pp. 6886–6896. doi: 10.1007/s10853-016-9976-6.

Wang, Q. *et al.* (2013) 'β-Ti alloys with low young's moduli interpreted by cluster-plus-glue-atom model', *Metallurgical and Materials Transactions A: Physical*

Metallurgy and Materials Science, 44(4), pp. 1872–1879. doi: 10.1007/s11661-012-1523-8.

Wang, Q. *et al.* (2015) 'Microstructures and Stability Origins of β-(Ti,Zr)-(Mo,Sn)-Nb Alloys with Low Young's Modulus', *Metallurgical and Materials Transactions A: Physical Metallurgy and Materials Science*. Springer US, 46(9), pp. 3924–3931. doi: 10.1007/s11661-015-3011-4.

Welsch, G. (1993) *Materials properties handbook*.

Williams, J. C. and Paton, N. E. (1973) 'The 0 ., -Phase as an Example of an Unusual Shear Transformation o', 4(December).

Xiang, L. *et al.* (2018) 'Effect of Pre-cold Rolling-Induced Twins and Subsequent Precipitated x -Phase on Mechanical Properties in a b -Type Ti – Mo Alloy', *Acta Metallurgica Sinica (English Letters)*. The Chinese Society for Metals, 31(6), pp. 604–614. doi: 10.1007/s40195-017-0687-z.

Xu, Y. H. and Cai, M. (2017) 'Influence of Loading System Stiffness on Post-peak Stress – Strain Curve of Stable Rock Failures', pp. 2255–2275. doi: 10.1007/s00603-017-1231-1.

Yong, L. I. U. *et al.* (2003) 'Microstructures and mechanical behavior of PM Ti-Mo alloy', 10(2), pp. 81–86.

Yu, L. *et al.* (1993) 'Agaricus bisporus'.

Zhang, J. *et al.* (2018) 'Materials Characterization Fabrication and characterization of a novel β metastable Ti-Mo-Zr alloy with large ductility and improved yield strength', *Materials Characterization*. Elsevier, 139(September 2017), pp. 421–427. doi: 10.1016/j.matchar.2018.03.031.

Zhang, L. *et al.* (2015) 'Effect of Nb addition on microstructure , mechanical properties and castability of ù -type TiíMo alloys', *Transactions of Nonferrous Metals Society of China*. The Nonferrous Metals Society of China, 25(7), pp. 2214–2220. doi: 10.1016/S1003-6326(15)63834-1.

Zhang, L. C. *et al.* (2005) 'Nucleation of stress-induced martensites in a Ti / Mo-based alloy', 0, pp. 2833–2836.

Zhang, L. C. *et al.* (2011) 'Manufacture by selective laser melting and mechanical behavior of a biomedical Ti – 24Nb – 4Zr – 8Sn alloy', *Scripta Materialia*. Acta Materialia Inc., 65(1), pp. 21–24. doi: 10.1016/j.scriptamat.2011.03.024.

Zhao, X. *et al.* (2012) 'Acta Biomaterialia Beta type Ti – Mo alloys with changeable Young ' s modulus for spinal fixation applications', *Acta Biomaterialia*. Acta

Materialia Inc., 8(5), pp. 1990–1997. doi: 10.1016/j.actbio.2012.02.004.

Zheng, Y. (2013) 'Nucleation Mechanisms of Refined Alpha Microstructure in Beta Titanium Alloys', (May 2013), p. 211. doi: osu1366296464.

Zhou, Y. and Luo, D. (2011) 'Microstructures and mechanical properties of Ti – Mo alloys cold-rolled and heat treated', *Materials Characterization*. Elsevier Inc., 62(10), pp. 931–937. doi: 10.1016/j.matchar.2011.07.010.

Zhou, Y. and Niinomi, M. (2009) 'Ti – 25Ta alloy with the best mechanical compatibility in Ti – Ta alloys for biomedical applications', *Materials Science & Engineering C*. Elsevier B.V., 29(3), pp. 1061–1065. doi: 10.1016/j.msec.2008.09.012.

Zhou YB (2000) 'No Title', *Titanium Alloys*.